LEABHARLANN CHOLÁISTE NA TRÍONÓIDE, BAILE ÁTHA CLIATH | TRINITY COLLEGE LIBRARY DUBLIN
Ollscoil Átha Cliath | The University of Dublin

Terms and Conditions of Use of Digitised Theses from Trinity College Library Dublin

Copyright statement

All material supplied by Trinity College Library is protected by copyright (under the Copyright and Related Rights Act, 2000 as amended) and other relevant Intellectual Property Rights. By accessing and using a Digitised Thesis from Trinity College Library you acknowledge that all Intellectual Property Rights in any Works supplied are the sole and exclusive property of the copyright and/or other IPR holder. Specific copyright holders may not be explicitly identified. Use of materials from other sources within a thesis should not be construed as a claim over them.

A non-exclusive, non-transferable licence is hereby granted to those using or reproducing, in whole or in part, the material for valid purposes, providing the copyright owners are acknowledged using the normal conventions. Where specific permission to use material is required, this is identified and such permission must be sought from the copyright holder or agency cited.

Liability statement

By using a Digitised Thesis, I accept that Trinity College Dublin bears no legal responsibility for the accuracy, legality or comprehensiveness of materials contained within the thesis, and that Trinity College Dublin accepts no liability for indirect, consequential, or incidental, damages or losses arising from use of the thesis for whatever reason. Information located in a thesis may be subject to specific use constraints, details of which may not be explicitly described. It is the responsibility of potential and actual users to be aware of such constraints and to abide by them. By making use of material from a digitised thesis, you accept these copyright and disclaimer provisions. Where it is brought to the attention of Trinity College Library that there may be a breach of copyright or other restraint, it is the policy to withdraw or take down access to a thesis while the issue is being resolved.

Access Agreement

By using a Digitised Thesis from Trinity College Library you are bound by the following Terms & Conditions. Please read them carefully.

I have read and I understand the following statement: All material supplied via a Digitised Thesis from Trinity College Library is protected by copyright and other intellectual property rights, and duplication or sale of all or part of any of a thesis is not permitted, except that material may be duplicated by you for your research use or for educational purposes in electronic or print form providing the copyright owners are acknowledged using the normal conventions. You must obtain permission for any other use. Electronic or print copies may not be offered, whether for sale or otherwise to anyone. This copy has been supplied on the understanding that it is copyright material and that no quotation from the thesis may be published without proper acknowledgement.

TRINITY COLLEGE
0 5 AUG 2008
LIBRARY DUBLIN
THESIS
8509

Methodological Considerations and Functional Correlates in Structural MR Image Analysis of the Brain

Erik O'Hanlon

A thesis submitted in for the degree of Doctor of Philosophy

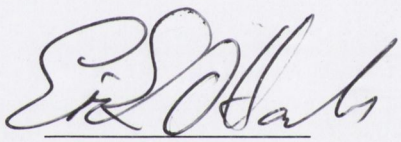
University of Dublin
Trinity College

2007

Declaration

I declare that this work has not been submitted previously as an exercise for a degree at this or any other university and that it is entirely my own work. I give my permission for the Trinity College Library to lend or copy this thesis upon request.

Signed



13.06.2008

Erik O'Hanlon

Date

Acknowledgements

Firstly, I would like to thank my supervisor Hugh Garavan for giving me the opportunity to pursue my studies. This thesis owes its existence to him, and his enthusiasm, interest, depth of knowledge and expertise. His willingness to mentor and guide my work in a challenging and meaningful way through novel and excellent ideas has been fantastic. I am truly grateful for his patience and understanding during the past three years as this work would not have been possible without his tireless efforts.

To my wife Janice, I couldn't have asked for more love, support and understanding and I can't thank you enough for the sacrifices you've made on my behalf during the last three years. Thanks, my love, you never cease to amaze me. To my children, Amie and Ethan, what can I say? I promise I'll make it up to you and love you both so much.

I have to thank all the members of lab, Cristina, Elena, Kevin, Clare, Liam, Gloria, Sarah, Alex, Gina, Karin and in particular Colm, for all the help and guidance over the last three years.

A special thanks to all my friends within the department especially Liam, Gloria, Cristina, Elena, Colm, Jason, Kylie, Christian, and Katherine for their support and enthusiasm during my time here.

My thanks to all the members of the Neurophysics team at Beaumont Hospital, in particular to Mary Fitzsimons, for the opportunity to work on a dataset that proved both challenging enlightening. A special thanks to Lisa Ronan for all her efforts, comments, questions *and* answers in our collaborations and for applying her expertise in Stereology and performing all the stereological measures referred to in this thesis. It's been a pleasure.

Not forgetting both Maria Fitzgibbon and Professor Ian Robertson for opening the door and allowing me to pursue my dream of studying at Trinity College for this Ph.D. Thank you both.

I'm sure there are many people I've neglected to mention and thank here and so deserve my apologies.

Lastly, to my parents, thanks Mum and Dad. Without your support and thoughtfulness over the past years this wouldn't have been possible.

Supported in part by USPHS grants DA09465, DA14100, DA11326, GCRC M01 RR00058 and by The Higher Education Authority (HEA) PLRTI grant to Trinity College Institute of Neuroscience 8AA.G03007.0.S11.

Summary

Structural magnetic resonance imaging is a complex and extremely powerful high resolution imaging mechanism that yields excellent soft tissue contrast. Recent times have seen the development numerous structural image analysis techniques that offer the researcher a means to perform whole brain voxelwise comparisons between various groups to capture and localize between-group differences. However, the researcher must be aware of the complexities involved in such analysis techniques and understand the implications of methodological variations. Addressing some of these concerns and applying these findings to perform inter-modal comparisons between functional MRI activation measures and structural volumetric measures to assess structure/function relations of the brain is the focus of this thesis.

The first study investigates a novel nonlinear modelling approach for event-related fMRI analysis and demonstrates the techniques ability to accommodate inter- and intra-subject variability in the haemodynamic properties of the BOLD response used as an indirect measure of neuronal activity. This investigation ensures that a suitably flexible and highly sensitive mechanism for fMRI analysis is employed to facilitate meaningful comparisons between the measures from an equally sensitive structural image analysis technique to examine structure function correlates.

The second study examines the sensitivity of Voxel-based morphometry to selectively identify and localize regions of effect associated with drug usage. Three independent drug using groups (cocaine, cannabis and nicotine) are compared to controls and each other to assess the ability of VBM to capture the drug specific brain regions targeted by

each particular substance of abuse and then compare all groups to investigate possible brain regions common to all groups that may imply a possible underlying mechanism of addiction processes. The sensitivity of the technique is clearly demonstrated as both unique and shared volumetric changes for the different drugs are identified.

VBM can be used to obtain quantitative brain volumetrics as well as the more common identification and localization of tissue concentration and volume differences. The third study examines the accuracy and reliability of volumetric measures from automated analysis techniques compared to 'gold standard' Stereological measures and incorporates a detailed volumetric comparison between three different automated analysis techniques to explore the variability the localization of global volume differences identified by the different fully automated techniques.

Finally both functional and structural VBM measures are compared to explore the correlates of brain volumetrics, functional activations and performance scores to further our understanding of the implications of anatomical variations on brain functions. Here the focus of volumetric analysis shifts from an approach where global group differences in tissue volumes in relation to drug use being explored to possible structural differences that may correlate to functional measures and cognitive performance scores. Differences in functional activation measures and performance scores are used to focus the search on brain regions involved in these cognitive processes and interrogate the possibility of structural differences in these specific regions being a key measure that drives these differences.

Publications

The following is a list of manuscripts that have been submitted for publication throughout the duration of this Ph.D.

Thesis chapters derived from the following articles:

Chapter 2:

O'Hanlon, E., Murphy, K., Ross, T..J., Stein, E., & Garavan, H. *A flexible nonlinear modelling technique for functional MRI data analysis.* (Under review).

Chapter 3:

O'Hanlon, E., Bloom, A., & Garavan, H. *Grey and white matter volume differences in cocaine, cannabis and nicotine users compared to controls.* (Under review).

TABLE OF CONTENTS

Declaration i

Acknowledgements ii

Summary iv

Publications vi

Table of Contents vii

Chapter 1 1

Introduction

1.1 A brief introduction to the physics of MRI 8

1.2 The physiology of blood flow, fMRI and the ***BOLD*** phenomenon 16

1.3 The mechanisms of voxelwise structural image analysis 19

1.4 Topics addressed in this thesis 27

Chapter 2 33

A Flexible Nonlinear Modelling Technique for Functional MRI data analysis

2.1 Introduction 34

2.1.1 Examples of the nonlinear technique 36

2.1.1.1. Modelling Pharmacokinetics 36

2.1.1.2. Modelling Emotional Processes 40

2.1.1.3. Application of non-linear regression to event-related fMRI 44

2.2 Methods 48

2.2.1 Subjects and Experimental Task Design 48

2.2.2 MRI Scanning Parameters 49

2.2.3 Image Preprocessing 49

2.2.4 Group Analysis 50

2.3 Results 51
2.4 Discussion 55
2.4.1 Haemodynamic Variability 55
2.4.2 Non-linear Regression for Event-related fMRI 58

Chapter 3 59

Grey and white matter volume differences in cocaine, cannabis, and nicotine users compared to controls, using Voxel-based morphometry

3.1 Introduction 60
3.2 Methods 63
3.2.1 Participants 63
3.2.2 MRI Scanning Parameters 65
3.2.3 Image Preprocessing 65
3.2.4 Template generation 66
3.2.5 Statistical Analysis 66
3.3 Results 68
3.3.1 Grey matter Comparisons 68
3.3.2 White Matter Comparisons 76

3.4 Discussion 83
3.4.1 Cannabis Group 84
3.4.2 Nicotine Group 86
3.4.3 Cocaine Group 87
3.4.4 Common Effects 90
3.5 Conclusions 91

Chapter 4 93

Comparison of grey and white matter whole brain volume measurements of temporal lobe epilepsy patients and controls using Stereology and fully automated voxel based volumetric techniques

4.1 Introduction 95
4.2 Methods 97
4.2.1 Participants 97
4.2.2 MRI Scanning Parameters 98
4.2.3 Stereological Volume Analysis 98
4.2.4 Automated Volumetric Analysis Techniques 102
4.2.4.1 Strategy 1: Optimized VBM analysis 102
4.2.4.2 Strategy 2: FSL FAST analysis 104
4.2.4.3 Strategy 3: FSL SIENAX analysis 105
4.2.5 Statistical Comparisons of Analysis Strategies 109
4.2.6 Statistical Analysis of Voxelwise volumetric Comparisons (fully automated techniques) 111
4.3 Results 112
4.3.1 Mixed Factorial ANOVA 114
4.3.2 Correlation Analysis 116
4.3.3 Voxelwise Comparison of fully automated techniques 119
4.4 Discussion 127

Chapter 5 137

Correlates of grey and white matter brain volumetrics using 'optimized' Voxel Based Morphometry with fMRI activation measures and behavioural performance scores

5.1 Introduction 139
5.2 Methods 142

5.2.1 Participants and Task design 142
5.2.2 MRI Scanning Parameters 143
5.2.3 Optimized VBM Analysis 144
5.2.3.1 Template generation 145
5.2.3.2 fMRI Group Analysis and Region of Interest Generation 146
5.2.3.3 Demographic Influences on Grey Matter Volumes. 148
5.2.3.4 Grey Matter volumes and Functional Activations. 148
5.2.3.5 Grey Matter Volume and Performance. 148
5.3 Results 149
5.3.1 Demographic Interactions 149
5.3.2 Grey Matter Volume and Functional Activity 150
5.3.3 Split-Group Comparisons of Grey Matter Volume and Performance. 150
5.3.4 Stepwise Multiple Regression Analyses. 151
5.4 Discussion 154
5.5 Summary 157

Chapter 6 159
6.1 Discussion 159
6.2 Summary of results 160
6.3 Proposed Analysis Strategy for 'Optimized' VBM 166
6.4 Interpretations: The Big Picture. 169
6.5 Future Directions 170
6.6 Conclusions 171

References 173

Chapter 1

Introduction

Magnetic resonance imaging (MRI) is a powerful imaging technique that has established itself at the forefront of the battery of modern neuroimaging tools used by clinicians and research scientist alike. The flexibility of this imaging modality to visualize high resolution anatomy with excellent soft tissue contrast, capture cellular chemical properties in-vivo using MR spectroscopy and offer a mechanism of indirectly visualizing cognitive functions in response to various forms of external stimulus via functional MRI, has contributed to the techniques position as a widely used tool for clinical diagnosis and research investigations. MRI has been extensively utilized to investigate numerous neurodegenerative and age related conditions (Bartzokis et al., 2001; Fotenos et al., 2005; Good et al., 2001a; Hermann et al., 2006; Hermann et al., 2003; Hsu et al., 2002; Huppertz et al., 2005; Kopelman et al., 2001; Matsuzawa et al., 2001; Persson et al., 2006; Scahill et al., 2003), cognitive impairment resulting from post traumatic brain injury (Carpentier et al., 2006; Ewing-Cobbs et al., 1998; Himanen et al., 2005; Kurca et al., 2006; McGowan et al., 2000; Pradat-Diehl et al., 1999; Soeda et al., 2005) and substance abuse (Bolla et al., 2004; Daumann et al., 2004; Fein et al., 2006b; Garavan et al., 2000b; Garavan and Stout, 2005; Lawrence et al., 2002; O'Leary et al., 2002; Parkinson et al., 2002; Pogarell et al., 2006; Rezvani and Levin, 2001; Wexler et al., 2001), mechanisms of language (De Carli et al., 2007; Kamada et al., 2007; Pouratian et al., 2002; Sakai et al., 2004; Tatsuno and Sakai, 2005), auditory

and visual processes (Elfgren et al., 2006; Pihlajamaki et al., 2004; Pins et al., 2004; Sekiyama et al., 2003; Sigman et al., 2005; Sokhi et al., 2005). Hence MRI offers various mechanisms to capture and quantify such features as underlying anatomical variations and the localization of brain functioning in response to cognitive demands using fMRI.

The presence of structural change in the brain is often routinely used to facilitate clinical diagnoses of numerous neurological clinical conditions and degenerative processes. The effects of anatomical change frequently manifest themselves in changes in cognitive performance, cognitive impairment and or dysfunction and hence suggest some mechanism of interaction between structure and function. The exact mechanisms of this complex relationship between brain anatomy and brain function, often more apparent in clinical populations compared to those of normal populations, remains elusive. A clear understanding of any underlying structure / function relationship would greatly benefit the early identification of possible biological markers that could predict the onset of a clinical condition, hence offering a more effective pre-emptive treatment mechanism for those at risk. Hence, the exact mechanisms of possible interactions between anatomical structure and brain function must be explored both in normal populations and in the presence of clinical conditions and pathologies. Understanding if the absolute volume of brain tissue is in any way influential or predictive of cognitive performance and related in any way to the extent of functional activity in the brain remains an important question yet to be definitively answered. Although the influence of anatomical differences associated with the performance of a certain task has been reported in the literature suggesting that some interactive mechanism relating brain structure and functional activity appears to exist under

certain conditions and featuring specific brain regions such as the hippocampus, corpus callosum, motor cortex, and cerebellum (Draganski et al., 2004; Maguire et al., 2000; Maguire et al., 2003; Munte et al., 2002; Schlaug, 2001). To investigate the relationship between structure and function, one must first develop a clear understanding of the individual mechanisms used to capture and analyse cognitive functioning and high resolution neuroanatomy. Both fMRI and volumetric image analysis offer the researcher a window of exploration that facilitates inter-modal comparisons between two different quantities. First, inherent sources of variability associated with each technique must be investigated to reduce the effects of these confounding influences. Once an understanding of the sources of variability associated with each individual technique has been gained, a clearer picture of the influences and importance of brain structure may unfold permitting, in due course, a systematic investigation of structure / function relations.

The use of fMRI to probe the underlying differences between various clinical groups displaying systematic cognitive variations compared to those of control populations is apparent by the numerous studies reported in the literature. Such functional differences have been successfully identified in clinical populations such as epilepsy (Deblieck et al., 2003; Oddo et al., 2003), ADHD (Bush et al., 1999; Bush et al., 2005; Roth and Saykin, 2004; Rubia et al., 2005; Seidman et al., 2004; Sunshine et al., 1997; Wolf et al., 2005; Zang et al., 2005), drug addiction (Bolla et al., 2003; Bolla et al., 2000; Desmond et al., 2003; Eldreth et al., 2004; Garavan et al., 2000b; Goldstein and Volkow, 2002; Hester and Garavan, 2004; Kaufman et al., 2003; Kumari et al., 2003; Risinger et al., 2005; Solowij N, 1997) and cognitive difference associated with demographic factors such as gender (Bell et

al., 2006; Bolla et al., 1999; Cowan et al., 2000; Gorbet and Sergio, 2007; Kastrup et al., 1999; Moulton et al., 2006; Nielson et al., 2002; Nielson et al., 2004; Persson et al., 2006; Siegler, 2007) and aging processes (Braver and Barch, 2002; Gazzaley and D'Esposito, 2007; Grossman et al., 2002; Hesselmann et al., 2001; Rypma et al., 2007; Taniwaki et al., 2007).

However, fMRI measures are intrinsically noisy and feature numerous sources of variability including natural biological variations in arterial blood flow and tissue composition, technological variations encountered during parameter optimization of imaging protocols during acquisition and those related to the various analyses strategies employed (Aguirre et al., 2002; Aguirre et al., 1998; Calhoun et al., 2001; Calhoun et al., 2004; Cohen, 1997; Dale, 1999; D'Esposito et al., 1999; Handwerker et al., 2004; Kwong et al., 1992; Lee et al., 1995; Logothetis, 2002; Lu et al., 2006; Murphy and Garavan, 2004a; Murphy and Garavan, 2005; Ogawa et al., 1990). The mechanisms of fMRI analysis employed must therefore be flexible to accommodate such sources of inter and intra-subject related variability and accurately remove confounds thus facilitating meaningful interpretations of the experimental findings.

MRI offers the clinician and researcher an imaging mechanism of high resolution suitable for the investigation of soft tissue regions and offering excellent tissue contrast between the various tissue types. Structural changes related to aging or pathology, are frequently captured by MRI and facilitate diagnosis and treatment interventional therapies (Garden and Roberts, 1996; Geuze et al., 2005; Gong et al., 2004; Lawson et al., 1997; Lawson et

al., 2002; Roberts et al., 1994; Salman et al., 2005b; Schad, 2001; Shi et al., 1998). More recently, detailed analysis techniques have permitted the whole brain voxelwise comparisons of various clinical groups to those of normal populations and have greatly improved our understanding of the biological mechanisms and markers of numerous conditions. These powerful analyses techniques aided by modern technological advances in computing, allow the researcher to probe the neuroanatomy at superb special resolution, frequently in the range of 1 mm^3. MRI based manual delineation and region of interest (ROI) techniques have been extensively utilized to provide accurate quantitative measures of anatomical structures routinely used in surgical planning and oncology treatment mechanisms (Castellanos et al., 2001; Castellanos et al., 1996; Garcia-Finana et al., 2003; Hermann et al., 2003; Hoshida et al., 1995; Kopelman et al., 2001; Lawson et al., 2000; Mackay et al., 2000; Rosen and Harry, 1990; Tisserand et al., 2002). Analysis techniques such as Stereology, which incorporates a mathematically unbiased sampling technique, can be employed to efficiently measure whole brain volumes and sub-structures and assess group volumetric differences between clinical and normal populations (Gong et al., 2000; Howard et al., 2003; McCloskey et al., 2006; Roberts et al., 1994; Roberts et al., 1998; Roberts et al., 2000; Ronan et al., 2006). More recent advances have seen the rise of fully automated voxelwise analysis techniques such as Voxel-based Morphometry (VBM) (Ashburner and Friston, 2000) that routinely segment whole brain volumes or more restricted regions of interest into tissue specific volumes of grey matter, white matter and cerebrospinal fluid (csf). Tissue specific group comparisons can then be performed to probe for localized changes in tissue composition between the various populations. These automated techniques have been extensively utilized and reported in the literature and have

proved successful in the identification of localized changes in the grey and white tissue partitions associated with numerous specific clinical conditions (Bonilha et al., 2006; Brody et al., 2004a; Carmona et al., 2005; Cowan et al., 2003; Good et al., 2001b; Keller et al., 2002b; Matochik et al., 2005; Matochik et al., 2003; Matsuzawa et al., 2001; McMillan et al., 2004; Mueller et al., 2006; Salmond et al., 2000; Semrud-Clikeman et al., 2006; Smith et al., 2007). These automated analysis tools continue to evolve and optimized versions (Good et al., 2001a; Jenkinson et al., 2002; Jenkinson and Smith, 2001) offer the researcher the ability to explore not only subtle tissue morphology (known as tissue concentration), but can also identify areas of volumetric change, quantify global and regional tissue volumes and identify, quantify and localize atrophy of brain tissue where present. Automated techniques have thus become very powerful and sophisticated analysis tools at the researcher's disposal but a clear understanding of the mechanisms of these techniques and their subsequent application to particular structural analyses must be gained to ensure the correct application of the most suitable analysis strategy is employed thereby producing meaningful results. This fact has lead to the difficulty comparing findings from different studies (sometimes contradictory) as the application and specific analysis methodology used can influence the results and induce a source of variability that makes such cross study comparisons difficult at times. Such comparisons can only be accurately performed if the analysis techniques are very closely comparable.

Both fMRI and voxelwise structural image analyses have independently provided meaningful and insightful details of the mechanisms, cognitive implications and structural morphologies of numerous clinical conditions and normative brain functions but few

studies have focused on the benefits that could be gained through the application of multi-modal MR imaging strategies and associated analyses techniques. The use of such multi faceted MR imaging techniques may offer an insight into the mechanisms of how brain structure directly or indirectly relates to functional activity and cognitive performance. Such investigations may uncover possible underlying interactions between the various brain measures in normal populations and how these complex interactions perform when pathology or degenerative processes arise. A clearer understanding of the methodological considerations associated with structural image analysis and the metrics of brain anatomy may reveal how the role brain structure plays in the mechanism of how the brain functions.

1.1 A brief introduction to the physics of MRI

Hydrogen atoms are the most abundant atoms found in the human body and have the highest sensitivity to magnetic resonance of any element in nature and hence are the focus of magnetic resonance imaging of the human body in a clinical environment. The hydrogen atom contains a single positively charged proton which is slightly magnetic in nature with an intrinsic momentum or spin associated with it. The characteristics of this intrinsic moment are frequently explained using both classical and quantum physics. The classical description focuses on the simple magnetic moment of isolated nuclei and is useful to gain a fundamental understanding of the principles involved in MR physics. The quantum description is used when considering the net effect on an assembly and describes the electromagnetic radiation in terms of discrete quantities (high energy state and low energy state) of energy (often referred to as packets of energy). In reality it is often very useful to use both classical and quantum explanations to describe the physics of MRI.

When placed in a large external magnetic field (B_0), the protons of the body tend to align themselves in either a parallel or anti parallel direction to that field. In reality, the number of parallel protons exceeds the number of anti parallel protons by a very small amount (typically 0.0005% for a 1.5 tesla magnetic and 0.001% for a 3 tesla magnet) and result in a net magnetization force (M), the size of which is proportional to the external magnetic field strength (see Figure 1.1).

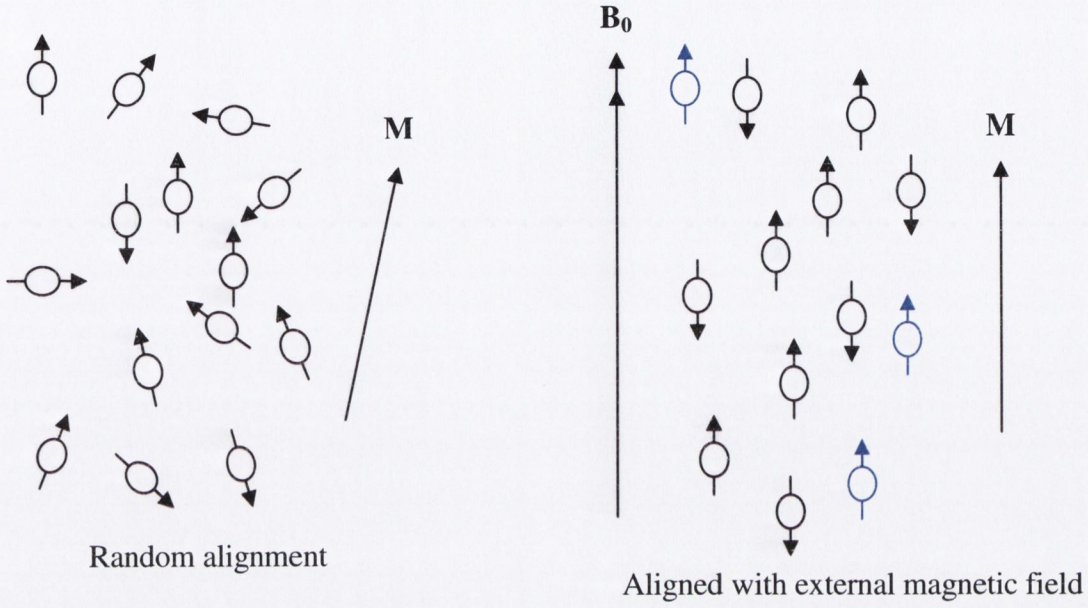


Figure 1.1: Protons without the influence of an external magnetic field have a random alignment with a net magnetization force of zero. When an external magnetic field ($\mathbf{B_0}$) is applied, the protons align themselves in either a parallel or anti parallel direction with it and result in a small excess of protons with parallel alignment (shown in blue) yielding a net magnetization vector **M** in the same direction as the external field. The number of aligned protons is much smaller than shown here and is used to facilitate the concept.

Each of the hydrogen nuclei that contribute to the overall net magnetization (M) precess or spin about their own axis without the presence of the external field. When initially immersed in the external field, the net magnetization vector of the protons may not be in parallel and so the force of the B_0 field will drive the M vector to line up with it over a short period of time. The path the protons follow during the alignment period is not a simple one and occurs in a spiral fashion. The largest force acting on the M vector induces a characteristic wobble or precession about the B_0 field vector in a clockwise direction. The

frequency of this precession is known as the Larmor frequency, measured in Hertz. The value of the Larmor frequency is governed by the Larmor equation

$$f = \gamma \cdot B_0 \quad \text{..... Equation 1}$$

where f is the frequency of precession or resonance, B_0 is the static magnetic field strength and γ is the proportionality constant referred to as the gyromagnetic ratio constant expressed in Megahertz/tesla and equals 42.57 for hydrogen protons. Hence the Larmor frequency of a 1 Tesla magnet is 42.57 MHz, 63.86 MHz for a 1.5 tesla magnet and 127.72 MHz for a 3 tesla magnet and so on. Under normal conditions this precession continues for the duration of the transitional period from disturbance (when the protons are placed in the external magnet field) until the equilibrium state (where protons are aligned in a parallel direction with B_0) has been reached. Thus when a subject is placed in the bore of the MR scanner, the hydrogen protons in their body align themselves with the external magnetic field of the MR scanner. A further disturbance is necessary to induce an excitation force that will push the now aligned M vector away from its state of parallel alignment with B_0 and induce a state of precession again at the Larmor frequency (see Figure1.2).

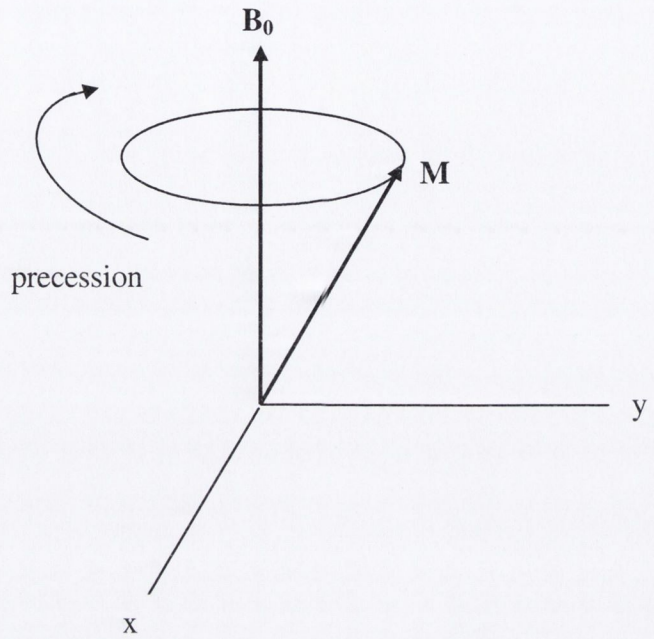


Figure 1.2: During the transition period where the magnetization vector aligns itself with the external field $\mathbf{B_0}$, the forces acting on **M** cause it to precess around the $\mathbf{B_0}$ axis in a clockwise direction following a spiral path.

This extra resonance or spin is achieved by applying extra magnetic fields or gradient fields that are not static in nature but vary linearly over time. This extra magnetic field is applied in three planes (X, Y and Z) using three gradient coils acting as electromagnets that vary the strength (positively and negatively) of the magnetic field in a controlled manner. When these gradients are turned off the precessing protons once again return to a state of equilibrium in a process called 'relaxation' and in doing so emit their excess energy (packets) in the form of an electromagnetic wave in the radio frequency (RF) range. This RF signal is captured by the RF receiver equipment (either the body coil of the scanner or a customized specific local coil) and forms the basis of the MR image. During the relaxation

period when the protons realign with B_0, the M vectors at any particular locations move at different rates as they return to the base state. Two independent relaxation processes influence the protons during this phase, namely spin-spin interactions commonly called T2 relaxation and spin lattice interactions known as T1 relaxation. These relaxation processes are the mechanisms that permit image contrast in MRI and can be selected by the choice of timing parameters within RF pulse sequence used. Variations in tissue compostion affect the relaxation parameters. A simple analogy would be to think of tiny spinning gyroscopes moving in numerous liquids of varying viscosity. Obviously a gyroscope spinning in water will spin faster than one spinning in oil which is turn would spin faster than one in treacle. This is equivalent to the action of hydrogen protons in the various tissue types in the human body and each signal collected from the various net magnetization vectors, M, are proportional to the discrete energy levels determined by the magnetic field strength at the various locations and these variations form the basis of tissue contrast in MR imaging. Both T1 weighted and T2 are utilized in MR imaging. T2 relaxation is the theoretical decay of the transverse magnetization that assumes a perfectly homogeneous magnetic field. In reality, inhomogeneities are present in the magnetic field and cause the T2 relaxation to decay at a faster rate. Hence, T2* relaxation takes into account the magnetic field inhomogeneities encountered in practice. The studies contained in the body of this work utilize T1 relaxation to form the basis of structural imaging and T2* relaxation for functional MRI (see Figure 1.3).

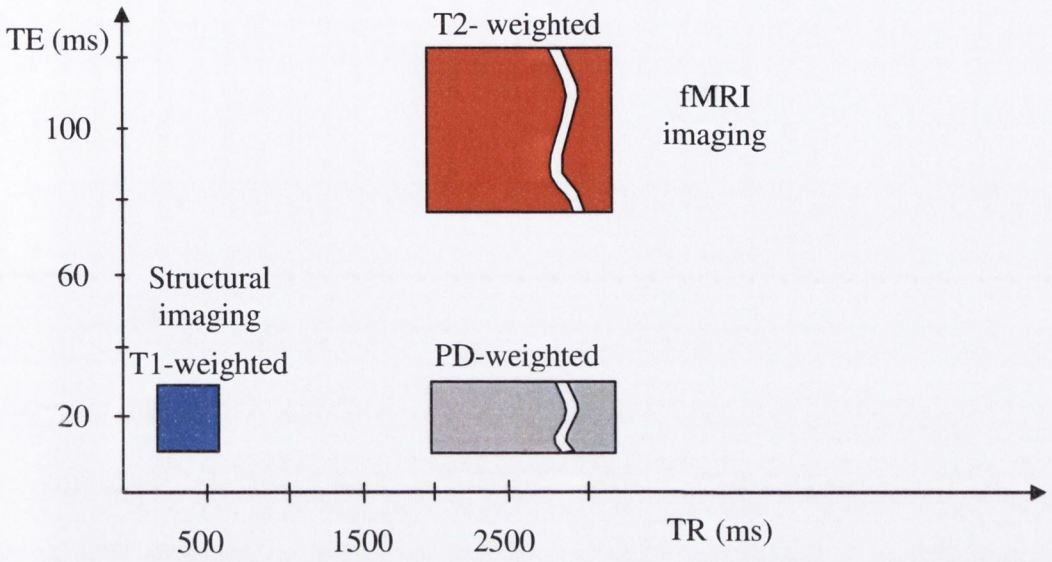


Figure 1.3: MR image contrast mechanisms and associated timing ranges. T1 weighted relaxation has short relaxation (TR) and echo (TE) times and forms the basis of the contrast mechanisms used in structural imaging. T2 (including T2*) feature long TR and TE times and forms the contrast mechanism used for fMRI and diffusion imaging. Note, a third contrast mechanism called proton density weighting is shown for information purposes only and is not focus of discussion here.

As previously mentioned, gradient fields or RF pulse sequences are applied in three directions (x, y and z) which enable the spatial localization of a point to be determined (see Figure 1.4). The frequency of the RF pulse varies about the Larmor frequency (f) by a known amount or bandwidth equal to $\pm \Delta f$. Spatial localization is achieved by firstly applying a gradient pulse in one plane known as the slice selection gradient, GS (say the z axis for axial slices). The RF pulse excites the protons at a particular point along the selected axis and over a frequency bandwidth of $\pm \Delta f$ about the central frequency f, and only the protons within this bandwidth are excited and hence are actively selected over a

particular slab of tissue. Next, the signals emitted from the selected slab of tissue must be collected along the other two axes of the image to facilitate spatial localization. The second gradient known as the frequency encoding gradient, (GR) occurs during the readout period of the sequence and is thus activated during the signal collection interval where signals from right to left of the image are linearly adjusted from lower to higher frequencies. Hence, the left side of the slab is encoded with frequencies lower than those on the right side and this process is know as frequency encoding. Finally a third gradient known as the phase encoding gradient (GP), is applied along the remaining axis, perpendicular to both the slice selection and frequency encoding gradients. The purpose of the phase encoding is to make the phase or angle of the emitted signal depend on its position along the third direction (top to bottom of the image) where protons at the top will precess at a slower speed than those at the bottom. Before the phase encoding gradient is switched on all the magnetization vectors in the selected slab of tissue have the same phase. When GP is activated (with the slice selection and frequency encoding gradients remaining constant) the M vectors along the phase encoding axis rotate at different frequencies due to the varying GP field being applied. When the gradient field is deactivated the frequencies of the M vectors return to normal once again but the phase of the M vectors remain out of synchronization or dephased by a specific amount in relation to their position along the phase encoding axis. This process is repeated numerous times and the quantification of dephasing is measured, hence enabling the position along the GP axis to be determined.

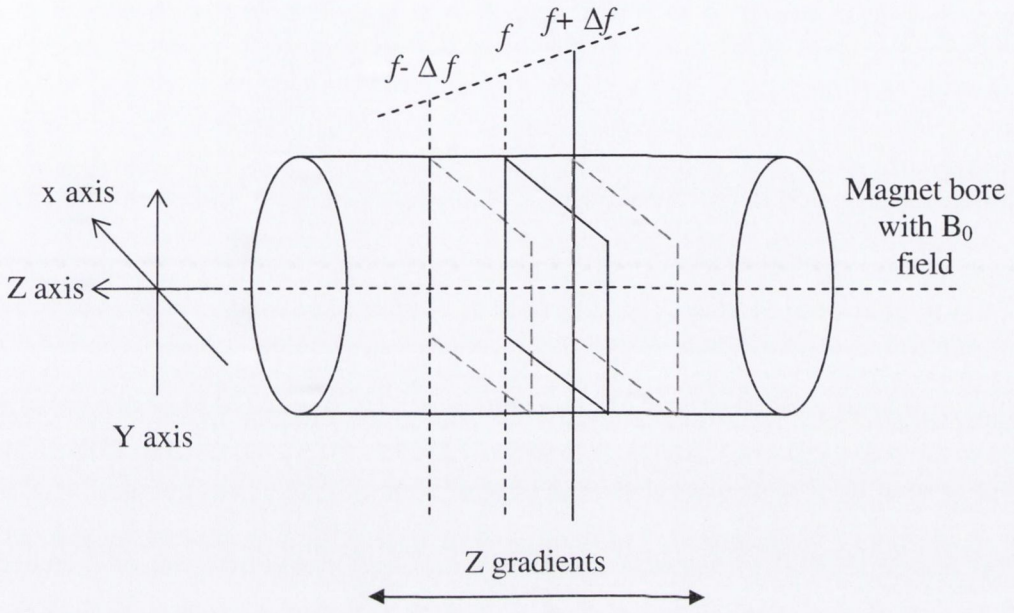


Figure 1.4: A schematic representation of the magnet bore of a typical MR scanner is shown indication the orientation of the magnetic field and relative axis directions with respect to the scanner. Magnetic gradient coils are applied in all three planes, x, y and z (shown above) to facilitate special localization of signals emanating from the excited protons within the sample of tissue selected by the RF pulse sequence. The central frequency of the selected slab of tissue corresponds to f (the Larmor frequency) and this frequency is varied over a known bandwidth to actively select a specific volume of tissue rather than just a single point in space, (located by applying a similar gradient pulse in the other two axes) and hence speeds up the imaging process by acquiring all signals from the selected slab at once and using frequency encoding to decode their spatial information.

1.2 The physiology of blood flow, fMRI and the BOLD phenomenon

Functional MRI is an imaging mechanism aimed at capturing neuronal activity. At present, the resultant electrical signals of neuronal activations or their associated magnetic tracers remain directly undetectable by standard MR imaging. This said, fMRI can capture signal changes due to the physiological properties of blood oxygenation (haemodynamic effects) in response to changes in neuronal activity and associated fluctuations in oxygen levels to the stimulated neurons. Thus an indirect mechanism of capturing neuronal activity is possible through fMRI. This mechanism relies on the contrast between oxygenated and deoxygenated haemoglobin which have different magnetic properties. Oxyhaemoglobin is diamagnetic whereas deoxyhaemaglobin is paramagnetic in nature. Paramagnetic substances induce inhomogeneities into the local magnetic field and these magnetic distortions detract from the MR signal causing a localized drop in signal. During activation, oxygen is metabolized as neurons fire and results in a localized small increase in deoxyhaemaglobin concentrations. The arterial response to this increase is a slight dilation of the blood vessels and hence a corresponding increase in the supply of oxygenated haemoglobin. This oversupply of oxyhaemoglobin causes a dilution in the level of deoxyhaemaglobin and thus induces a localized increase in MR signal in the proximity of the neuronal activity. This phenomenon is called the *BOLD effect* (blood oxygen level dependence). The fluctuations in the MR signal are very short in duration and thus require an extremely fast imaging sequence such as an echo planar imaging (EPI) sequence to capture them and typically give whole brain coverage in approximately 1-2 seconds . In contrast to this, the actual haemodynamic properties are very sluggish (see Figure 1.5) with

a typical delay in onset of the response between neuronal activation and associated increased blood flow being in the order of 1-2 seconds after stimulation. The signal can then take a further 4-6 seconds to reach its peak level before beginning to return to its pre-excitation level or baseline. The stabilization of the signal to baseline is further complicated by the haemodynamic property of *post-undershoot* as the signal actually drops below the baseline level before retuning to the initial state.

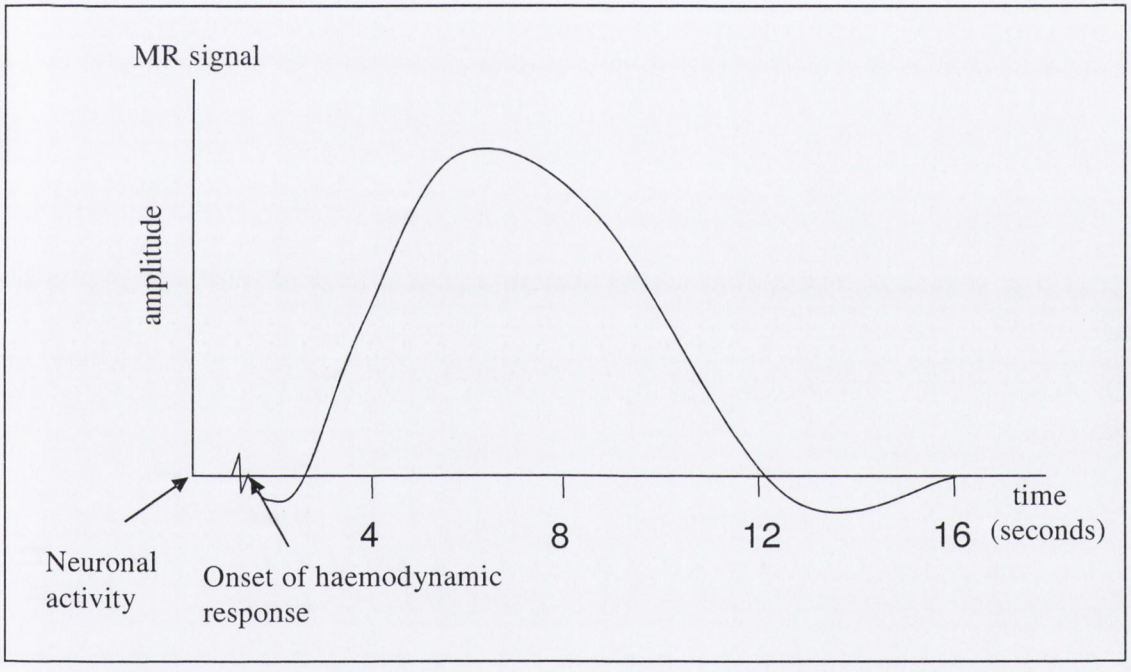


Figure 1.5: The haemodynamic response represented schematically. Typical characteristics of pre and post undershoots are shown with a temporal lag of typically 1-2 seconds between the occurrence of neuronal activity and the associated onset of the haemodynamic response. Typical times for the response to reach its peak are between 6-10 seconds before beginning its transition back to the baseline between 14-18 seconds. Time points in diagram are approximations only.

Using sequences that concentrate on the detection of the BOLD signal, the haemodynamic behaviour of every voxel in the brain at a temporal resolution of 1-2 seconds can be obtained. Hence the BOLD signal from voxels in close proximity to the stimulus driven neuronal activity can be compared to those in a state of rest and facilitate the localization of bran regions associated with the particular stimulus task being used. The complexity of such fMRI analysis techniques is by no means trivial as considerable inter- and intra-subject variability exists within the haemodynamic response functions that form the basis of event related fMRI analysis (Aguirre et al., 1998; Calhoun et al., 2004; Handwerker et al., 2004; Miezin et al., 2000; Miller and Van Horn, 2007; Murphy et al., 2006; Murphy and Garavan, 2004b; Neumann et al., 2003; Nielson et al., 2002; Nielson et al., 2004). In attempting to establish structure-function relationships at voxelwise resolution, it will be important to employ a functional MRI analytic technique that accommodates this intre- and intra-subject variability, an issue that is addressed in Chapter 2.

1.3 The mechanisms of voxelwise structural image analysis

Structural image analysis is very complex in its entirety but frequently comes as part of some fully automated analysis software. These programmes routinely employ a tissue segmentation technique to differentiate between the various tissue boundaries in the brain for the purpose of identifying between-group localized regions of change based on tissue-specific characteristics. This usually means that all subject images are transformed or warped into some standard reference plane to facilitate direct comparisons while minimizing variations in global brain size and shape. The structural image analysis components of this thesis utilize two of the main fully automated voxelwise techniques currently available, namely Voxel-based morphometry (VBM) and FSL's structural analysis toolbox, both of which are freely available for research purposes. Hence a brief explanation of the various processing pipelines for each method follows.

The VBM methodology for structural image analysis

Normalization

Normalization is the process where each image is registered to a template image to transform them into a common stereotaxic space thus removing global differences in shape and size while retaining individual differences for the purpose of between-group comparisons. This process within VBM is based on a 'non-labelled' (not landmark based) voxel intensity based approach that attempts to optimize some measure of voxel similarity between the source image and the standard space image. In order to make this comparison both images need to be in the same stereotaxic space, namely the standard image space

(Ashburner and Friston: Spatial Normalization). This is achieved by minimizing the residual sum of the squared differences between the template image and each subject image by first undergoing linear transformations followed by non-linear transformations.

- Linear transformations: are in the form of the optimum12 affine or closely related transformations to accommodate for positional differences such as x, y, z, role pitch yaw etc and variations in individual brain shape and size. This is achieved by a Bayesian framework whereby the maximum a posteriori (MAP) estimate of spatial transformation is made using prior information about normal variability in brain size.
- Non-linear transformations: are used to account for global non-linear brain shape differences and this process is modelled by a linear combination of smooth basis functions including a masking procedure to weight the normalization process to brain rather than non brain tissue.

Two important points must be mentioned; first the normalization process does not try to match every brain feature exactly but merely tries to accommodate global brain shape differences. If every feature was matched exactly then no differences would be found between the groups as all images would be identical. Second, all images must be high resolution images (1.5x 1.5 x 1.5 mm approximately) to reduce partial volume effects resulting where voxels contain a mixture of tissue types thus making it difficult to determine the classification of the tissue in that voxel as determined by the segmentation step in the VBM processing train. Small voxel sizes (high resolution images) reduce this effect as the likelihood of a small voxel consisting of different tissues is much smaller than

a large voxel size covering a larger brain volume and thus possibly encompassing a mixture of different tissues.

Segmentation

The VBM segmentation method is based on a modified Gaussian Mixture Model and incorporates image intensity non-uniformity (RF bias) correction based on a Bayesian Model. Tissue probability maps are used to assist in the classification process and the objective function is optimized by an Iterated Conditional Modes (ICM) approach and employs an Expectation Maximization Algorithm to update the mixture parameters of the objective function. Basically segmentation is the process where the brain tissue is partitioned into three distinct tissue groups, grey, white and CSF, and a further three background classes using a mixture model cluster analysis technique and to correct for smooth intensity variations (common in MR images). The tissue classification is based on the actual voxel intensity value. All voxels in the image have been spatially transformed by normalization but voxel intensity values have so far remained the same. The segmentation step attempts to classify the tissue type of every voxel of the image. This is achieved by firstly employing a mixture model cluster analysis that identifies the voxel intensity value and matches it to known intensity values for grey, white and CSF tissue based on predefined tissue probability maps or 'priors' for the predefined cluster of tissue.

Assume that the brain (F) is subdivided into small cubes or voxels, each with dimensions l x m x n, and that each of these voxels (h in number) forms part of one of a predefined number of clusters (k).

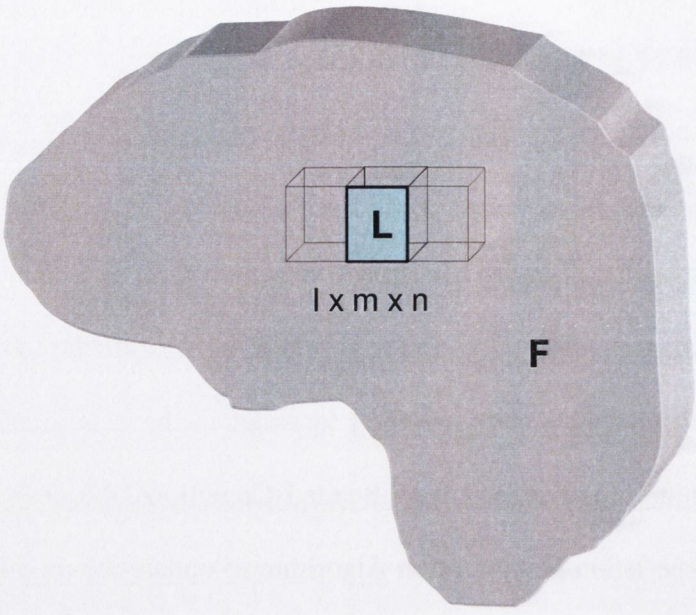


Figure 1.6: Schematic representation of the brain (F) showing three voxels (l x m x n millimetres in size) with the centre voxel labelled L for explanatory purposes.

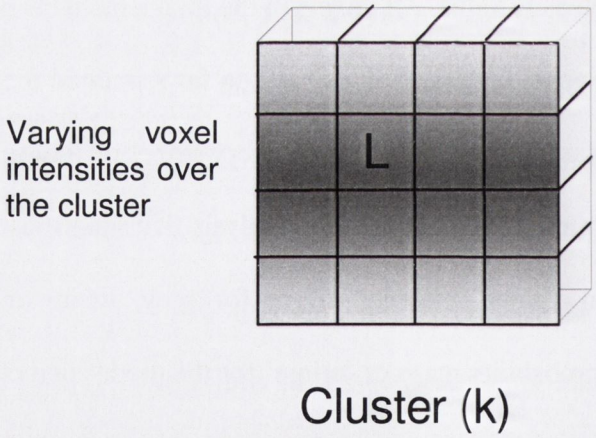


Figure 1.7: A representation of a cluster k containing 16 voxels including the voxel of interest L is shown. Each voxel has a specific grey scale intensity determined by its composition, associated with it. The mean voxel intensity is calculated by

averaging the voxel intensities over a predefined number of voxels (say the eight neighbouring voxels of L).

The distribution of voxel intensities within each of the clusters is defined by the number of voxels within the cluster multiplied by the mean voxel intensity for each cluster multiplied by the variance around the mean. As the image has been normalized each voxel has a prior probability of belonging to a particular tissue group as determined by the a priori tissue maps in the SPM package for grey, white and CSF. So the Prior probability is multiplied by probability density function for a cluster at each voxel (likelihood function). This process is an iterative process and the algorithm continues to run until the difference between log of the likelihood function and that of the previous iteration becomes negligible. This information is then convolved with a modulation function that estimated the intensity non-uniformity of the image. This gives the final probability of the voxel or the concentration. VBM segmentation thus normalizes, segments, corrects for RF intensity non-uniformity in a combined process. This value has to be convolved with a smoothing kernel to render it normally distributed Now comparisons between groups is possible for each tissue type to determine if the concentrations differ in any particular region.

The FSL Methodology for Structural Image Analysis

Normalization

FSL uses the FLIRT (FMRIB's Linear Image Registration Tool) tool to perform *linear* /affine registration between two images (source image and standard space image for

example) with variable degrees of freedom (DOF) possible with a maximum of 12 DOF (3 rotations, 3 translations, 3 scaling, and 3 skews/shears). Registration is achieved based on voxel intensity and not landmark based. Initial robust alignment is carried out to obtain the transformation matrix and then a process that optimizes or maximizes the similarity between the reference and the source image based on the minimization of a mathematical 'intensity based' cost function that quantifies the dissimilarity between the two images. The default cost function and interpolation methods used are correlation ratio and trilinear interpolation but these are easily changed if needed. FSL has focused on the optimization method to reduce the likelihood of misregistration due to being trapped in local minima and hence improve the accuracy of registration process. The optimization process uses two approaches (a) to apodize the cost function to reduce small scale dips and (b) employ a hybrid global-local optimization technique based on prior information about brain registration that combines the speed of local optimization with the robustness of global optimization which is much slower. FLIRT provides an automated mechanism of trade off between local and global optimization (Jenkinson 2002, Jenkinson 2001).

FSL Segmentation

FSL employs a Hidden Markov Random Field Model and Expectation-Maximization algorithm

(HMRF-EM) for the segmentation of brain MR images into three tissue types, grey matter, white matter and CSF (Zhang et al., 2001a). The HRFM model is a stochastic process based on the hidden Markov model using Markov chains which are designed as a one dimensional system. Since MR images are three dimensional, the Markov chain model is

substituted with a special case, the Markov random field model (MRF). Here the stochastic processes are generated by Markov Random fields whose state sequence cannot be directly observed but instead is indirectly estimated through observations. The advantage of the HRFM model over more commonly used finite mixture (FM) models is its ability to capture spatial information by encoding it through mutual influences of neighbouring sites. In real terms, the segmentation of the MR image into a number of different tissue types involves assigning each pixel in the image a class label. The HMRF-EM algorithm starts by estimating tissue parameters and classifications based on image intensity values. This approach doesn't employ the use of a-priori maps for the initial classification of the various tissue types but instead bases the initial estimates on histogram analysis to obtain statistics such as means and variances of the distribution of pixel values. Statistical approaches are then used to label the pixels with probability values determined from the image intensity distributions. Both Maximum *a posteriori* (MAP) and maximum likelihood (ML) principles are examples of this type of statistical approach used to solve tissue parameter class labelling. The expectation maximization (EM) algorithm then follows with a three-step process that iteratively updates the tissue classes using Markov random Fields (MRF) Maximum *a posteriori* (MAP) approach, tissue parameters using a maximum likelihood (ML) approach and bias field estimation using a MAP approach. The resulting output from the algorithm is a segmented image corrected for bias field inhomogeneities. This segmentation approach assumes that both skull and scalp tissue have been removed from the MR image prior to segmentation as we are not concerned with these parts of the head and are only interested in segmenting into three distinct tissue types, grey, white and CSF.

Post Segmented Image Smoothing for Statistical Group comparisons

Both VBM and FSL employ a final smoothing step to facilitate statistical group comparisons. This involves convolving the segmented images with a Gaussian smoothing kernel to make the final images more normally distributed and hence obey the random Gaussian field theory. This smoothing usually comes in the form of a blurring filter whose spatial effect is determined by the size (in millimetres) of Gaussian filter at the full width value at half maximum height of the kernel. Careful consideration of the filter size employed is necessary to ensure that the scale of the localised changes match the extent of the blur. Thus, if the research hypothesis suggests possible changes in small anatomical structures, a suitably small smoothing filter must be used to reduce the possibility of these small scale morphologies being diluted over a large spatial extent and hence rendering them undetectable. The size of the smoothing kernel can introduce a considerable source of variability into the results (Jones et al., 2005). Unfortunately there is no hard and fast rule for calculating the size of the smoothing kernel and the researcher much develop a good sense of what may be suitable for a particular investigation and sometimes may even consider the possibility of repeating the final stages of the analysis incorporating a variety of blurring filters to assess which ones yield the most meaningful results in relation to the hypothesis being explored.

1.4 Topics addressed in this thesis

This thesis presents an investigation of the methodological considerations in structural MR image analysis and how carefully selected analysis strategies must be used to facilitate a clearer understanding of brain structure and investigate interactions between neuroanatomy and brain functions during the performance of cognitive tasks. In particular the focus is directed towards the methodological complexity of structural volumetric image analysis techniques, in an attempt to clarify and hence minimise some of the possible confounding effects frequently encountered. Armed with a clearer view of the dynamics of voxelwise structural image analysis and the application of such sophisticated structural analysis strategies, it is hoped that the complex mechanisms and interactions between functional activity, performance measures and structural morphologies may become more apparent. Such inter-modal comparison can only be attempted through the application of an equally sophisticated analysis technique for event-related fMRI that possesses the flexibility to accommodate both intra and inter-subject related variability and thus yield robust and reliable measures of functional activation in response to an external visual stimulus. Hence the initial focus of this thesis establishes a novel approach for event–related fMRI analysis to be utilized at a later stage of this thesis to facilitate comparisons of multi-modal analysis techniques. More specifically, the aim of Chapter 2 is to assess the ability of a nonlinear modelling technique to model and subsequently cope with inherent sources of variability known to exist in fMRI. Event-related fMRI is a very flexible and powerful analytical tool that offers the researcher an indirect mechanism of capturing task-related neuronal activity. Extensive evidence exists demonstrating the extent and variability associated with haemodynamic properties throughout the brain and one must ensure that

where possible, this variability is either removed or accommodated by the analysis technique employed to ensure accurate and meaningful comparisons between various populations of interest can be made. Chapter 2 presents a study that demonstrates a novel non-linear analysis technique that is flexible and can accommodate inherent sources of variability associated with the haemodynamic properties of blood flow. This chapter aimed to explicitly measure and quantify the variability of the BOLD response to a GO/NOGO cognitive task by quantifying the modelling parameters of the gamma variate function (known to successfully model the haemodynamic response) across the whole brain and hence determine if the model is suitably flexible to accommodate inter and intra subject variability in the BOLD response. The suitability and adaptability of this non-linear modelling technique to various applications in event-related fMRI such as pharmacological and emotional studies is shown and a detailed investigation (featuring 58 subjects) of the techniques ability to cope with both inter and intra-subject differences in the observed haemodynamic response function (HRF) while performing an even-related cognitive task is shown. It was determined that the nonlinear modelling technique was a suitably sensitive mechanism to capture the intra and inter subject variability of the BOLD signal. Hence, with the identification of a suitably sophisticated fMRI analysis technique, the focus shifts to methodological concerns in structural image analysis applied to various clinical and control samples and finally culminates in an investigation into the interrelations of both structural and functional measures incorporating both the nonlinear modelling technique for fMRI and the methodological considerations for structural MR image analysis.

The sensitivity of Voxel-based morphometry (VBM) to detect whole brain localized regions of volumetric change has lead to the prolific use of the technique in recent times.

Chapter 3 presents a study that focuses on a voxelwise volumetric VBM comparison featuring three separate drug using samples (cocaine, cannabis and nicotine) and a matched control sample. Drug-associated volumetric changes in the brain have been reported in the literature and Chapter 3 specifically aims to demonstrate the sensitivity of the technique to detect drug specific localized regions of effect while also trying to assess common regions of effect that may be involved in generic addictive processes across all drug using groups. The results clearly demonstrate the ability of VBM to identify the variability in drug-specific localized grey and white matter regions of volumetric change and offer further support of structural brain changes related to drug use and identifies volumetric changes that are shared and/or unique to different drugs.

The reliability of fully automated analyses techniques to accurately quantify volumes and localise areas of volumetric change is a major source of concern. Chapter 4 introduces a study featuring a clinical population of epilepsy patients and matched controls where the aim was to access the accuracy of whole brain volumetric measures output by the various fully automated analysis techniques (VBM and FSL analysis techniques) compared to those of a 'gold standard' volumetric quantitative analysis technique, namely Stereology. All data were provided by the Department of Neurophysics, Beaumont Hospital, Dublin, and subsequent stereological measures were performed by Ms Lisa Ronan, member of the Neurophysics team and expert in quantitative Stereological techniques. Detailed methodological variations featuring VBM, FSL FAST and FSL SIENAX were performed and systematically compared to Stereological measures. Volumetric results indicted that both fully automated techniques provided significantly greater grey matter volumes and significantly smaller white matter volume measurements compared to those of Stereology

demonstrating a methodological bias toward grey matter associated with the automated techniques. These findings stress the necessity for 'gold standard' quantitative measures and highlight the importance of such measures for clinical purposes such as surgical planning and quantitative volume measures of tumour size in oncology treatment assessment, as the automated measures routinely provide biased volumetric measures of grey and white matter for whole brain measures. Hence careful consideration of the use of quantitative volumetric measures from fully automated techniques is necessary when investigating quantitative whole brain volumetric variations and associated functional activations. Furthermore, a detailed comparison of localized regions of volumetric changes identified by the various fully automated techniques revealed that considerable variations identified regions existed for these data specific to the analysis technique employed. These results may be specific to some artefact within the dataset employed and a further investigation is needed to clarify these results as such variation could have considerable impact in the validity of these automated techniques.

Having gained an insight into some of the fundamental mechanisms and complexities of both structural and fMRI analyses, Chapter 5 introduces a study that specifically focuses on the correlates of brain volumetrics with fMRI activation measures and behavioural performance scores in a control sample. A combined dataset consisting of 41 participants that featured in a larger previously published event-related fMRI study(Murphy and Garavan, 2004a), the data also used in the study reported in Chapter 2 of this body of work, was conducted to explore whether brain structure and volume correlates with functional activations and cognitive performance measures. Hence this study investigates the interaction and correlations of structural brain volumetrics in regions found to show task-

specific localized areas of increased functional activity (determined by fMRI). Behavioural performance scores relating to the stimulus presentation of a GO/NOGO inhibition task were recorded to further explore possible interactions between performance and the structural and fMRI activation measures obtained by the analyses. Thus, this chapter attempts to merge fMRI, Volumetric and behavioural analyses and explore if and how these independent measures correlate. In contrast to the results in Chapter 3 investigating drug related volumetric changes, possible volumetric variations were examined in specific functionally defined regions. Thus the analysis strategy employed in Chapter 5 differs from Chapter 3. Here the focus of investigation changed from the exploration of drug induced whole brain structural changes to a more subtle volumetric examination confined to brain regions based on the pattern of functional activations in response to the GO/NOGO cognitive task. Hence the influence of possible structural differences and their relationship to functional and cognitive measures in specific brain regions became the focus. The results show that effects of sex on both structural grey matter volumetrics and fMRI activation measures must be carefully considered as gender specific local regions of effect are present in the results of both analyses techniques. These results appear to demonstrate that functional activation measures are predominately unaffected or determined by the specific grey matter volume in the localised regions of increased functional activity. Only two regions (right inferior frontal lobe and right middle frontal gyrus) of the 17 regions examined demonstrated a significant difference in grey matter volume and associated activation measure. The lack of structure-performance relations remains unclear as no difference in performance scores were found even though gender specific volume differences were identified predominantly in parietal and frontal regions. The complexity of

such structure-performance correlates is further demonstrated by split-group comparisons based on top and bottom performance scores. These finding appear to suggest an apparent advantage of greater grey matter volumes being associated with top performance scores in male participants. Further research to probe the interactive mechanisms of structure, functional activations and performance scores featuring a larger heterogeneous sample is needed to gain a clearer understanding of the exact mechanism of these measures.

Chapter 2

A Flexible Nonlinear Modelling Technique for Functional MRI data analysis

Abstract

Analysis techniques used for event-related functional magnetic resonance imaging must be sufficiently sensitive to accommodate inter- and intra-individual differences in the observed haemodynamic response function (HRF). Frequently, analyses test for a goodness-of-fit between the observed data and a predetermined HRF, which may lead to false negatives for brain regions that are responsive to a task but that deviate in haemodynamic properties from the predetermined response. We describe an analysis technique that combines standard deconvolution and model-fitting approaches to determine a best-fitting HRF on a voxelwise basis. Quantitative descriptors of each voxel's HRF are calculated as are measures that can be usefully employed for group activation analyses. The technique is shown to reveal the variability in haemodynamic responses in a dataset of 58 subjects performing an event-related cognitive task. The analytic technique is general and examples are provided of it being adapted to include a wide range of modelling parameters including relatively slow responses such as those found in emotional or pharmacological studies.

2.1 INTRODUCTION

Functional MRI is a non-invasive imaging technique that has become an important tool in the study of human neurobiological processes. The technique does not require the use of an intravenous contrast agent but, instead, typically uses an echo planar imaging sequence that monitors dynamic changes of several blood parameters including oxygen level, blood volume and blood flow (Ogawa et al., 1990). The contrast mechanism known as BOLD (Blood Oxygen Level Dependent) is understood to provide an indirect measure of neuronal activity by measuring changes in relative levels of deoxyhaemaglobin resulting from metabolic changes due to activity at a particular brain location (Bandettini et al., 1992; Kwong et al., 1992; Ogawa et al., 1990).

The resultant signal acquisition yields a time-series dataset at each spatial location on the order of 10^5 voxels for full brain imaging. In general, two main categories of fMRI experimental design are used: block design and event-related, although mixed model designs featuring aspects of both block and event related designs are also used (Mechelli et al., 2003; Wenger et al., 2004). Both methods require the use of an external stimulus (the input signal) that is presented to the subject and generates neuronal activity when reacted to by cognitive, motor or sensory processes. Block designs typically use stimuli of the same type presented in blocks that are interspersed with periods of rest or a control condition. The regressor for the alternating stimulus and rest periods is usually modelled as a square wave function, often convolved with a standard haemodynamic response function (HRF) so as to accommodate the haemodynamic filter. Alternatively, event-related designs present

individual trials, the analysis of which typically involves convolving the event stimulus train with a standard HRF to produce a regressor. For both block and event-related designs the time-series data are then compared to the regressor with amplitude-of-fit and goodness-of-fit between the two being possible activation measures.

The use of a standard HRF, particularly in event-related designs, may present certain analytical compromises as such a standard implicitly assumes that the haemodynamic response is sufficiently similar between brain regions within a subject and between subjects. However, recent empirical evidence demonstrates that haemodynamic variations do exist and these differences can impact statistical analyses (Handwerker et al., 2004; Neumann et al., 2003). For example, anatomical differences such as vascular diameters can lead to variations in BOLD response where longer delays in onset are partly attributed to larger vessels (Lee et al., 1995); the inclusion of temporal derivatives is frequently used to account for such delays. Despite this variability, existing techniques often use a standard HRF for all subjects and all brain regions or calculate a HRF from one brain region of a subject (e.g., visual cortex) that is then used for all regions of that subject (Aguirre et al., 1998). Ideally, what is needed is a method for event-related analyses that tests for haemodynamic responses but without making assumptions about the uniformity of that response within- and between-subjects.

This paper is divided into two major sections. In the first we provide some brief examples of the application of a nonlinear modelling technique to studies of pharmacological and emotional responses as well as an example examining the *post-undershoot* of the HRF. In

the second section we provide a more complete example of the analysis of an event-related study demonstrating the flexibility of the technique by employing a data set of fifty-eight subjects performing an event-related GO/NOGO task. All examples use the same basic analysis strategy. All voxels are fit to a model that is non-linear in some of its parameters using the simplex algorithm (Nelder and Mead, 1965). In order to eliminate the possibility of a divergent fit, we mandate that each parameter be limited to a user-specified bounded range. A large number of random sets of starting parameters (1000 in all examples) are chosen at each voxel; a smaller set of those that fit best (10 in these examples) undergo the full nonlinear simplex algorithm fit to find the global minimum. Optimal values for model parameters, derived parameters such as time-to-peak and an F-value (comparing the fit to the model to a fit to a reduced model such as a straight line) are returned.

2.1.1. Examples of the nonlinear technique

2.1.1.1 Modeling Pharmacokinetics

For this example, subjects were given a one-minute intravenous injection of nicotine after a four minute baseline period, with a total scan time of 20 minutes. The model chosen for the nonlinear regression was the difference of two exponentials, one representing absorption of the drug, the other its clearance. This model has been shown to effectively model the pharmacokinetics of the plasma concentration of a drug (Evans, 1992), and it is hypothesized that it is also a good model of pharmacologically-induced neuronal activity (Bloom et al., 1999; Stein, 1999). The NL modelling algorithm frees one from the *a priori* assumptions that the rate constants are homogeneous or are identical to those of the plasma

concentration. It also allows one to see which parameters are critical in a drug challenge. The full model used in this example was:

$$y(t) = a + mt + k\left(e^{-\alpha_1 (t-t_0)} - e^{-\alpha_2 (t-t_0)}\right)u(t-t_0) \quad \text{...Equation 2.1}$$

Here a is a constant offset, m is the slope of any linear trend, α_1 and α_2 are the rate constants for elimination and absorption respectively, k is an overall scale of response, t_0 is the onset time and u is the Heavyside unit step function such that

$$u(x) = \begin{cases} 1 \; for \; x \geq 0 \\ 0 \; for \; x < 0 \end{cases}$$

This function constrains the signal onset to occur in a specified range of time after the injection. The parameter ranges used were: $-500 < a < 500$, $-10 < m < 10$, $-1000 < k < 1000$, $27 < t_0 < 40$ (in units of TR, where TR was 6000 msec), $0.0035 < \alpha_1 < 0.0231$ (corresponding to a half life of elimination of 3 to 20 min.), and $0.04621 < \alpha_2 < 0.2773$ (corresponding to a half life of absorption of 15 to 90 sec.) Figure 2.1 shows example time courses, along with their location in the brain, and their associated F-values indicating statistical significance of model fit. The lower two voxels in the figure would not be considered active, since the full model did not explain significantly more variance than the reduced model, leading to the relatively low F-values. Conversely, the upper two voxels fit the model very well, leading to high F-values and the consideration that they have been "activated" by the pharmacological challenge.

FIGURE 2.1

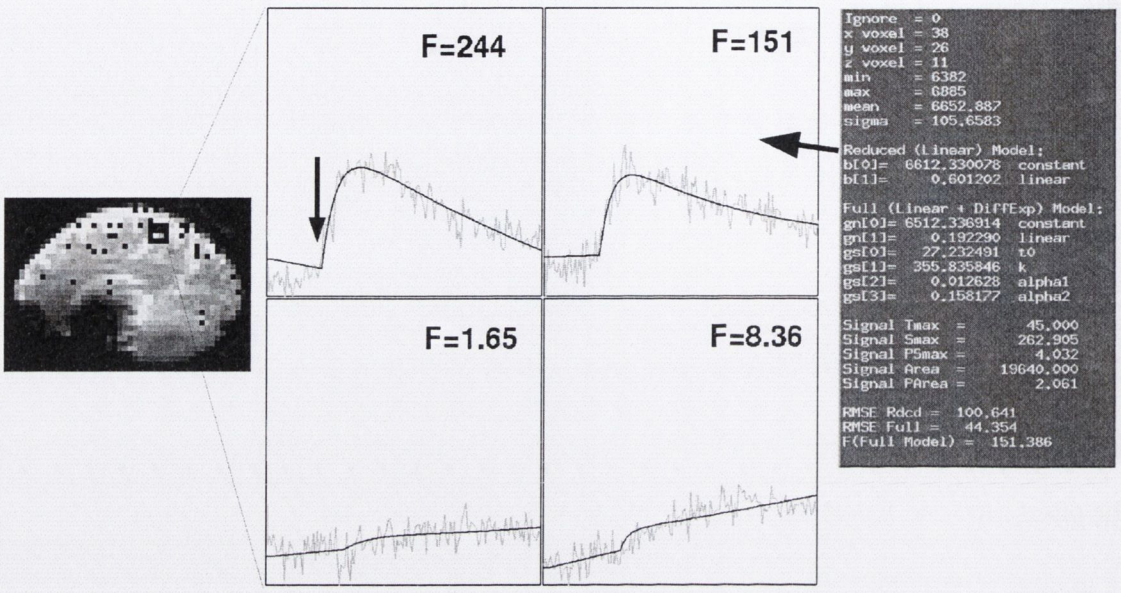


Figure 2.1: Four adjacent voxel time series from a subject showing example nonlinear fits using the difference of exponentials model following an acute injection of nicotine. The associated F-values, indicating goodness-of-fit for each voxel, are also given. The lighter lines are the actual BOLD EPI data, the darker lines the model fit. The arrow indicates the time of the injection. The figure on the left is an echo-planar anatomy with significant voxels, as measured with the F-test, coloured black. The box indicates the location of the four voxels. On the right side of the figure is the diagnostic output for the upper right-hand voxel, which indicates, from top to bottom, information about the voxel, optimal parameters for the reduced model (a straight line), optimal values for the full model (see Equation 3), derived parameters based on the best-fitting full model (time to peak, maximum amplitude, maximum amplitude expressed as a percentage of the baseline, area under the curve

[AUC], AUC expressed as a percentage of the area under the baseline) and the errors of the fits and the associated F statistic.

2.1.1.2 *Modelling Emotional Processes*

There are instances where a researcher does not have an *à priori* hypothesis as to the exact shape of the resultant fMRI time courses. For these situations, a data-driven approach such as Independent Components Analysis (ICA) may prove useful (McKeown et al., 1998). However, even these techniques require some knowledge of either the expected response (to select the interesting temporal components) or the expected activated regions (to select the interesting spatial maps). Furthermore, an interesting component does not provide quantitative information about the response. Finally, there is no consensus in the literature on how to use these techniques at a group level to make group inferences (Calhoun et al., 2001; Schmithorst and Holland, 2004).

Often, the *a priori* hypothesis is as simple as the expectation of a single-phasic response for each stimulus. Such is the case for this example data set. Experienced cocaine users watched a four-minute long film, consisting of two males smoking what appeared to be crack cocaine, designed to elicit cue-induced cocaine-craving. The film was preceded by a three-minute baseline period during which the subjects saw only a blank blue screen and were instructed to relax. We expected that the film would cause a BOLD response that would be dependent upon the individual subject's emotional response to the film. This type of response is empirically well modelled by the beta variate function described as:

$$y(t) = a + mt + k\left(\left(\frac{t-t_0}{t_f-t_0}\right)^{\alpha-1}\left(1-\left(\frac{t-t_0}{t_f-t_0}\right)\right)^{\beta-1}\right)u(t-t_0)\,u(t_f-t) \quad \text{..Eq 2.2}$$

Here, α and β characterize the shape of the curve, and t_f is the time the curve returns to baseline. All other parameters have the same meaning as in the previous examples. This model was chosen for its ability to represent a variety of response types. As can be seen in Figure 2.2, varying the relationship between the parameters changes the curve from sharply rising/slowly falling to slowly rising/sharply falling, or somewhere in between. Varying the size of α and β changes the width of the response. Additionally, manipulation of the t_f parameter has the effect of "stretching" the curve in the time dimension, even past the acquisition window such that the curve never returns to baseline. For this particular example, the parameter ranges were: $-1000 < a < 1000$, $-1 < m < 1$, $-5000 < k < 5000$, $27 < t_0 < 42$ (TRs, where TR was 6000 msec; corresponding to the onset of the film until 90 seconds thereafter), $73 < t_f < 250$ (film offset until 17.5 minutes thereafter), $0 < \alpha < 10$ and $0 < \beta < 10$, with a voxel and its best fit shown in Figure 2.3. Note that by allowing t_f to extend beyond the end of the film, we permit the possibility of the emotional response to continuously increase during the duration of the film.

FIGURE 2.2

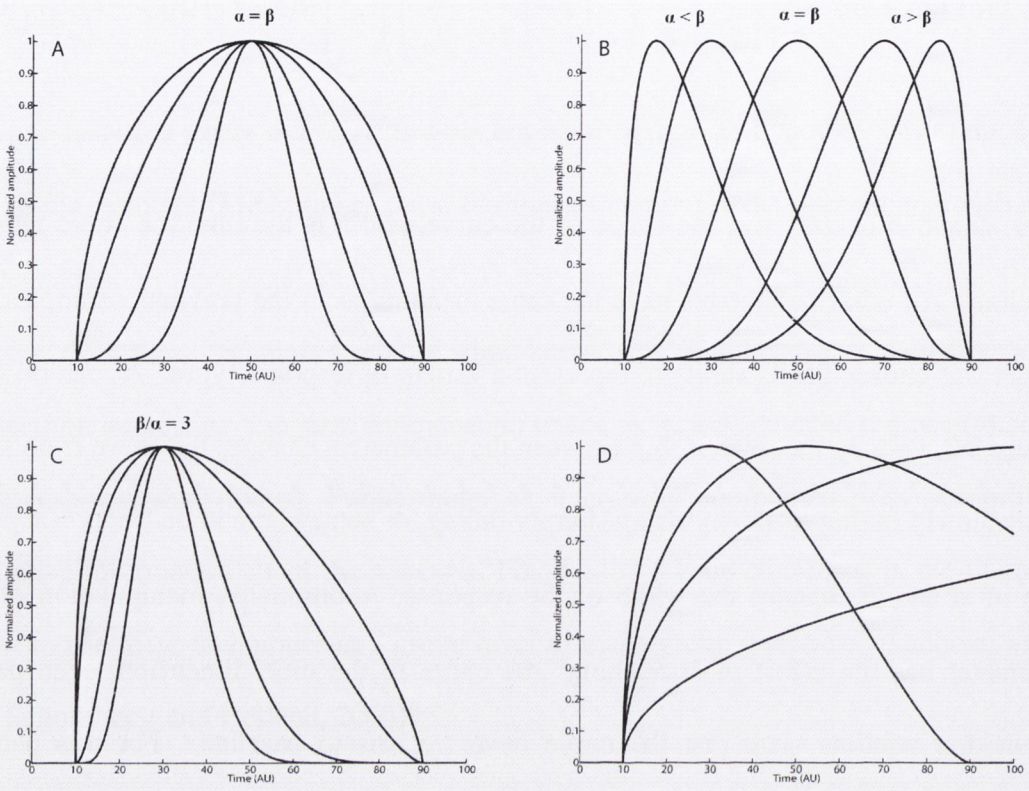


Figure 2.2: Examples of the beta function for various parameter ranges. See Equation 2.4 for the definition of the function. A) A family of curves where $\alpha=\beta$, for several values of α, changing the width of the curve. B) A family of curves varying the ratio of α and β ($\alpha<\beta$ rising early and $\alpha>\beta$ rising late). C) A family of curves for a constant ratio of $\beta/\alpha=3$, varying each. D) Varying the t_f parameter, in this case for a constant ratio of α and β, stretches or compress the curve in the time dimension; setting t_f greater than the number of images modifies the curve such that it never returns to baseline.

FIGURE 2.3

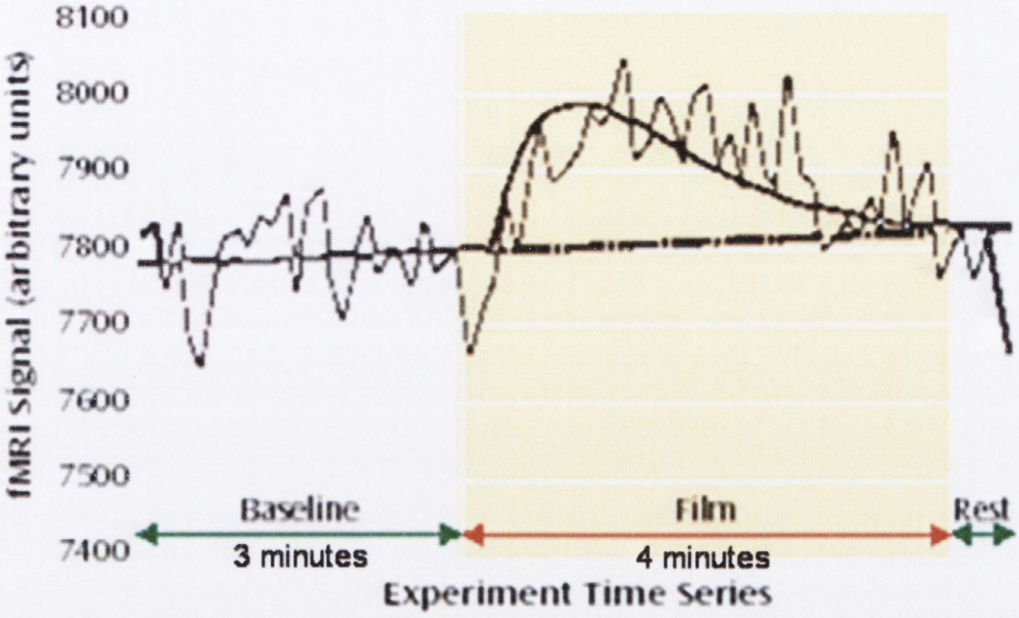


Figure 2.3: Time course of fMRI signals for a responsive brain voxel in an experienced cocaine user during exposure to a film scene of cocaine use. The jagged line represents the time course of fMRI signals from a voxel that showed increased activation. The time series, which was first filtered to remove frequencies greater than 0.01Hz, was modified with a beta function (shown by the continuous smooth line) that was constrained to depart from baseline only during the first 90 seconds of film. The time series before this departure point was fitted with a linear trend. The percentage of area under the curve measure was calculated by continuing the linear portion of the fit (the dashed line), calculating the area between the dashed line and the beta fit, and expressing as a percentage of the total area under the flat line (linear portion of the fit and the dashed line).

2.1.1.3 *Application of non-linear regression to event-related fMRI*

The gamma variate function (Equation 2.3) has been shown to effectively model the haemodynamic response in the human visual cortex (Cohen, 1997).

$$\gamma = k(t - t_0)^r e^{-(t-t_0)/b} \quad \text{.....Equation 2.3}$$

Parameters k, r, b and t_0 are variables: k is the scaling factor that describes the amplitude of the curve, r characterizes the rise time of the curve, b characterizes the decay and t_0 represents the time to onset of the curve (Ward et al., 1998).

An estimation of the HRF for each individual voxel is calculated using a deconvolution technique. This technique employs a multiple regression analysis to obtain the signal contribution to the overall time series data resulting from each individual event type. Using multiple regression techniques, this procedure calculates the IRF that follows each event. To achieve this, a regressor that specifies where each event occurs is first defined. This regressor is then time-shifted by 1 TR to create a new regressor that specifies events 1 TR later. This is repeated up to 8 TRs (i.e., 16 seconds). The deconvolution procedure then calculates a scaling value for each regressor using a least-squares multiple regression algorithm and these scalar values define the HRF for each voxel. The deconvolution procedure also calculates intercept and slope parameters for a baseline regressor, which can be used to calculate a baseline (i.e., the ongoing mean activity level after excluding the variance due to the events) for the HRF. The parameters of the fit are converted into an activation measure for the purposes of group comparison. For example, the estimated HRF for each voxel can be converted into a percentage area under the curve score (%AUC) by

expressing the area under the haemodynamic curve and above the horizontal baseline divided by the area under the baseline (Figure 2.4). The %AUC scores are signed so as to accommodate negative-going responses and can then be used as descriptive voxelwise statistics for determining group activation maps.

FIGURE 2.4

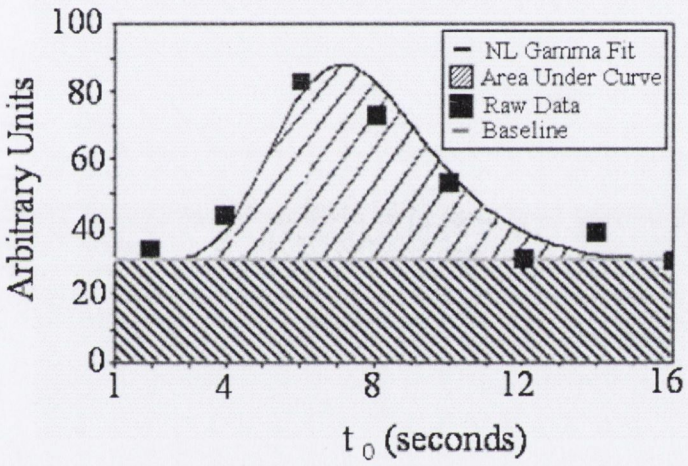


Figure 2.4: Composite diagram showing the raw data IRF points as black squares, the gamma-variate function fitted to these data and the area under the fitted curve. The area-under-the-curve can be expressed as a percentage of the baseline area and can be used as an activation measure.

An advantage of the proposed methodology is that it is easily extended. For example, in event-related designs, the current model might be altered by addition of another term such

as a second gamma variate term thus rewriting the gamma-variate model of the HRF to include a post-undershoot as:

$$h(t;a,k_1,k_2,r_1,r_2,b)=a+k_1\left[\left(\frac{t-t_0}{r_1 b}\right)^{r_1} e^{-\left(\frac{(t-t_0)}{b}-r_1\right)}-k_2\left(\frac{t-t_o}{r_2 b}\right)^{r_2} e^{-\left(\frac{(t-t_0)}{b}-r_2\right)}\right] \quad \text{Eq. 2.4}$$

This model contains 2 gamma-variate functions with the same exponential damping factor (in principle different damping factors could be used for each), both normalized (although the second scaled by k_2, such that $0<k_2<1$) and h_i peaking at $r_i b$. In SPM, h (t;1,1/6,4,15,1) and its temporal derivative are often used as basis functions in event-related designs.

Data from a high-temporal resolution (TR=300ms, brief visual stimulation every 15s, epochs averaged before nonlinear regression) event-related experiment were fit twice to the above model, once to the full model, and once with $k_2 = 0$ (also fixing the now-meaningless b_2 to free up a second degree of freedom) to remove the post undershoot. The parameter ranges for the full model were: $-10 \leq a \leq 10$, $-30 \leq k_1 \leq 30$, $0 \leq k_2 \leq 0.6$, $1 \leq r_1 \leq 10$, $10 \leq r_2 \leq 20$ and $0.2 \leq b \leq 2$. An F-test was performed to see if the addition of the post-undershoot was significant. Figure 2.5 shows 9 voxels from the visual cortex and their best-fitting curves. For most of the data shown, improved fits were obtained by including a post-undershoot term. Over the set of voxels in visual cortex that were significant at $p<0.001$ in a linear regression, 44% were significantly improved (at $p<0.05$) by including the extra

term. Note that this is meant to be an example of the power and flexibility of the proposed technique and not a thorough systematic study of the post-undershoot. Further note that in this example the extremely short TR permitted the use of many parameters in the model. In a typical full-brain study, using 6 parameters likely over-specifies a model of the HRF.

FIGURE 2.5

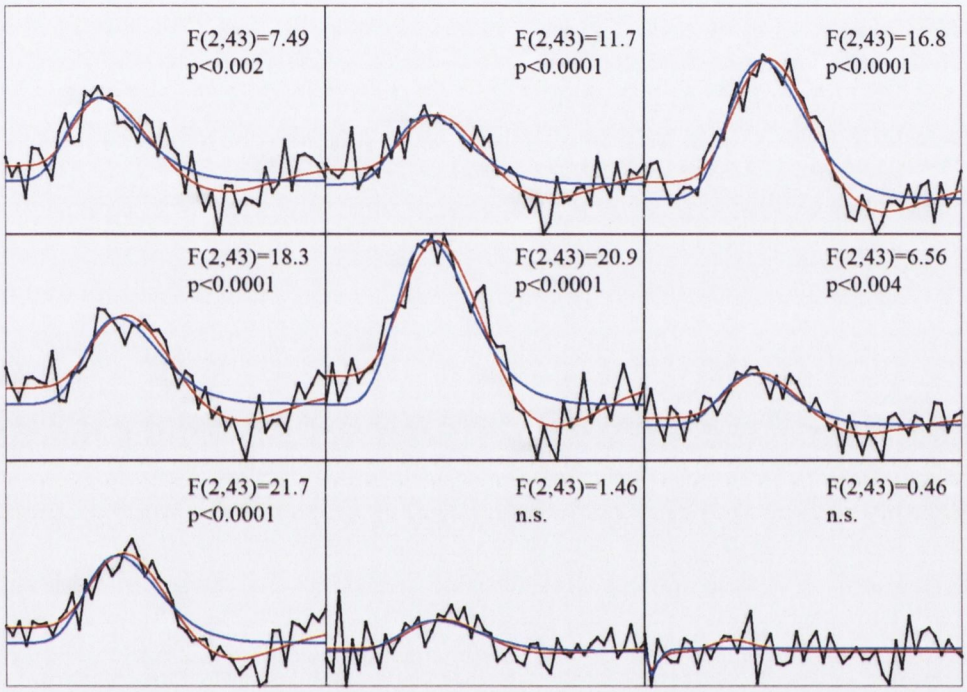


Figure 2.5: Timecourses from a block of 9 individual voxels in visual cortex showing average haemodynamic responses (HRF) following brief visual stimulation. Variability of the HRF in each independent voxel is apparent in the shape and amplitude where the time periods are consistent in each of the voxels. The black lines are the average HRF for that voxel, the blue (red) curves are the best fit to the data using a gamma variate model without (with) a post-undershoot term. F-values indicate the improvement of the fit by including the extra parameters.

An application of nonlinear regression to an event-related study now follows.

2.2 METHODS

2.2.1. *Subjects and Experimental Task Design*

Fifty-eight right-handed subjects (35 female, mean age: 30, range: 18-46) completed a GO/NOGO task after providing written informed consent. The GO/NOGO task required frequent responses and occasional response inhibitions. A serial stream of letters consisting of X and Y were presented to the subjects in an alternating pattern that required a response for each letter and an inhibition of response upon the observation of a break in the alternation pattern. For example, the subject would respond to all stimuli except the fifth in the following sequence XYXYYX. Minor variations of the task were presented to four different groups. Fourteen subjects (six female, mean age: 30, range 19-44) completed the task in which additional letters were interspersed between the X and Y letters with all letters presented serially at a frequency of 2 Hz with 0s interstimulus interval (Garavan et al., 1999). A response inhibition was required, on average, every 20s with GO trials occurring, on average, every 3.5s. Another fourteen subjects (10 female, mean age: 31, range: 19-45) completed an experiment in which only the target letters, X and Y, were presented at 1Hz (Garavan et al., 2002). Fifteen subjects (9 female, mean age: 29, range: 18-46) completed the task in which the stimulus duration was 900ms followed by a 100ms blank (Garavan et al., 2003). The final variation, completed by fifteen subjects (10 female, mean age: 30, range 23-40), introduced a visual cue to this task, 2-7s before half of the NOGO events (Hester et al., 2004b), but the present analysis only included the uncued

NOGO events. Previous analyses have shown that activation differences between the groups were no greater than that expected given the sizes of the group samples (Murphy and Garavan, 2004a)

2.2.2. MRI Scanning Parameters

Scanning for three of the studies (Garavan et al., 1999, 2002, 2003) was conducted using contiguous 7mm sagittal slices covering the entire brain from a 1.5T GE Signa scanner using a blipped gradient-echo, echo-planar pulse sequence (TE = 40 ms; TR = 2000 ms: FOV =24 cm; 64 x 64 matrix; 3.75 x 3.75 mm in plane resolution). High resolution spoiled GRASS anatomic images (TR = 24 ms, TE = 5 ms, flip angle = 45°, FOV = 24 cm, thickness = 1.0 mm with no gap, matrix size = 256 x 256 x 124) were acquired before functional imaging. Scanning for the fourth study (Hester et al., 2004b) was conducted on a 1.5-T Siemens VISION scanner. Contiguous 5 mm sagittal slices covering the entire brain were collected using a single-shot, T2* weighted echo planar imaging sequence (TE = 50 ms; TR = 2000 ms; FOV 256 mm, 64 x 64 mm matrix; 4 x 4 mm in plane resolution). High-resolution T1-weighted structural MPRAGE images (FOV = 256 mm isotropic 1 mm voxels) were acquired following functional imaging.

2.2.3. Image Preprocessing

All data processing was performed using the AFNI software package (Cox, 1996) *http://afni.nimh.nih.gov*. First, the time-series data were shifted using sinc interpolation to align the slices to a common temporal origin. Each 3D volume corresponding to a particular time point was then volume registered to a chosen "base" image, acquired at the

midpoint of the time series, to correct movement artefacts. This process was performed by the application of a Fourier interpolation algorithm to align the voxels. Voxels lying outside the brain were then removed by an edge detection routine.

An estimation of the HRF for each individual voxel was calculated using the deconvolution technique described above. The best fitting haemodynamic shape based on the gamma variate function (Equation 2.3) was determined for each voxel for the event type of interest (the STOP and ERROR HRFs in this case) using a non-linear regression algorithm (Ward et al., 1998). Parameters k, r, b_0, and t_0 were free to vary over a range in order to capture and describe the varying HRFs. The parameter ranges used were: $-1000 < k < 1000$, $0 < t_0 < 2$, $8.0 < r < 9.0$, $0 < b < 0.5$ where both t_0 and b are in TR units (1 TR = 2 seconds). These parameter ranges were shown to accommodate the optimal parameter values of r = 8.6 and b =0.547 as suggested from modelling the HRF of the human visual cortex, (Cohen, 1997).

A correct inhibition (STOP) regressor and a commission error (ERROR) regressor were included but further analyses were limited to STOP activations. The inclusion of an ERROR regressor, which removes variance associated with error events, leads to a more accurate STOP activation map (Murphy and Garavan, 2004b). The estimated HRF for each voxel was converted into a signed percentage area under the curve score (%AUC) to determine activation maps.

2.2.4. Group Analyses

In the present GO/NOGO data, one-sample t-tests against the null hypothesis of no activation changes were conducted for the successful inhibition events. The %AUC maps were resampled to the higher resolution of 1µl and then converted to the standard

stereotactic coordinate system of Talairach and Tournoux (Talairach and Tournoux, 1988) and spatially smoothed using a Gaussian kernel with 3 mm r.m.s. isotropic deviation. Significantly active areas were required to pass a voxelwise statistical threshold of $p \leq 0.00001$ and to be part of a larger cluster of 31 µl significant, contiguous voxels ($p \leq 0.05$ corrected). Twenty activated regions were identified. In order to ensure that cluster sizes did not bias the analyses of haemodynamic properties, the clusters were constrained to have the same size. This was accomplished by increasing the statistical threshold for each cluster until only 100 voxels (i.e., 100 µl) remained. Average HRFs were calculated for these ROIs and the gamma variate parameters t_0, r, b and the parameter T_{max} (the time to peak of the curve; derived from the other fit parameters) were calculated for the average HRF of each ROI and the extent of the variability of each of these parameters over the data from 58 subjects was calculated.

2.3 RESULTS

Statistical comparisons were carried out using SPSS (version 12.01 for Windows) and Microsoft ^{R} Excel 2002 (10.4302.4219) SP-2. The group analysis identified 20 activated regions that included frontal, parietal, temporal and sub-cortical areas (see Table 2.1). A 'repeated measures ANOVA' found no significant differences between the 20 ROIs for any parameter. For the subsequent results, parameter estimates were collapsed across region and subject and all distributions are based on 1160 (58 subjects x 20 regions) estimates. Variability of the non-linear gamma variate parameters is represented in histogram form (Figure 2.6) for the parameters t_0, r, b, and T_{max}. Parameter t_0, ranging from 0-4 seconds

about a mean of 1.97 seconds, shows an appreciable degree of fluctuation associated with the onset of the haemodynamic response; the rectangular distribution here is notable. It could be argued that permitting t_0 to range much higher than demonstrated could result in responses being attributed to later events and not those emanating from the event of interest. This influenced our choice of range for t_0 from 0-4 seconds, which also corresponds well to empirically derived values (Buckner et al., 1996; Neumann et al., 2003). The parameter r, reflecting the rise time of the HRF, ranges from 8-9 with a mean of 8.44 while the curve's fall time parameter b ranges 0-1.0 with a mean of 0.528. These mean parameter estimates closely correspond to parameter estimates derived from the human visual cortex (Cohen, 1997). The parameter T_{max}, representing the time to peak of the HRF, ranges from 0-12 with a mean of 6.4. The relationship between the time to onset t_0 and parameters r and b were investigated and scatterplots of t_0 versus gamma variate parameters were plotted. A voxel's onset time was not highly correlated (as determined by Pearson's correlation coefficient) with either the r or b parameters ($r = .19$ and .36, respectively). It is important to note that the boundaries of these ranges are somewhat artifactual insofar as the parameter estimates were constrained within pre-specified ranges (see Methods). However, with the exception of the t_0 parameter, the pre-specified ranges would seem to have been reasonable given the observed distributions which tended to fall well within the boundaries.

FIGURE 2.6

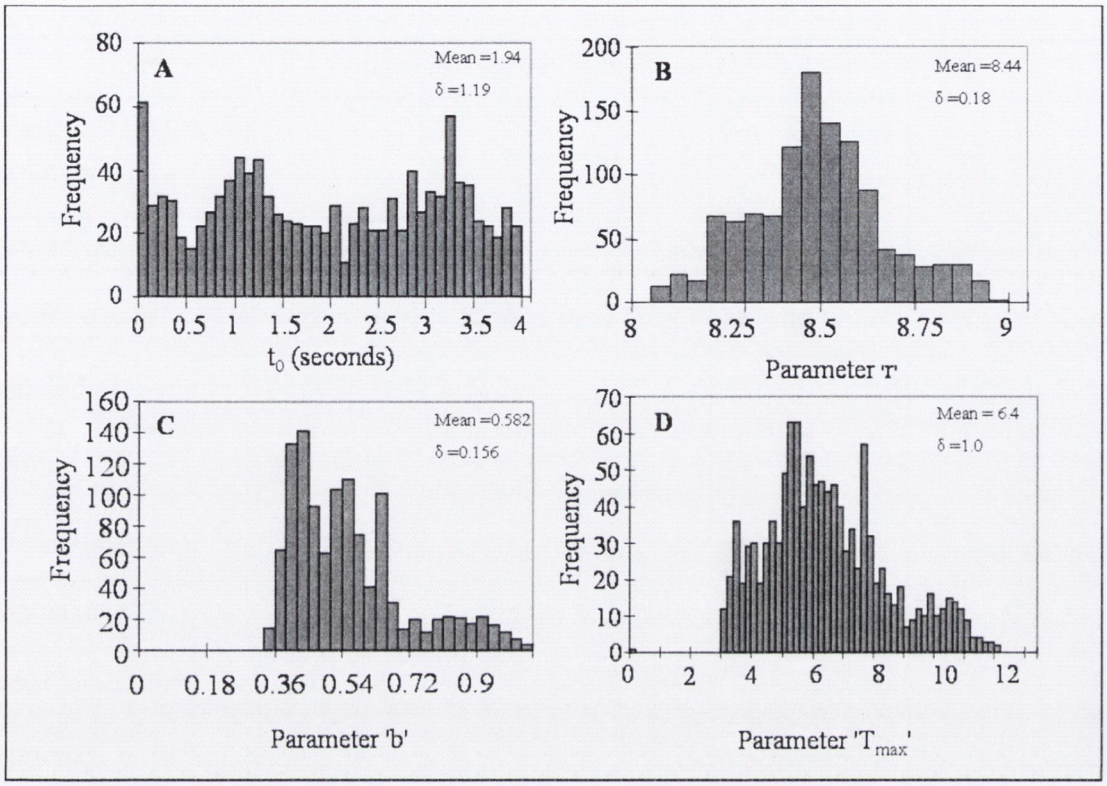


Figure 2.6: Histogram representations of the gamma variate parameters t_0, r, b, and T_{max}. Graph A shows the 'time to onset' parameter 't_0' ranging from 0-4 seconds (0-2 TR's); Graph B represents the variability of the gamma variate parameter 'r' characterizing the rate of rise of the HRF curve ranging from 8 to 9 about a mean of 8.44; Graph C represents the variability of the gamma variate parameter 'b' characterizing the decay of the curve over a range of 0-1 with a mean value of 0.528; Graph D details the variability of T_{max} from 0-6.5 about a mean value of 3.19 and a standard deviation of 1.0.

TABLE 2.1

Cluster Positions for the 100µl Map			
Lobe/Gyri	Broadman Area BA *	Brain Stucture	Talairach Coordinates X, Y, Z
Left Frontal	6	Left Precentral Gyrus	-46, 1, 35
	6	Left Middle Frontal Gyrus	-26, 10, 53
Left Parietal	40	Left Inferior Parietal Lobule	-34, 48, 37
	40	Left Inferior Parietal Lobule	-45, 41, 42
	7	Left Superior Parietal Lobule	-23, 61, 46
Left Sub-cortical	-	Left Lentiform Nucleus/Left Putamen	-23, -10, 9
Right Frontal	44	Right Precentral Gyrus	50, -10, 8
	9,44,45	Right Inferior Frontal Gyrus	47, -15, 20
	9	Right Middle Frontal Gyrus	39, -32, 26
	6	Right Precentral Gyrus	45, -1, 29
	40	Right Middle Frontal Gyrus	40, 49, 42
	6	Right Middle Frontal Gyrus	25, 6, 47
	6	Right Medial Frontal Gyrus	-0, 1, 53
Right Temporal	22	Right middle Temporal Gyrus	52, 37, 0
	37	Right middle Temporal Gyrus	51, 58, 5
	13	Right Superior Temporal Gyrus	55, 44, 18
Right Parietal	40	Right Inferior Parietal Lobule	40, 49, 42
Right Sub-cortical	4	Right Claustrum/Right Insula	30, -13, 6
	-	Right Thalamus	7, 12, 5
	--	Right Caudate	12, -0, 10

* Note: Regions assigned Broadman numbers closest to the listed brain structure where possible.

Table 2.1. Functionally-defined 100µl regions-of-interest from the GO/NOGO dataset

2.4 DISCUSSION

The present results have described the extent to which variability exists in the haemodynamic response. This survey has been facilitated by a reasonably large sample size, a cognitive task paradigm that produces significant levels of activation in a number of distinct brain regions, thus allowing the haemodynamics of many cortical areas to be assessed, and an analytic technique that provides quantitative estimates of the haemodynamic response with voxelwise resolution. The existence of variability in the HRF, although not extensive in the regions activated here, must be carefully modelled as extensive differences in shape and amplitude can introduce model fitting problems and hence underscores the importance of employing a flexible analytic approach. The GLM approach is to use a standard HRF across brain regions but this may impact on the sensitivity to detect subtle regional differences in the HRF and in so doing desensitise the model to the presence and detection of such differences. The nonlinear modelling technique based on a gamma variate function is proposed as one such technique.

2.4.1 Haemodynamic Variability

Variability in haemodynamics was most pronounced in the t_0 parameter, which measures the onset of the haemodynamic response, that is, its departure from baseline. A common practice in fMRI data analysis is to desensitise the data to temporal offsets due to activation delays or slice timing acquisitions by the addition of 1st and 2nd order temporal derivative terms to the haemodynamic model (Calhoun et al., 2004). Failure to do so can induce mismatches between the data set and the fitted haemodynamic function approximation,

which in turn may affect the statistical analysis of the data. In the present data, an interpolation preprocessing step corrected for temporal offsets produced by differences in slice acquisition timing, thus the persistent differences in onset times cannot be attributed to the data acquisition artefact.

It is likely that factors other than neuronal activity are responsible for altered HRF latency and magnitude between and within subjects. For example, intrinsic anatomical differences such as vascular diameters may underlie variations in the BOLD response whereby longer delays in onset may be partly attributed to larger vasculature (Lee et al., 1995). Changes in hemodynamic coupling, oxygen consumption or differences in, for example, the number of large vessels could also account for differences in HRF. This is a very real concern as Henson et al (2002) and Meizen et al (Miezin et al., 2000) have reported shorter latency in motor cortex HRF than in visual cortex when performing a visual response task. Vascular dynamics between brain regions has also been implicated for differences in BOLD signal rather than differences in cognitive processes (Lee et al., 1995). Since multiple types of receptors are known to exist on the cerebral vasculature [e.g. dopamine (Krimer et al., 1998) and acetylcholine (Graham et al., 2002)], it is also possible that differences in such drug use history as smoking or medications that are known to affect dopamine receptors (e.g. stimulants, neuroleptics, etc) could also act upon the vasculature independent of changes in neuronal activity.

Mismatches in onset time between a standard HRF and the observed data of as little as 1 second have been shown to impact parameter estimates and variations of 2.5 seconds

adversely impact false negative rates (Handwerker et al., 2004). Less variability was observed for the rise and fall times of the haemodynamic response. Previous estimates for the r and b parameters for the human visual cortex reported by Cohen (1997) are 8.6 and 0.547, respectively. The estimates obtained in this paper adhere closely to these values but are slightly smaller at 8.44 and 0.528, respectively. These slight differences could be due to the large sample size of 58 subjects yielding a more accurate estimation of the two parameters or that slight inter-regional differences render these somewhat smaller values better whole-brain parameter estimates. Variability in the shape of the haemodynamic response due to prolonged activations can cause errors in the estimation of the time to peak (T_{max}), which is a problem often encountered in the GLM approach of fMRI analysis and successfully countered by careful consideration of the design model. The estimates obtained for T_{max} outlined in the results yielded 3.19, 6.0 and 1.5 for the mean, maximum and minimum respectively, which match reasonably well to the estimates of 4.0, 6.5 and 2.5 reported by Handwerker et al (2004).

The present results reveal that variability in the HRF waveform between regions was not statistically significant. This result is consistent with previous findings of within-subject haemodynamic differences being smaller than between-subject differences (Aguirre et al., 1998; Handwerker et al., 2004). While this result underscores the merit of determining an individualised HRF for each subject based on event-related visual activity that is used for subsequent analyses (Aguirre et al., 1998), the (albeit non-significant) variability between regions may raise concerns that some percentage of activated voxels may nonetheless be missed (Lu et al., 2006).

2.4.2 *Non-linear regression for event-related fMRI*

Inter-voxel variability in HRFs can be accommodated by the gamma-variate modelling approach. By fitting a separate model to each voxel this approach can adjust for differences in haemodynamic shape and can provide quantitative information describing both the voxel's haemodynamic shape as well as measures that can be used for constructing activation maps such as an area-under-the-curve or signal maximum. The quantification of the HRFs can prove informative in assessing the integrity of haemodynamics in special populations such as elderly participants (Nielson et al., 2004) or clinical groups such as nicotine or cocaine users for whom vascular compromise might be suspected (Murphy et al., 2006). Activation measures such as the area-under-the-curve expressed as a signed percentage of the area-under-the-baseline (%AUC) have previously been used successfully for determining activation maps in both normal and clinical samples (Garavan et al., 1999; Hester and Garavan, 2004; Kaufman et al., 2003). The %AUC measure also has the advantage of yielding stable activation measures that asymptote after relatively few events and contain less noise than goodness-of-fit statistics: unlike goodness-of-fit statistics which tend to improve as more events are added, the %AUC measure derives an activation estimate that is relatively insensitive to the addition of random noise around the HRFs central tendency (Murphy and Garavan, 2005).

Chapter 3

Grey and white matter volume differences in cocaine, cannabis, and nicotine users compared to controls, using Voxel-based morphometry.

Abstract

Cognitive, neurophysiological and functional deficits associated with drug use have all been reported in the literature. This study used optimized voxel based morphometry to examine the possibility of drug-related brain volumetric changes in cocaine, cannabis and nicotine users when compared to a drug-naïve control group. The most extensive grey matter changes were observed in cocaine users with reductions observed in bilateral thalamus / red nucleus, left inferior semi lunar lobule, right cerebellar tonsil and left inferior parietal lobe. Parietal, occipital and temporal volume reductions were also identified in the nicotine using group. Grey matter volume reductions were identified in the left parahippocampus and left thalamus for cocaine and cannabis users while cerebellar deficits were observed for both nicotine and cocaine users. White matter morphologies (both increases and decreases) were noted for all drug using groups, with cocaine users again demonstrating the most pronounced effects. These results offer further support of structural brain changes related to drug use and identify volumetric changes that are shared and/or unique to different drugs.

3.1 INTRODUCTION

Drug use and its possible effects on brain function and structure continue to fuel public concern and, consequently, research interest (Rogers and Robbins, 2001). Various imaging techniques such as fMRI and PET have facilitated a better understanding of the biological mechanisms of substance abuse and subsequent effects on cognitive functions (Breiter et al., 1997; Volkow et al., 2002). More recently, analysis techniques such as voxel-based morphometry (VBM) have enabled the interrogation of structural images resulting in the identification of anatomical differences in the brains of those who use cocaine (Franklin et al., 2002; Matochik et al., 2003), MDMA (Cowan et al., 2003), cannabis (Matochik et al., 2005), and nicotine (Brody et al., 2004c), thus providing evidence for structural differences accompanying the neurocognitive deficits of drug users.

There is accumulating evidence for cognitive deficits and associated brain function and brain structure deficits in drug abusers. For example, a body of evidence has identified cognitive deficits in heavy cannabis users (Nester et al., 2008; Pope, 2001; Pope, 1996; Solowij N, 1997; Solowij et al., 2002b). Similarly, marijuana induced cognitive deficits for very heavy marijuana usage has been shown to persist during periods as long as 28 days after drug abstinence starts (Bolla et al., 2002). Persistent performance deficits and faulty decision making were also demonstrated in 25 day abstinent heavy marijuana users (Bolla et al., 2005) performing the Iowa Gambling Task. Thus the evidence of cognitive deficits associated with heavy marijuana use has been shown and these effects remain for periods up to 28 days of drug abstinence. Consistent with this evidence for persistent cognitive

effects, recent structural imaging studies have reported anatomical differences in the prefrontal and orbitofrontal cortex (Eldreth et al., 2004), (Bolla et al., 2005), and the hippocampus and parahippocampal regions of cannabis users (Eldreth et al., 2004; Matochik et al., 2005). The hippocampus contains very high densities of endogenous cannabinoid receptors in the human brain and is thus a likely region to show volumetric changes resulting from chronic cannabis use.

Neuropsychological and functional deficits associated with cocaine abuse have been well reported in the literature. Cognitive dysfunction has been demonstrated for inhibitory control, attention and decision-making (Bolla et al., 2003; Kaufman et al., 2003; Kubler et al., 2005; Verdejo-Garcia et al., 2005), and key brain areas previously associated with cocaine-related dysfunction include lateral prefrontal cortex (Bolla et al., 2004), anterior cingulate cortex (ACC), orbitofrontal cortex, insula (Franklin et al., 2002), and nucleus accumbens (Breiter et al., 1997). Neurobiological models of drug addiction highlight the involvement of the dopaminergic system in the reinforcement mechanism of the drug addiction process while also stressing the role of the frontal cortex in drug cravings and deficient cognitive control (Goldstein and Volkow, 2002). Several recent studies have reported volumetric changes and or tissue density / concentration decreases in many of the same brain regions implicated in the cognitive deficits associated with cocaine use (Bartzokis et al., 2000; Franklin et al., 2002; Liu et al., 1998; Matochik et al., 2003).

To date, there is relatively less evidence that nicotine affects cognition, although acting through its agonist activity in the acetylcholine system it may affect complex mental

processes such as memory and learning. Nicotine related enhancement of attention and working memory function on an 'n-back' task was demonstrated by increased BOLD activations in the prefrontal cortex, thalamus, anterior cingulate, superior frontal cortex and superior parietal cortex during task performance and cerebellum during rest (Kumari et al., 2003; Lawrence et al., 2002). A more recent volumetric study reported grey matter changes in PFC primarily in bilateral dorsolateral prefrontal cortex, but also bilaterally in the ventrolateral prefrontal cortex, left dorsal ACC and right cerebellum for smokers (Brody et al., 2004a).

The extant literature on the cognitive effects of cannabis, cocaine and nicotine and the few studies that have addressed brain volumetric changes associated with these drugs can guide predictions for the present volumetric analyses. Between these three drugs of abuse, cocaine would be expected to demonstrate the largest changes due to the evidence of its neurotoxicity (Li et al., 1999) and its cognitive sequelae. The profile of cognitive dysfunction within this group and cocaine's effects on the dopamine system leads to the prediction of volumetric changes in prefrontal cortex. The evidence of memory impairment coupled with knowledge of the distribution of the cannabinoid receptors suggest tissue morphology changes within the temporal and medial regions of cannabis users. Finally, the attention-enhancing effects of nicotine suggest that any observed brain volumetric changes may be observed in fronto-parietal areas associated with attention. In addition to these drug-specific predictions, the present study was also able to test for common effects across drugs. Common volumetric effects might result from common mechanisms of the drugs (e.g., alterations in the sites of dopaminergic activity) or could be

driven by secondary effects such as stress common across drug users. Another consideration is that any observed effects may have preceded use rather than resulted from it and any brain volumetric marker of risk dependence may be common across different drugs of abuse.

These predictions were tested using whole-brain VBM to investigate the structural changes in grey and white matter volumes of three distinct drug using groups (cannabis, cocaine and nicotine) compared to a drug naïve control group. The inclusion of three drug groups enabled us to determine if any observed volumetric effects were particular to a drug or common to all, as volumetric changes present in all three groups may reflect a general addiction process.

3.2 METHODS

3.2.1 Participants

The experimental data set consisted of seventy-two right handed subjects (29 female, mean age: 29, range: 18-46) who each provided written informed consent prior to their participation in the study. Subjects were assigned to one of four possible groups, namely controls (n=25), cocaine (n=16), nicotine (n=11) and cannabis (n=20) depending on their individual drug history.

The control group consisted of 25 participants (14 female; mean age: 25 ± 1.1; range: 18-36) and had no prior history of cocaine, cannabis or nicotine use. The Cocaine group

consisted of 16 participants (4 female; mean age 39 ± 1.6 range: 22-45) and had been using cocaine for an average of 12.5 years spending approximately $350 per week on the drug. The nicotine group consisted of 11 participants (6 female, mean age 33 ± 3.1, range: 22-46) with an average cigarette consumption of 25 cigarettes per day over an average smoking duration of 18 years (average Fagerstrom score 5.3). The cannabis group consisted of 20 participants (5 female, mean age 23 ± 1.4, range: 19-45) who had been using the drug for a period of 6.5 years on average with a typical drug use pattern of 6 days per week. The mean age for both the nicotine and cocaine groups differed significantly from controls ($p \leq 0.009$ and $p \leq 0.001$, respectively) but the cannabis group showed no significant age difference.

Within the cocaine group, nine smoked cigarettes (group averages for nicotine use of 9 years and 6 cigarettes per day) while 8 of the cannabis group smoked (group average for nicotine use of 4 years and 7 cigarettes per day). However, the nicotine usage in the nicotine group was significantly greater in both period of usage (Chi Squared = 13.71, df = 2, $p \leq 0.001$) and number of cigarettes per day (Chi Squared = 21.57, df = 2, $p \leq 0.0005$) and thus these participants were included in their primary drug use group. Each participant of the cocaine and cannabis groups was abstinent from their preferred drug of use for a 24 hour period prior to their MR scan. Nicotine users had smoked within hours of scanning thus avoiding concerns of acute withdrawal in this group.

3.2.2 MRI Scanning Parameters

Scanning was conducted using a 1.5T GE Signa scanner. High resolution spoiled GRASS anatomic images (TR = 24 ms, TE = 5 ms, flip angle = 45 °, FOV = 24 cm, thickness = 1.0 mm with no gap, matrix size = 256 x 256 x 124) were acquired for all subjects.

3.2.3 Image Preprocessing

The MR images were collected in DICOM format and were converted to the Analyze 7.5 image format via the software package MRIcro; http://people.cas.sc.edu/rorden/mricro.html and a subsequent voxel-based morphometry (VBM) image analysis was performed using the statistical parametric mapping software (SPM2; http://www.fil.ion.ucl.ac.uk/spm/). Voxel based morphometry is a voxel-wise automated analysis technique performed on high resolution structural images to investigate structural differences in local concentrations of grey and white matter and volumetric differences of the brain. The output from the VBM technique is a probability measure of a voxel being classified as grey or white tissue as determined following normalization and segmentation routines based on an *a priori* image template used for affine registration and tissue classification maps (see (Ashburner and Friston, 2000; Good et al., 2001a)) for detailed descriptions of the standard and optimized VBM methods). The output from the analysis is commonly referred to in the literature as grey/white matter concentration or tissue density and statistical analysis is performed to examine between-group differences in tissue concentrations/densities

3.2.4 Template generation

Template images for normalization of grey, white and CSF tissue classification maps were constructed from the complete data set of 72 subjects. All images were spatially normalized to the same stereotaxic space by a process of linear and non-linear transformations based on the Montreal Neurological Institute (MNI) coordinate system and registered to a template image compiled from the 152 brain average of the MNI brain. A mean normalized image was then created from the 72 normalized images and smoothed using an 8mm FWHM Gaussian smoothing kernel. All normalized images were segmented into grey matter, white matter and CSF partitions using *a priori* grey, white and CSF maps provided in the SPM software package which uses a mixture model cluster analysis for the identification of voxel intensities for tissue classification purposes. A study specific template for grey, white and CSF tissue was made from the average segmented image files and smoothed using an 8mm FWHM Gaussian kernel. The optimized VBM strategy employs a 'modulation' step to correct for partial volume effects resulting from the non-linear normalization process.

3.2.5 Statistical Analysis

All normalized and segmented images output from the optimized VBM routine were smoothed with a 4mm FWHM Gaussian kernel and converted into AFNI data files for the purpose of statistical analysis. A series of t-tests compared each drug using group to the control group. Significant voxels passed a voxelwise statistical threshold (Cocaine: $t = 3.56$, $p \leq .001$; Nicotine: $t = 3.6$, $p \leq .001$; cannabis: $t = 3.53$, $p \leq .001$) and were required to be part of a larger cluster of contiguous significant voxels. The cluster size criterion differed

between the group and tissue-type comparisons and ranged between 83 and 138 µl. The cluster size was determined through Monte Carlo simulations which, when combined with the voxelwise statistical criterion, resulted in a 5% probability (corrected) of a cluster surviving due to chance.

Next, the clusters from each control / drug group pairing were subjected to an ANCOVA with age as a covariate. Sex differences for each control /drug group pairing were accommodated by a further set of ANCOVA's (with age as the covariate) in which each control / drug group pairing was matched for sex by randomly selecting equal numbers of males and females from each group while ensuring no significant differences between the original age demographic profile based on the entire data set and that of the smaller sex matched sample occurred. This resulted in a reduced sample of four females and five males in each group (the minimum number of each sex across all four groups).

The grey matter volumetric maps of significant differences between the controls and each of the drug-using groups were next combined. That is, the combined map included the voxels of volumetric differences indicated as significant from any one of the initial *t*-test maps. The clusters of this combined map were subjected to an ANCOVA (with age as a covariate) that included all four groups so as to determine if regions shown to be different between one drug group and controls were specific to that control/drug group comparison or differed between the drug groups. Sex differences between the groups were accommodated by a second four group ANCOVA (with age as the covariate) in which the groups were reduced, as before, to four females and five males. Bonferroni corrected *post-hoc* pairwise comparisons across all groups were conducted. Finally, all analysis procedures were then repeated for the white matter volumetric maps.

3.3 RESULTS

3.3.1 Grey Matter Comparisons

Grey matter t-tests and ANCOVA results are presented in Table 3.1. The initial t-tests revealed 23 regions with significant grey matter volume differences between controls and the cocaine group compared to three between controls and the nicotine group and one between the controls and the cannabis group, (see Figure 3.0 & Table 3.1).

Table 3.1

Grey Matter Analysis

Voxelwise *t*-test Cluster Report for Cocaine vs. Control Group Comparison					**Cocaine** group **ANCOVA** comparissons with age as covariate (***P*** value)	
Lobe / Gyri	Cluster size (µl)	Structure / Location	MNI Coordinates **XYZ**	Broadmann Area	vs Controls	vs Controls (sex-matched)
Frontal	995	Right inferior frontal gyrus	62 26 15	45	0.038^{+}	*0.132^{+}*
	1063	Left Orbital / rectus gyrus	-3 41 -34	11	0.028^{-}	0.035^{-}
	402	Left inferior frontal gyrus	-59 17 17	44	0.033^{+}	*0.110^{+}*
	191	Right anterior cingulate	15 36 -13	32	0.030^{+}	0.046^{+}
Temporal	414	Left parahippocampus	-29 -2 -36	36	0.004^{+}	0.00^{7+}
	290	Left middle temporal gyrus	-67 -47 -0	22	0.030^{+}	*0.107^{+}*
	230	Middle / Superior Temporal Gyrus	-58 -67 23	39	0.035^{+}	*0.179^{+}*
Parietal	1186	Left inferior Parietal / supramarginal	-63 -45 36	40	0.027^{+}	*0.196^{+}*
	1090	Left Precuneus	-0 -76 51	7	0.017^{+}	0.051^{+}
	570	Left Post central	-60 -24 25	2	0.012^{+}	*0.096^{+}*
	326	Right Cuneus	2 -93 7	8	0.039^{+}	*0.086^{+}*
	214	Left Precuneus	-29 -74 30	19	0.015^{+}	*0.085^{+}*
	208	Left inferior parietal gyrus / Cuneus	-10 -77 6	17, 18, 30	0.019^{+}	0.032^{+}
	196	Left inferior Parietal gyrus / Precuneus	-31 -53 41	40	0.017^{+}	*0.128^{+}*
	189	Left inferior Parietal Lobule	-57 -27 51	2	0.048^{+}	0.041^{+}
Sub-cortical	7587	Left Inf. Semi Lunar Lobule (Cerebellum)	-41 -79 -41		0.019^{+}	0.003^{+}
	2862	Right Brainstem Cerebellar Tonsil	16 -37 -47		0.001^{+}	0.001^{+}
	978	Left Cerebellar tonsil	-19 -39 -43		0.001^{+}	0.001^{+}
	595	Left Uvula	- 0 -78 -40		0.008^{+}	0.003^{+}
	248	Right Declive (cerebellum)	25 -82 -19		0.004^{+}	0.014^{+}
	8017	Bilateral Thalamus / Red Nucleus	-1 -21 -13		0.001^{+}	0.001^{+}
	176	Right thalamus / caudate	21 -34 21		0.005^{-}	0.002^{-}

Voxelwise *t*-test Cluster Report for Cannabis vs. Control Group Comparison					**Cannabis** group **ANCOVA** comparisons with age as covariate (***P*** values)	
Lobe/ Gyri	Cluster size (µl)	Structure / Location	MNI Coordinates **XYZ**	Broadmann Area	vs Controls	vs Controls (sex-matched)
Temporal	509	Left parahippocampus	-28 -0 -35	36	0.001^{+}	0.001^{+}
Sub-cortical	187	Left Thalamus	-15 -21 1		0.001^{+}	0.005^{+}

Voxelwise *t*-test Cluster Report for Nicotine vs. Control Group Comparison					**Nicotine** group **ANCOVA** comparisons with age as covariate (***P*** values)	
Lobe/ Gyri	Cluster size (µl)	Structure / Location	MNI Coordinates **XYZ**	Broadmann Area	vs Controls	vs Controls (sex-matched)
Temporal	197	Right parahippocampus/ Sup temp gyrus	44 2 -23	38	0.001^{+}	0.004^{+}
Parietal	1037	Right precuneus	25 -66 40	7	0.001^{+}	0.001^{+}
	190	Left interior parietal lobule	-46 -44 47	40	0.005^{+}	0.010^{+}
	146	Left interior parietal lobule	-57 -28 35	40	0.004^{+}	*0.056^{+}*
Precentral	369	Right cingulate gyrus/ precentral	29 -10 46	6, 24	0.001^{+}	0.016^{+}
Occiptal	287	Left superior occipital gyrus	-31 -78 35	19	0.001^{+}	0.001^{+}
Post central	207	Left post central gyrus	-19 -39 67	4	0.001^{+}	0.004^{+}
Sub-cortical	1098	Right cerebellum (pyramis)	12 -82 -24		0.001^{+}	0.002^{+}

Note: + = Mean control cluster volume > mean drug using group cluster volume . - = mean controls cluster volume < mean cluster volume of drug using group. MNI coordinates given are for the centre of mass of given cluster. Each cluster may traverse multiple BA's and listed BA is where the largest portion of the cluster is felt to reside. P values no longer reaching significance are in italics.

Table 3.1: Grey matter cluster report detailing areas of volumetric change for the Cocaine, Cannabis and Nicotine drug groups as determined by voxelwise *t*-test comparisons of each drug group versus controls and individual control vs. drug group ANCOVA's with age as a covariate. ANCOVA's with age as a covariate and matched for sex, with a reduced sample are also reported.

FIGURE 3.1

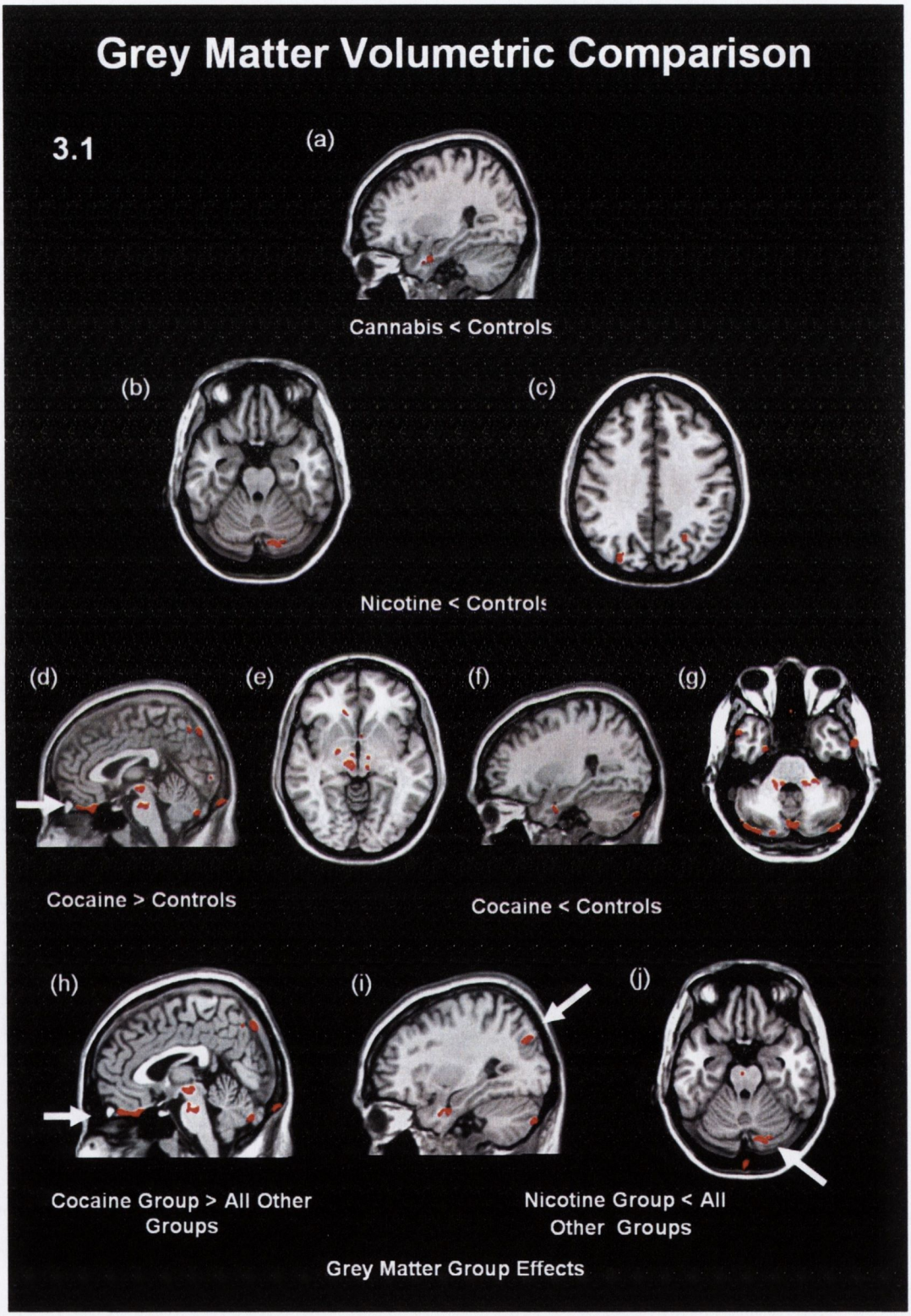

Grey Matter Volumetric Comparison
3.1
(a)
Cannabis < Controls
(b)
(c)
Nicotine < Controls
(d)
(e)
(f)
(g)
Cocaine > Controls
Cocaine < Controls
(h)
(i)
(j)
Cocaine Group > All Other Groups
Nicotine Group < All Other Groups
Grey Matter Group Effects

Figure 3.1: Regions of grey matter volumetric change in each of the three drug using groups compared to controls: Regions shown include (a) left parahippocampal gyrus /Uncus, (b) right declive, (c) Right and left precuneus, (d) left orbital gyrus /rectal gyrus, left precuneus and bilateral red nucleus, brain stem ,left inferior parietal lobe and right cingulate gyrus / precentral gyrus, (e) left anterior cingulate and bilateral red nucleus and left thalamus (f) left parahippocampus /uncus, left cerebellum, (g) left parahippocampus / Uncus, left inferior temporal gyrus, right middle temporal gyrus, bilateral cerebellar tuber, bilateral cerebellar tonsil and pyramis of Vermis (h) Grey matter overlap or common effect site determined by *post-hoc pairwise* comparisons (N = 72) showing grey matter region in the left orbital / rectal gyrus where cocaine users showed a larger grey matter volume compared to controls, nicotine and cannabis users, (i) left parahippocampus / Uncus, left inferior temporal gyrus, right middle temporal gyrus, bilateral cerebellar tuber, bilateral cerebellar tonsil and pyramis of Vermis, (j) Grey matter overlap or common effect site determined by *post-hoc pairwise* comparisons (N = 72) showing grey matter region in the left precuneus where nicotine users showed a decrease in grey matter volume compared to controls, cocaine and cannabis.

In all these comparisons, all but three regions showed decreased grey matter volumes in the drug groups relative to controls. The exceptions were the left orbital /rectal gyrus, the left

anterior cingulate and the right cuneus which showed increases in grey matter in cocaine users. Large deficits were found bilaterally in the red nucleus and left parahippocampal gyrus for the cocaine group and left parahippocampal gyrus for the cannabis users (Figure 3.1 (a) & (b)). In addition, extensive volumetric reductions were found in the right and left cerebella and right cuneus and left precuneus, the brain stem, and frontal gyrus in cocaine users (Figure 3.1 (f), (g), (h) & (i)). The comparison of nicotine versus controls identified two parietal regions (left and right precuneus) as well as a cluster of grey matter volume deficit in the right cerebellum.

Group differences in the pairwise drug group/controls comparisons remained significant in all clusters when covaried for age. Accommodating the sex imbalance between the groups with the smaller sex-matched groups had minimal impact on the ANCOVA results between the controls and the cannabis users (with the cluster in the parahippocampus / uncus remaining significant) and between controls and nicotine users (with one of the original three clusters, the right cerebellar declive, failing to show a significant group effect, $p \leq 0.10$). The cocaine-control comparison was affected with five of the original 23 clusters failing to show group effects (these were the left anterior cingulate, left middle temporal gyrus, left inferior parietal gyrus, left precentral gyrus and the right cuneus). Notably, all previously identified sub-cortical regions and the extensive cerebellar volumetric reductions remained significant (Table 3.1).

Combining the significant clusters from the individual drug group/controls t-tests resulted in a map of 26 regions of between-group volumetric change. The results from this ANCOVA (with age as the covariate) performed for all four groups on each cluster are reported in Table 3.2. Examination of Bonferroni-corrected, *post hoc* pairwise comparisons revealed one region in the left precuneus where nicotine users showed a grey matter decrease compared to controls ($p \leq 0.001$), cannabis users ($p \leq 0.008$) and cocaine users ($p \leq 0.011$) (Figure 3.1 (l)), one region in the right precuneus where nicotine users showed a grey matter decrease compared to controls ($p \leq 0.001$), cannabis users ($p \leq 0.05$) and cocaine users ($p \leq 0.018$) and one region in the right declive where, again, nicotine users showed a grey matter decrease compared to controls ($p \leq 0.001$), cannabis users ($p \leq 0.005$) and cocaine users ($p \leq 0.012$). In the left orbital /rectal gyrus, cocaine users showed a grey matter increase compared to controls ($p \leq 0.001$), cannabis users ($p \leq 0.002$) and nicotine users ($p \leq 0.001$). Controls were found to have greater grey matter volumes compared to both cannabis and cocaine users in four regions: the left thalamus, the left uncus /parahippocampus, the left precentral gyrus and the right precuneus.

Table 3.2

Grey Matter Volume Between-Group ANCOVA with age as a covariate							
Lobe	Cluster size (µl)	Structure	M N I Coordinates **XYZ**	Brodmann Area	Group Significance ***P*** (N = 72)	Sex matched ***P*** (N=36)	***Post Hoc*** Pairwise comparisons
Frontal	394	Left Orbital / Rectal gyrus	-2 36 -33	11	0.001	0.029	c-, e-, f - (*f* -)
	270	Right inferior frontal gyrus	59 28 15	45,46	0.001	not sig	c+ ,f+
	176	Left Anterior Cingulate	-12 29 -8	6	0.006	not sig	e- ,f -
Temporal	341	Left Uncus/parahippocampus	-28 -1 -33	36	0.001	0.006	a+ , c+ (*c* +)
	234	Left middle temporal gyrus	-52 9 -38	21	0.003	not sig	c+
	225	Right Inferior temporal gyrus	59 1 -39	20	0.021	not sig	
	159	Left Inferior temporal gyrus/fusiform	-59 2 -34	21	0.021	not sig	f +
	143	Left Middle Temporal gyrus	-52 -71 26	39	0.002	not sig	a+
Parietal	589	Left Inferior Parietal gyrus	-59 -46 40	40	0.015	0.042	c+, (*c* +)
	468	Right Precuneus	0 -79 47	7	0.001	not sig	a+, c+
	234	Left Precuneus	-29 -78 33	19	0.001	0.001	b+,d+,f-,(*b* +,*d* +)
	222	Right Cuneus	2 -94 7	18	0.009	not sig	
	184	Left pre central gyrus	-57 -7 42	6	0.003	0.026	a+ ,c+ (*c* +)
	163	Right Cuneus	9 -98 36	19	0.001	0.005	c- ,f - (*c* - ,*f* -)
	160	Left Post Central gyrus	36 -37 69	1	0.004	not sig	c+ ,e+
	148	Right Precuneus	24 -66 38	7	0.001	0.020	b+ ,d+ ,f - (*b* +)
Sub-cortical	1485	Bilateral Red Nucleus	-1 -19 -10		0.001	0.039	c+
	1376	Left Pyramis/Tuber	-35 -83 -42		0.004	0.004	c+, (*c* +)
	814	Brain Stem	-0 -24 -30		0.001	0.010	c+, (*c* +)
	441	Right Cerebellar tonsil	16 -39 -36		0.002	0.001	c+, f +,(*c* +,*f* +)
	332	Left lentiform nucleus/globus pallidus	-18 -5 -4		0.035	not sig	f +
	283	Left Thalamus	-18 -28 -2	27	0.001	not sig	a+, c+
	240	Left Cerebellar tonsil	-12 -41 -36		0.015	0.036	c+
	161	Right Cerebellar tonsil	30 -39 -43		0.002	0.001	c+, f+,(*c* +,*e* +,*f* +)
	143	Left Caudate	-4 5 -2	25	0.008	0.004	f-, (*b* - ,*c* -)
	138	Right Declive	16 -99 -25		0.001	0.001	b+,d+,f- (*b*-,*d*-)

Notes: a = Controls vs. Cannabis, b = Controls vs. Nicotine, c = Controls vs. Cocaine
d = Cannabis vs. Nicotine, e = Cannabis vs. Cocaine, f = Nicotine vs. Cocaine
(a,b c,d,e,f) = Sex matched comparisons
+ and - indicate direction of mean volume change ie. a+ = Controls > Cannabis
a- = Controls < Cannabis, not sig = no significant difference

Table 3.2: Grey matter four-Group ANCOVA with age as a covariate showing between-group volumetric comparisons. Bonferroni corrected *post-hoc* pairwise comparisons for each statistically significant cluster are listed. Between–group ANCOVA's with age as a covariate and matched for sex are also reported (n =36).

The sex-matched four-group ANCOVA (with age as the covariate) results were substantially affected with only 15 of the original 26 clusters persisting to show overall between-group effects. Regions that failed to show a significant group difference were, right inferior frontal gyrus, left anterior cingulate, two regions in left middle temporal gyrus, right inferior temporal gyrus left inferior temporal gyrus, right precuneus, right cuneus, left post central gyrus, left lentiform nucleus and left thalamus (Table 3.2). As with the analysis conducted on the entire dataset, Bonferroni-corrected, *post-hoc* pairwise comparisons were examined for the sex-matched sample. Of the three regions showing decreased grey matter volume in nicotine users compared to all other groups and the region of increased grey matter volume in cocaine used compared to all other groups previously revealed by *post hoc* pairwise comparisons based on the entire dataset, none remained significant. However, the regions in right declive and left precuneus where nicotine was found to have reduced grey matter compared to all other groups did persist for both cocaine and controls but failed to show an effect for cannabis.

3.3.2 White Matter Comparison

Similar to the grey matter comparisons, the cocaine group t-test contrast against controls for white matter yielded the largest number of significant clusters (n = 12) compared to three regions in the cannabis-controls comparison and two in the nicotine-controls comparison (see Figure 3.2 and Table 3.3). However, in contrast to the grey matter differences, the white matter volume differences were largely in the opposite direction to those found in the grey matter with controls having smaller volumes than users in all but

one region, the left inferior parietal / supramarginal gyrus. The largest of the clusters showing increased white matter volumes in cocaine users relative to controls were found in the right cuneus, right dentate, left parahippocampus / uncus, left culmen, bilateral anterior cingulate, bilateral red nucleus and the brainstem. The cannabis comparison identified two regions (the left superior parietal gyrus and the left parahippocampus / uncus where cannabis users showed a white matter volume increase compared to controls and one site in the left middle occipital gyrus where controls had a higher white matter volume. The nicotine group comparison identified two clusters in the right insula /post central gyrus and the left culmen where controls showed larger white matter volumes than nicotine users. Group differences remained significant in all clusters even when covaried for age. Repeating these ANCOVAs with the smaller, sex-matched groups mainly affected the cocaine group/control comparison. Here, two of the original 12 group differences failed to reach significance. These regions included the left anterior cingulate gyrus, and the left parahippocampus / thalamus. The sex matched cannabis / control comparison found only two of the three identified regions (the left middle occipital gyrus and the left parahippocampus / uncus) remained significant. The sex-matched nicotine / control comparison remained unaffected with both regions of group difference remaining significant.

Table 3.3

White Matter Analysis						
Voxelwise *t*-test Cluster Report for Cocaine vs. Control Group Comparison					**Cocaine** group **ANCOVA** comparisons with age as covariate (***P*** value)	
Lobe	Cluster size (µl)	Structure / Location	MNI Coordinates **XYZ**	Brodmann Area	vs. Controls	vs. Controls (sex matched)
Frontal	321	Left Anterior cingulate	-2 33 6	24	0.030-	*0.064-*
	243	Right Anterior cingulate	6 33 6	24 / 32	0.006-	0.050-
Temporal	913	Left parahippocampus / uncus	-21 -6 -34	36	0.001-	0.005-
	208	Left Parahippocampus/ Thalamus	-13 -31 -4	27	0.012-	*0.104-*
	227	Right Parahippocampus /uncus	24 -5 -37	36	0.001-	0.002-
Parietal	115	Left Inferior Parietal / Supramarginal gyrus	-54 -44 39	40	0.002+	0.001+
Occipital	239	Left Cuneus / lingual gyrus	-14 -70 3	18	0.027-	0.032-
Sub-cortical	1231	Right Dentate	14 -44 -31		0.001-	0.003-
	792	Left Culmen / Nodule (cerebellum)	-6 -46 -31		0.002-	0.009-
	788	Bilateral Red Nucleus	1 -17 -11		0.003-	0.036-
	495	Brain Stem	-1 -22 -31		0.002-	0.023-
	201	Right Insula	34 13 -11	13	0.001-	0.018-
Voxelwise *t*-test Cluster Report for Cannabis vs. Control Group Comparison					**Cannabis** group **ANCOVA** comparisons with age as covariate (***P*** value)	
Lobe	Cluster size (µl)	Structure / Location	MNI Coordinates **XYZ**	Brodmann Area	vs. Controls	vs. Controls (sex matched)
Occipital	127	Left Middle Occipital gyrus	-47 -82 -3	18/19	0.001+	0.001+
Parietal	98	Left Superior parietal lobule	-38 -78 47	7	0.001-	*0.270-*
Temporal	118	Left parahippocampus / Uncus	-20 -7 -35	28, 35, 36	0.001-	0.001-
Voxelwise *t*-test Cluster Report for Nicotine vs. Control Group Comparison					**Nicotine** group **ANCOVA** comparisons with age as covariate (***P*** value)	
Lobe	Cluster size (µl)	Structure / Location	MNI Coordinates **XYZ**	Brodmann Area	vs. Controls	vs. Controls (sex matched)
Temporal	159	Right Insula/ post central gyrus	56 -20 21	43	0.001+	0.002+
Sub-cort.	119	Left Culmen (cerebellum)	-14 -31 -18		0.001+	0.001+

Note: + = Mean control cluster volume > mean drug using group cluster volume , - = mean controls cluster volume < mean cluster volume of drug using group. MNI coordinates given are for the centre of mass of given cluster. The BA is the location where the bulk of the cluster is fell. P values no longer reaching significance are in italics.

Table 3.3: White matter cluster report detailing areas of volumetric change for the Cocaine, Cannabis and Nicotine drug groups as determined by voxelwise *t*-test comparisons of each drug group versus controls and individual control vs. drug

group ANCOVA's with age as a covariate. ANCOVA's with age as a covariate and matched for sex, with reduced sample are also reported.

FIGURE 3.2

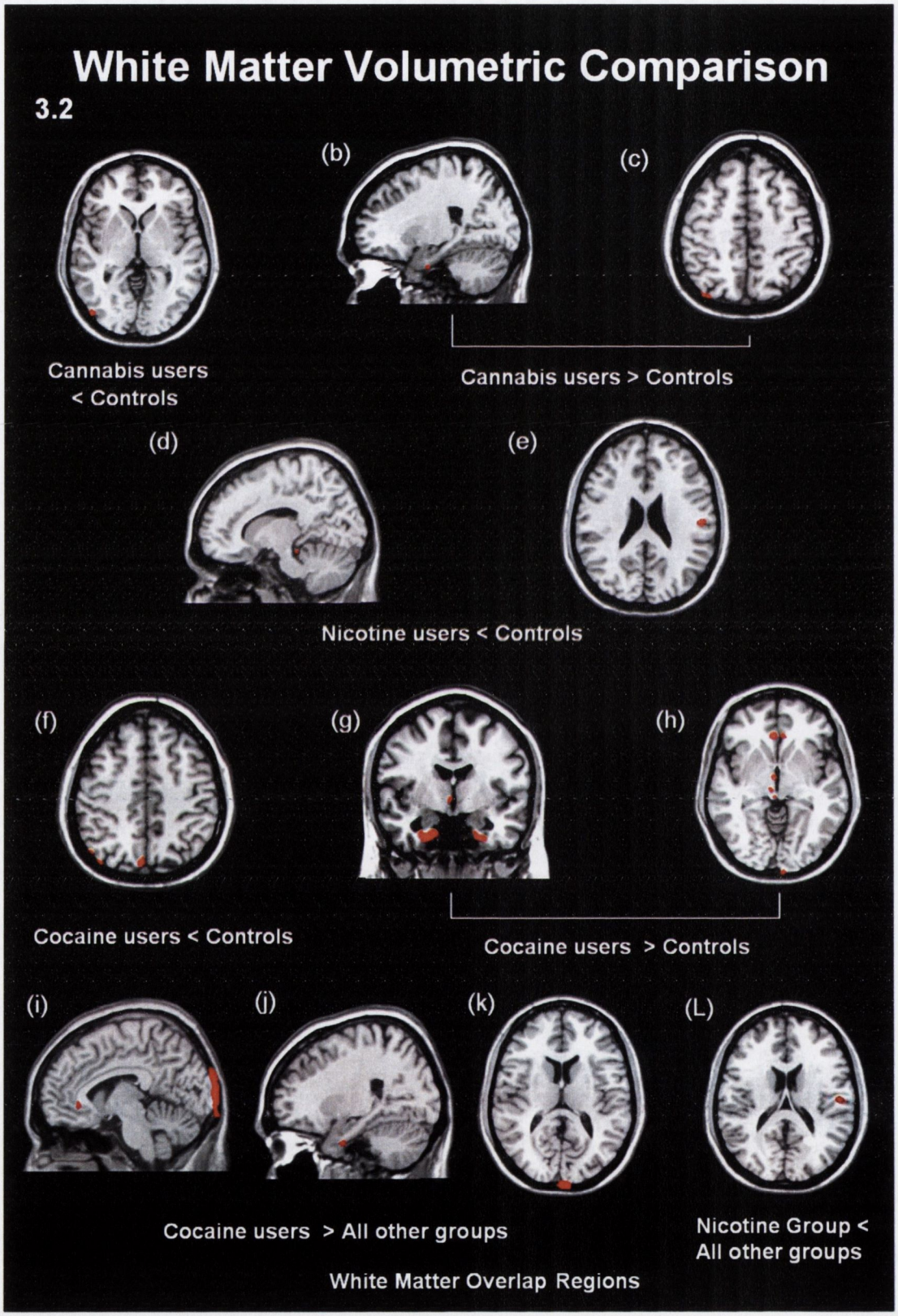

White Matter Volumetric Comparison
3.2
(b)
(c)
Cannabis users
< Controls
Cannabis users > Controls
(d)
(e)
Nicotine users < Controls
(f)
(g)
(h)
Cocaine users < Controls
Cocaine users > Controls
(i)
(j)
(k)
(L)
Cocaine users > All other groups
Nicotine Group <
All other groups
White Matter Overlap Regions

Figure 3.2: Regions of white matter volumetric change for each of the three drug using groups compared to controls: Regions shown include (a) left middle occipital gyrus, (b) left parahippocampus, (c) left superior frontal gyrus, (d) right inferior parietal lobe, (e) right insula / post central gyrus and right posterior cingulate, (f) left cuneus, (g) left parahippocampus and (h) bilateral anterior cingulate, bilateral parahippocampus and red nucleus, (i) white matter overlap site as determined by a comparison of the paired voxelwise *t*-test result found between cocaine (shown in red) and cannabis (shown in blue), (j) white matter overlap or common effect site determined by *post-hoc pairwise* comparisons (N = 72) showing white matter region in the right insula / postcentral gyrus where nicotine users showed decreased white matter volume compared to controls, cocaine and cannabis users.

The combined map of white matter drug group / control differences contained 17 clusters (see Table 3.4). Examination of the Bonferroni-corrected *post hoc* pairwise comparisons revealed that nicotine users had a statistically significant decrease in white matter volume in the right insula / postcentral gyrus when compared to controls ($p \leq 0.001$), cannabis ($p \leq 0.049$) and cocaine users ($p \leq 0.001$) and in the left Culmen when compared to controls ($p \leq 0.001$), cannabis ($p \leq 0.049$) and cocaine users ($p \leq 0.001$). Cocaine users had increased white matter volumes compared to controls, cannabis and nicotine users in two regions, the right anterior cingulate and right parahippocampus / uncus (Table 3.4). Cocaine users were found to have greater white matter volume than controls and nicotine users in four sub-

cortical regions (right dentate, left culmen/nodule, bilateral red nucleus, and the right insula). Controls were found to have greater white matter volume than cannabis and cocaine users in the left middle occipital gyrus and cocaine users had greater white matter volume than both controls and nicotine users in the right dentate. As with the grey matter analyses, the ANCOVA was repeated with the groups matched for sex. The results were substantially affected with only ten of the original 17 clusters persisting to show overall between-group effects. The areas with persistent between group differences, having matched for sex and co-varied for age included the right insula, right insula /post central gyrus, left and right parahippocampal gyrus, left cuneus / lingual gyrus, left inferior parietal / supramarginal gyrus, the left middle occipital gyrus, the right dentate, left culmen and left culmen/ nodule (see Table 3.4). The examination of Bonferroni-corrected, *post hoc* pairwise comparisons revealed only one of the previously identified regions, the right parahippocampal gyrus in which cocaine users were found to have greater white matter volumes compared to cannabis ($p \leq 0.036$), nicotine users ($p \leq 0.029$) and controls users ($p \leq 0.003$). None of the regions in which nicotine users had decreased white matter compared to the other groups persisted. The previously identified region in the left middle occipital gyrus where controls were found to have greater white matter volume than cannabis and cocaine users was found to persist in the sex matched comparison along with the region in the right dentate where cocaine users had greater white matter volume than both controls and nicotine users. No regional effects where cannabis users differed from all other groups were identified.

Table 3.4

White Matter Volume Between-Group ANCOVA with age as a covariate (*p* values)							
Lobe	Cluster size (µl)	Structure	M N I Coordinates **XYZ**	Brodmann Area	Group Significance (N = 72)	Sex matched (N=36)	**Post Hoc** Pairwise comparisons
Frontal	321	Left Anterior Cingulate	-2 33 6	24	0.031	not. sig	c-,
	243	Right Anterior Cingulate	6 33 -6	24	0.008	not. sig	c-, e- ,f -
Temporal	919	Left Parahippocampus/ Uncus	-21 -6 -34	36	0.001	0.019	a-,c-,f -, *c-*
	227	Right Parahippocampus/ Uncus	24 -5 -37	36	0.001	0.004	c-,e-,f-, (*c-, e-,f -*)
	208	Left Thalamus/ Parahippocampus	-13 -31 -4	27	0.003	not. sig	c-
	402	Left Inferior Parietal gyrus	-41 -76 48	7	0.008	not. sig	a-,c-
	239	Left Cuneus/ Lingual gyrus	-14 -70 3	18	0.031	0.033	c-, (*c-*)
	136	Left Precuneus	-6 -78 46	7	0.013	not. sig	a+
	115	Left Inf. Parietal /supramarginal	-54 -44 39	40	0.015	0.002	a+, (*b +, c +*)
Occipital	175	Left Middle Occipital gyrus	-47 -82 -3	18 / 19	0.001	0.001	a+,c+,d- (*a +,d-,f +*)
sub-cortical	1231	Right Dentate (cerebellum)	14 -44 -31		0.001	0.001	c-,f-, (*c-,f -*)
	792	Left Culmen / nodule	-6 -46 -31		0.001	0.033	c-, f -
	788	Bilateral Red Nucleus	1 -17 -11		0.003	not. sig	c-
	495	Pons/ Brainstem	0 -22 -31		0.001	not. sig	c-, f -
	201	Right Insula	34 13 -8	13	0.001	0.024	c-, f-, (*c -*)
	159	Right Insula / Ppost Central Gyrus	56 -20 21	43	0.001	0.009	b+, d +, f-, (*b +*)
	119	Left Culmen	-14 -31 -18		0.001	0.001	b+, d +, f-, (*b +, f-*)

Note: a = Controls vs. Cannabis, b = Controls vs. Nicotine, c = Controls vs. Cocaine
d = Cannabis vs. Nicotine, e = Cannabis vs. Cocaine, f = Nicotine vs. Cocaine
(a,b c,d,e,f) = Sex matched comparisons (pairing as above)
+ and - indicate direction of mean volume change ie. a+ = Controls > Cannabis
not sig. = no significant group difference

Table 3.4: White matter four-Group ANCOVA with age as a covariate showing between-group volumetric comparisons. Bonferroni corrected *post-hoc* pairwise comparisons for each statistically significant cluster are listed. Between–group ANCOVA's with age as a covariate and matched for sex are also reported (n =36).

3.4 DISCUSSION

In this study grey and white volumetric changes were identified in the three groups of cocaine, nicotine and cannabis drug users when compared to a drug-naïve control group. The grey matter tissue examination revealed the most substantial changes to be in the

cocaine group with multiple clusters of reduced volume being identified. Moreover, both volumetric differences unique to each drug-using group and differences shared by groups were observed. In contrast, the drug groups showed many instances of greater white matter volumes, often in regions adjacent to the grey matter reductions. When sex differences were accounted for, both grey and white matter results were affected. In the case of the grey matter analysis, only two of the 26 regions (the right inferior frontal gyrus and the left inferior temporal gyrus) of grey matter volume difference failed to persist indicating very strong effects in the identified regions that remained true even when the sample size was halved from 72 to 36. The white matter differences on the other hand, were dramatically affected with only 10 of the 17 regions of white matter volume differences persisting. This difference between the initial and the sex-matched analysis could be due to the reduction in statistical power in the reduced sample. Moreover, fewer white matter tissue differences have been reported in the literature due perhaps to the more heterogeneous tissue compostion found in white matter regions which, in turn, may render these effects less robust and more sensitive to the sample size reduction.

3.4.1 Cannabis Group

The cannabis users had reduced grey matter volumes in parahippocampal and thalamic regions when compared to controls (Tables 3.1 & 3.2). The cognitive deficits associated with cannabis use are consistent with Δ^9-Thetrahydrocannabinol (THC), the main psychoactive ingredient in cannabis, targeting the cannabinoid CB1 and, to a lesser extent, CB2, receptors (Iversen, 2003; O'Leary et al., 2002). High concentrations of the CB1

receptor are found in the parahippocampus, hippocampus and thalamic regions of the brain consistent with the observed volume reductions. The grey matter reductions in both the parahippocampal gyrus and the thalamus lay in close proximity to regions of higher white matter volumes in the cannabis group. This apparent inverse relationship between grey matter reduction and white matter growth has previously been reported for the hippocampus and parahippocampal regions in heavy marijuana users (Matochik et al., 2005) and may reflect a mechanism wherein reductions in grey matter produce compensatory increases in neighbouring white tissue. The observed grey matter changes may result from drug induced neuronal atrophy (Campbell, 2001) caused by the neurotoxic effects of Δ^9–Thetrahydrocannabinol (Downer et al., 2003) although this pattern of hippocampal grey matter atrophy accompanied by white matter volume increase has also been identified in methamphetamine users (Thompson et al., 2004) and suggests that this effect may not be specific to cannabis Indeed, the present data show grey matter reductions in the cocaine group in this same area. Localized white matter volume increases are possibly due to cannabis's protective mechanism as a promoter of oligodendrocyte progenitor survival (Molina-Holgado et al., 2002) as oligodendroglial cells are responsible for myelination. Possible inflammatory mechanisms due to drug exposure could also be responsible for the observed white matter increases or it could be that white matter volume which typically continues to increase with age may mask or counteract to some extent, the effect of substance abuse in this tissue type.

3.4.2 Nicotine Group

The region of grey matter deficit in the right cerebellum observed in smokers confirms previous reports (Brody et al., 2004a; Domino et al., 2000), although it should be noted that it did not survive the more stringent sex-matched and age-controlled comparison with controls. In contrast to the findings of Brody et al., 2004, identifying prefrontal regions of volumetric change, this study failed to identify any significant regions of volumetric change in the dorsolateral prefrontal cortex (DLPFC) and the ventrolateral prefrontal cortex (VLPFC). This apparent lack of agreement could be partly attributable to the differences in the threshold limits used ($p \leq .001$ uncorrected with a minimum cluster criteria of 50 contiguous significant voxels reported by Brody et al. compared to our voxelwise statistical threshold, $t = 3.6$, $p \leq .001$ and minimum cluster size of 138 µl contiguous significant voxels). When our results were examined at $p \leq 0.001$ uncorrected with a minimum cluster criteria of 50 contiguous significant voxels, similar areas of volumetric change were observed in the DLPFC and VLPFC but these effects failed to remain significant at the more conservative threshold level. The larger sample of 19 smokers compared to 11 in this study could be a factor in the more robust prefrontal regions of volumetric change identified by Brody et al., 2004 which included two regions that survived Bonferroni correction ($p \leq 0.5$).

Nicotine has been reported to act on cholinergic receptors in the cerebellum and to increase cerebellar blood flow (Domino et al., 2000; Domino et al., 2004; Zubieta et al., 2005) but the complex nature of these actions, which produce both therapeutic (Guan et al., 2003; Opanashuk et al., 2001) and neurotoxic effects (Guan et al., 2003; Zubieta et al., 2005) do

not suggest an obvious mechanism for the observed volumetric reductions. The largest regions of volume reduction in the right and left precuneus could lend support to the involvement of these regions in episodic retrieval (Krause et al., 1999) given nicotine's effects on memory functioning (Kumari et al., 2003). The specificity of the nicotinic effect on the precuneus is evident from the four-group ANCOVA *post-hoc* pairwise comparisons (Table 3.2) in which nicotine users showed decreased grey matter volume compared to controls, cocaine and cannabis users. The precuneus has been reported to be involved in episodic memory, semantic tasks (Fernandes et al., 2005; Krause et al., 1999) and spatial location encoding and recognition (Frings et al., 2006) and has recently been suggested to play a key role in cognitive mechanisms that integrate multiple tasks and modulate conscious processes (Cavanna and Trimble, 2006). The very high metabolic rate of the precuneus at rest (Gusnard et al., 2001; Gusnard and Raichle, 2001; Raichle et al., 2001) could contribute to its apparent susceptibility to nicotine exposure as the neurotoxic effects could accumulate along possible memory associated connections such as the retrosplenial pathways culminating in an increased exposure level due to the relative high blood profusion rate of this region. It has been suggested that the insula plays a key role in the addition to cigarette smoking (Naqvi et al., 2007) and our results identifying a white matter reduction in the insula in smokers compared to controls appear to offer further support to the involvement of the insula in nicotine addition.

3.4.3 Cocaine Group

Cocaine is one of the most potent stimulants and a sizeable body of research into the effects of the drug has revealed cognitive impairments and, more recently, structural brain changes

in key sites where the drug's pharmacological effects are most pronounced. Left thalamus and right inferior frontal gyrus as well as extensive parietal regions showed reduced grey matter volumes. These reductions, some in areas rich in dopamine receptors that have been implicated in the cognitive impairments of cocaine users, may constitute the neurobiological substrates for the pattern of deficits and behavioural profiles of users. For example, a reduced volume in right inferior prefrontal cortex may reflect the diminished inhibitory control of cocaine users (Fillmore and Rush, 2002; Kaufman et al., 2003). The most substantial volumetric changes were observed in the cerebellum. The human cerebellum shows large metabolism increases in response to methylphenidate (Volkow et al., 2003) while rat models show altered function here resulting from cocaine exposure (Jimenez-Rivera et al., 2000) and our findings appear consistent with previously identified cocaine induced cerebellar changes reported in the literature (Hester and Garavan, 2004; Jimenez-Rivera et al., 2000; Sim et al., 2007).The sensitivity of the cerebellum to oxidative stress (Pae et al., 2005; Sim et al., 2007) which in turn, could be accentuated by the vasoconstrictive mechanism of cocaine (Kaufman et al., 2003) and the vascular toxicity of the drug also offers support to the extensive volumetric changes identified in the cerebellum. Functional imaging studies have also shown atypical cerebellar activation patterns in cocaine users in response to cognitive task challenges (Hester and Garavan, 2004), a pattern also observed in alcoholics (Desmond et al., 2003) and cannabis users (Bolla et al., 2005) together with our results identifying cerebellar grey matter volume reductions in cocaine and nicotine uses appearing to lend further evidence suggesting a common non-drug-specific mechanism (e.g., stress or drug-related lifestyle) of volumetric change (Cohen et al., 2006; Kitayama et al., 2006; Yamasue et al., 2003). More recently,

substantial cerebellar grey and white matter volume changes have been reported (Sim et al., 2007) in which a negative correlation between bilateral cerebellar hemispheric grey matter volume and duration of cocaine use was identified. Right cerebellar white matter volume also demonstrated a negative correlation with the Groove pegboard test for motor performance (GPT) completion times (Sim et al., 2007). In contrast, the white matter analysis of the present study found controls to have less white matter than cocaine users in the cerebellum. This pattern is also evident in the anterior cingulate region and parahippocampal gyrus where cocaine users had reduced grey but increased white matter volumes. In interpreting these effects, it should be noted that they may be partially attributable to an edge effect phenomenon at the grey /white matter tissue boundary where, for example, boundary variations due to atrophy in one tissue type can lead to misidentification as tissue of the second type (Good et al., 2001*b*).

Curiously, both the left anterior cingulate gyrus and the left orbitofrontal cortex in the vicinity of the Rectal Gyrus showed increased grey matter volumes for cocaine users compared to controls, although the cingulate result did not survive in the sex-matched and age-controlled analysis. The extant literature identifies cocaine usage with reduced grey matter volumes (Bartzokis et al., 2002; Bartzokis et al., 2000; Bolla et al., 2004; Franklin et al., 2002; Liu et al., 1998; Matochik et al., 2003). This said, increases in grey matter volumes have been identified in parietal and frontal regions in schizophrenic patients treated with the atypical neuroleptic drug 'clozapine' (Molina et al., 2005) and the caudate and left accumbens with risperidone (Massana et al., 2005), and in pituitary volume in concurrent cocaine and heroin users (Teoh et al., 1993). Further investigation of these

volume increases is needed given the possibility of an artifactual finding driven, as mentioned above, by features of the brain segmentation mechanism around grey /white matter tissue boundaries and around the nasal and ocular cavities.

3.4.4 Common Effects

The grey matter comparison revealed no areas of effect common to all drug using groups compared to controls but four regions (the left parahippocampus / uncus, right precuneus, left thalamus and the left precentral gyrus) showed grey matter volume decreases in both cannabis and cocaine users compared to controls. Both drugs might affect the dopaminergic receptors found abundantly in the thalamus and parahippocampal gyral or, as mentioned, secondary effects due to stress (Bremner and Narayan, 1998; Gurvits et al., 1996; Villarreal et al., 2002) and associated lifestyle factors driven by drug addiction processes (Thompson et al., 2004) could be responsible for the apparent common effect. A further three regions were found that showed very specific individual drug effects compared to controls and the other drug using groups. These regions were the left precuneus and right declive where nicotine users had decreased grey matter compared to controls, cocaine and cannabis users and the left orbital / rectal gyrus where cocaine users showed an increased grey matter volume compared to all other groups. White matter comparisons revealed no areas of effect common to all drug using groups compared to controls but identified two regions, the left parahippocampus/ uncus and the left inferior parietal lobe with increased white matter volume in cocaine and cannabis users compared to controls and one region, the left middle occipital gyrus, which showed a white matter volume decrease in cocaine and cannabis

compared to controls. A further three regions showed specific individual drug effects compared to controls and the other drug using groups. These regions were the right cuneus, right anterior cingulate, and right parahippocampus / uncus where cocaine users showed increased white matter volumes compared to all other groups. A further two regions, namely the right insula / postcentral gyrus and the left culmen where nicotine users had decreased white matter compared to controls, cocaine and cannabis users were identified.

3.5 CONCLUSIONS

While the present results have identified cortical regions that would appear to be adversely affected in drug abusers, a number of qualifiers should be noted. The nicotine and cocaine groups are relatively small when compared to the controls and cannabis group although this concern is mitigated to some extent by the observed group effects being largest in the cocaine group. Further, the groups were not ideally matched in either age or sex, although the group results did persist in the ANCOVA in which age was controlled for. The difference in the proportions of the sexes in each group (there was a greater proportion of females in the control group) did impact on the results obtained in the cocaine / control comparison. The extent to which this was driven by between-group sex differences or by the reduction in statistical power in the smaller sample of the sex-matched comparison is unclear and will require further investigation with larger samples. Finally, while the VBM analysis permits the investigation of tissue density/concentration it does not speak to the mechanisms of biological changes in the brain that might be associated with drug use.

Detailed quantitative histological measurements are needed to illuminate the cellular and structural changes that underlie the observed, relatively course, volumetric changes observed. The present results, however, do offer some preliminary evidence of brain structural changes that are unique to cocaine, cannabis and nicotine and appear to support, by and large, those identified by previous volumetric studies. Overall, the present results demonstrate no common regions of volumetric differences across all users groups providing no support for a volumetric reduction that can be associated with a general addictive process. However, drug-specific effects were observed and may be related to the specific cognitive profiles of users of each drug.

Chapter 4

Comparison of Grey and White matter whole brain volume measurements of temporal lobe epilepsy patients and controls using stereology and fully automated voxel based volumetric techniques.

Abstract

Fully automated volumetric techniques are becoming more widely used for between-group comparisons of brain structure and volume. The 'optimized' method of voxel-based morphometry (VBM), FMRIB's FAST segmentation and SIENAX tools are examples of the fully automated techniques that are frequently used. The aim of this paper was to validate volume measurements generated via these fully automated processes using the mathematically unbiased, manual technique of stereology. In this experiment both stereological and fully automated methods were applied to 17 temporal lobe epilepsy patients and 17 neurologically normal controls. Volumes were generated for whole-brain grey and white matter. Derived variables of grey / white matter ratio and total intracranial volume (TIV; grey matter + white matter) were also generated. Although the measurements of the fully automated techniques were highly correlated with the stereological measurements, the fully automated techniques identified significantly greater grey matter volume and significantly smaller white matter volume measurements compared to those via

stereology. Moreover, while the stereological results indicated significant group differences between patients and controls in white matter volumes and the grey / white matter ratio, the fully automated techniques failed to detect these effects. The results indicate that a grey matter overestimation by the automated techniques affects volume estimates and can impact on the sensitivity of these techniques for detecting group differences.

Results of the voxelwise comparison study appear to agree with those of previous studies that identified both hippocampal and extrahippocampal (frontal, parietal and cerebellar) grey matter volume decreases in TLE patients relative to controls and also identified cerebellar, parahippocampal and temporal white matter changes. The extent of variability between the regions identified by each method was surprisingly greater than expected and warrants further investigations with new data from other patient-control comparison studies to determine the robustness of the inaccuracies between the automated techniques.

4.1 INTRODUCTION

Accurate and reliable measurements of global and regional brain volumes are increasingly used as an informative and important part of neurophysiological and cognitive assessment. Neurodegenerative conditions where brain morphology changes are known to exist such as epilepsy and Alzheimer's disease and oncology treatment planning and assessment could benefit from an accurate and reliable fully automated brain volume measurement technique. With advances in imaging techniques such as Magnetic Resonance Imaging (MRI), analysis techniques to obtain and quantify whole-brain and regional brain volumes have been developed (Good et al., 2001a; Good et al., 2001b; Thompson et al., 2003) and have facilitated the assessment and treatment of diseases such as dementia (Bigler et al., 2004). Volumetric change observed in grey and / or white matter tissue can be very informative in numerous applications such as detecting the onset and tracking the progression of degenerative diseases (Colchester et al., 2001; Fotenos et al., 2005), oncological assessments of tumour size (Joe et al., 1999; Salman et al., 2005a), and investigating the cognitive and structural effects of substance abuse on the brain (Liu et al., 1998; Matochik et al., 2005; Matochik et al., 2003) or the effects of ageing (Good et al., 2001b; Matsuzawa et al., 2001; Wolf et al., 2003).

To date, there is no standard fully automatic mechanism employed to perform *in vivo* brain volume measurements resulting in large variations in brain volumetric measurements being reported in the literature (Colchester et al., 2001). These variations may be partly attributable to the techniques employed to perform the measurement and analyses. For the purpose of this analysis we have broadly split the various techniques into two categories,

namely manual techniques (manual delineation and stereology), and automated techniques. Although considered the gold-standard method for quantitative brain measurement, manual techniques such as manual delineation are often time consuming. They require knowledge on the part of the rater in order to accurately define the boundary of the region of interest. Stereology or 'proper sampling' can be used to obtain unbiased volume estimates by the application of the Cavalieri method. The precision of a volume estimate obtained using the Cavalieri sections method may be measured by its coefficient of error (CE), the prediction of which is complex (Gundersen and Jensen, 1987; Roberts et al., 2000). Stereology is also a manual technique, however it is more time efficient in that the structure is sampled and its volume estimated. Hence, the choice of stereology as a validation tool for fully automated volumetric measurement techniques is due to the mathematically unbiased nature of the method for geometric property estimation (Gundersen and Jensen, 1987). The unbiased nature of the applied sampling means that stereological measures may be considered to be accurate contingent on the accurate identification of the structure by the rater and the density of the sampling. The accuracy and reliability of stereological measures has previously been demonstrated by Ronan *et al* (2006), Doherty *et al* (2000), and Garcia-Finana *et al* (2003).

In contrast to manual-based techniques, fully automated quantitative methods are time-efficient requiring minimal user-driven measurement. However, there are a number of steps in the automated processing pipeline (normalisation, segmentation and smoothing) that might have consequences for the accuracy of the volume measurements and, in turn, the sensitivity of these techniques for between group comparisons. Consequently, a clear

understanding of the differences between these analyses techniques is needed and the strengths and weaknesses of each need to be considered for the particular application at hand. The first focus of this paper is a comparison of two MRI based techniques, namely stereology (in this case taken as the 'gold standard' technique) and the fully automated volumetric analysis techniques of Voxel Based Morphometry (VBM) and those of the FMRIB's FSL package (category two as described above) to assess global grey and white matter tissue volumes in a clinical group of temporal lobe epilepsy (TLE) patients compared to a matched control population. The second focus is the consistency between the fully automated analysis techniques to perform between-group (TLE and controls) whole-brain voxelwise comparisons for the identification and localisation of regions of volumetric change in grey and white matter tissue.

4.2 METHODS

4.2.1 Participants

Seventeen control subjects with no neurological deficit (10males, 7 females, mean age = 30 years, range 21-43) were chosen at random from a bank of controls in an MR-image data library at Beaumont Hospital, Dublin, Ireland and compared to a sample of 17 TLE patients (10 males, 7 females, mean age = 30 years, range 14-40). The patient profile consisted of six patients, diagnosed with left TLE, four of whom showed evidence of mesial temporal lobe sclerosis (MTS), one with small hippocampus bilaterally and one non lesional. A further six were diagnosed with right TLE, four of whom, with evidence of MTS, one with right posterior hippocampal abnormality and one non lesional. Finally, five patients had

bilateral TLE including one patient with left MTS, one with subtle right temporal focal polymicrogyria, one with lesional Cavernoma and two non lesional. All patients attended the epilepsy service at Beaumont Hospital. Diagnosis for each patient was made by clinical assessment and included a three-dimensional (3D) MR scan for each patient, reviewed by a radiologist, and this qualitative report was used to aid diagnosis. Informed consent was obtained for subjects involved. The medical research ethics committee at Beaumont Hospital Dublin approved this study.

4.2.2 MRI Scanning Parameters

Scanning was conducted using a 1.5 T GE MRI scanner using a standard head coil. A 3D spoiled gradient (SPGR) sequence was acquired from a sagittal localizer in the coronal plane. High resolution anatomical images (TR = 10.1 ms, TE = 4.2 ms, TI = 450 ms, flip angle = 20°, FOV =24 cm, slice thickness = 1.5 mm, matrix size = 256 × 256 × 124) were acquired for all subjects resulting in 124 × 1.5mm thick image slices.

4.2.3 *Stereological Volume Analysis*

The MR images were collected in DICOM format. Stereological estimates were subsequently carried out by a single rater using the specialized interactive software package *Measure,* developed at John's Hopkins, Maryland (Barta et al., 1995). Volume estimates were calculated using the Cavalieri principle which has previously been described (Roberts et al., 2000; Ronan et al., 2006). In this method a volume is initially separated into a series of equidistant section planes. In order to ensure that estimates are unbiased, the position of the first slice is random with respect to the volume (Figure 4.1). This generates a series of

systematic random slices through the volume. The Cavalieri principle states that the volume may be estimated by multiplying the sum of the area of the object of interest on each sample slice by the slice separation "T". At this stage a second level of sampling may be employed; the area of the object of interest may itself be estimated. This is done by superimposing at random a uniform grid of points on each slice (see Figure 4.1). Each point has an area associated with it, a/P. The area of interest is calculated by summing the total number of points (P) within the boundary of interest, and multiplying this by the area per point of the sample grid. By combining the information due to sectioning and point counting, the volume of the structure may be estimated (see Equation 4.1).

$$\hat{V} = T\frac{a}{P}\sum_{i=1}^{n} P_i \qquad \text{(Eq. 4.1)}$$

where P_i is the point counter of the i^{th} sample slice, and n is the total number of sample slices generated through sampling.

FIGURE 4.1

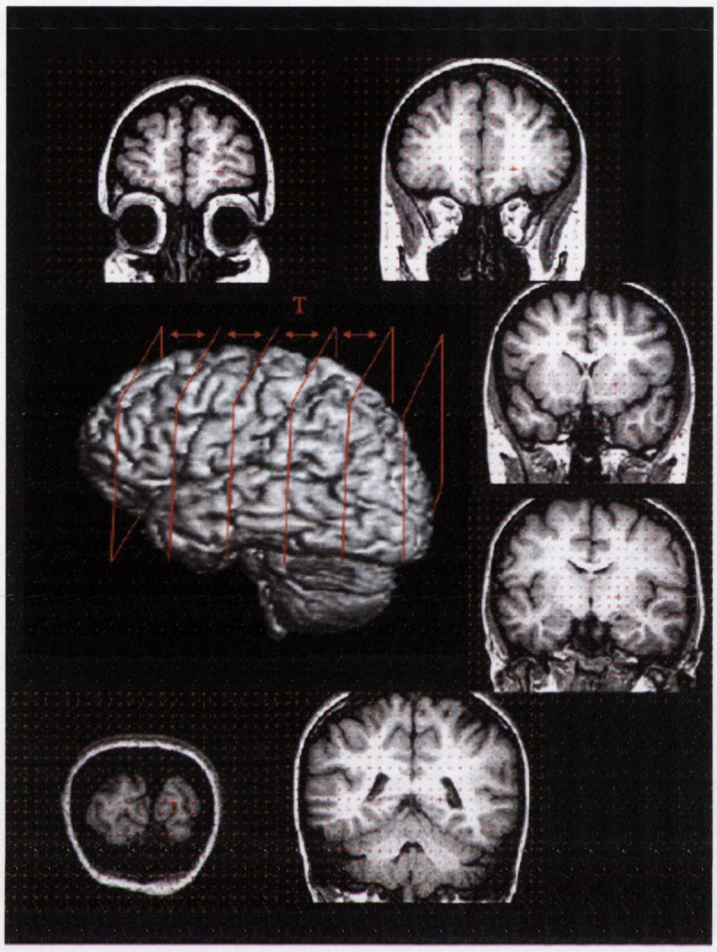


Figure 4.1: showing an example of 6 Cavalieri sections through a cerebral volume. "T" indicates the uniform slice separation. The position of the first slice is randomly generated within an interval [0, T]. A point grid with an associated area per point (a/P) is randomly overlaid on each slice to generate an area estimate. The final volume estimate is calculated by multiplying the total number of points marked within the object of interest by the slice separation and the area per point (see Equation 4.1).

Because of the randomness of sampling, stereological estimates may be considered unbiased, where the precision of the volume estimate obtained using the Cavalieri sections

method can be measured by its coefficient of error. The error prediction formula proposed by Gunderson and Jenson (Gundersen and Jensen, 1987) is shown in Equation 4.2 below. Thus, the precision of these estimates is determined by the intensity of sampling, that is, the number of points counted through the structure and the number of slices generated. In this paper, a sampling strategy was employed to generate approximately 350 – 400 points per brain over 10 – 11 equidistant slices. At this level of sampling, experiments conducted by the Neurophysics team at Beaumont hospital suggest the resultant variance of estimates to be less than 5%.

$$CE(V) = \left(\sum_{i=1}^{n} A_i \right)^{-1} \times \left[\frac{1}{12} \left(3 \sum_{i=1}^{n} A_i^2 + \sum_{i=1}^{n-2} A_i A_{i+2} - 4 \sum_{i=1}^{n-1} A_i A_{i+1} \right) \right]^{1/2} \quad \text{Eq. 4.2}$$

In this study a single rater carried out all stereological measurements. The intra-rater reliability of grey and white matter volumes was demonstrated to be acceptable and repeatable with an intraclass correlation coefficient (ICC) = 0.8, 0.79, for grey and white volumes, respectively based on a repeated measurement of 10 randomly selected subjects and sampled with a variance of less than 5%. In addition, the current study's stereological estimates agreed well with a similar stereological study carried out by Garcia-Fiana et al (2003) which reported a grey / white matter ratio of 1.17 based on MR image data and 1.04 based on post-mortem data; the present data observed a grey / white ratio of 1.18. A stereological estimate for white matter volume by (Tang, 1997) was 475cm^3 compared to our estimate of 521.3 cm^3.

4.2.4 *Automated Volumetric Analysis Techniques*

4.2.4.1 Strategy 1: Optimized VBM analysis

The DICOM format MR images were converted to the Analyze 7.5 image format via the software package MRIcro; http://people.cas.sc.edu/rorden/mricro.html and a subsequent voxel-based morphometry (VBM) image analysis was performed using the statistical parametric mapping software (SPM2; http://www.fil.ion.ucl.ac.uk/spm/). Voxel-based morphometry is a voxel-wise automated analysis technique performed on high resolution structural images to investigate structural differences in local concentrations of grey and white matter and volumetric differences of the brain when the 'optimized' VBM strategy including the modulation step is employed (see below for details). The standard VBM methodology incorporated three processing steps, namely (a) normalization to transform all images to a common standard space, (b) segmentation to partition the brain into grey, white and CSF tissue types and finally (c) smoothing by convolving with a Gaussian smoothing kernel to conform to the Gaussian field model and render the data more normally distributed to facilitate statistical analysis. The output from the VBM technique is a probability measure of a voxel being classified as grey or white tissue as determined following normalization and segmentation routines based on an *a priori* image template used for affine registration and tissue classification maps (see (Ashburner and Friston, 2000) and (Good et al., 2001b) for detailed descriptions of the standard and optimized VBM methods). The output from the analysis is commonly referred to in the literature as

grey/white matter concentration or tissue density and statistical analysis is performed to examine between-group differences in tissue concentrations/densities. More recently, the standard VBM strategy was adapted to overcome some of the criticisms and shortcomings of the technique in what is commonly referred to as the 'optimized VBM' strategy (see the methods section Good et al. 2001a). The optimized VBM strategy employs a 'modulation' step to correct for partial volume effects resulting from the non-linear normalization process. This 'modulation' or volume correction accommodates variance in brain size as it is normalized to standard space. The normalized images are convolved with the determinants of the Jacobian transformation matrix to achieve the volume correction as the image is transformed from its native space to a standard space to facilitate group comparisons. Volumetric between-group comparisons can thus be investigated using the optimized VBM technique incorporating the volume modulation step. This study incorporated the optimized VBM analysis strategy to specifically examine volumetric change (Draganski et al., 2004; Good et al., 2001b; Good et al., 2001a; Keller et al., 2004). A major source of concern with VBM analyses is the possible error induced by poor image co-registration during normalization (Ashburner and Friston, 2001; Bookstein, 2001). The residual error of the mean was reported (Fein et al., 2006a) to be effectively reduced by up to 30% by first removing the skull and scalp from the brain images. Thus, all images were skull stripped using FMRIB's Brain Extraction Tool (BET) (Smith, 2002) skull stripping routine; http://www.fmrib.ox.ac.uk/fsl/ and these images were used as the input for the fully automated techniques used in this paper except for FSL SIENAX which uses unstripped brains as an input but performs the skull stripping routine in the initial stages of its scripted processing pipeline.

Template generation

Template images for normalization of grey, white and CSF tissue classification maps were constructed from the complete data set of 34 subjects. All images were spatially normalized to the same stereotaxic space by a process of linear and non-linear transformations based on the Montreal Neurological Institute (MNI) coordinate system and registered to a template image compiled from the skull stripped 152 brain average of the MNI brain included in the FSL tool box. A mean normalized image was then created from the 34 normalized images and smoothed using an 8mm FWHM Gaussian smoothing kernel. All normalized images were segmented into grey matter, white matter and CSF partitions using *a priori* grey, white and CSF maps provided in the SPM software package which use a mixture model cluster analysis for the identification of voxel intensities for tissue classification purposes. A study specific template for grey, white and CSF tissue was made from the average segmented image files and smoothed using an 8mm FWHM Gaussian kernel.

The output from the 'optimized' VBM analysis resulted in an optimally normalized, segmented and modulated image file. Each image file was smoothed with an 8 mm FWHM kernel and was used for statistical analysis to examine regional differences in the volumes of grey and white matter.

4.2.4.2 Strategy 2: FSL FAST analysis

All images were skull stripped using the FSL BET skull stripping routine; http://www.fmrib.ox.ac.uk/fsl/ and these images were used as an input to the FSL toolbox to perform an automated segmentation routine using FMRIB's Automated Segmentation

Tool (FAST) (Zhang et al., 2001a) to obtain separate grey, white and CSF tissue maps. The output files consisted of tissue type segmented files including partial volume estimates. These grey and white matter tissue images were then used to calculate the total brain volumes (grey + white matter) and the grey/white matter ratio for each subject in their native space using the FSL *avwstats* tool provided in the additional FSL utilities. At this stage the images were normalized to standard MNI space using FMRIB's Linear Registration Tool (FLIRT) (Jenkinson et al., 2002; Smith, 2002) and smoothed using an 8mm FWHM Gaussian kernel for the purpose of statistical comparisons examining regional volume differences in grey and white matter between controls and the clinical group.

4.2.4.3 Strategy 3: FSL SIENAX

Here FMRIB's Structural Image Evaluation using Normalization of Atrophy (cross sectional single time point brain analysis) (SIENAX) was employed (Smith et al., 2004). SIENAX starts by extracting brain and skull images from the single whole-head input data (Smith, 2002). The brain image is then affine-registered to MNI152 space (Jenkinson et al., 2002; Jenkinson and Smith, 2001) using the skull image to determine the registration scaling; this is primarily in order to obtain the volumetric scaling factor, to be used as a normalization for head size. A standard brain image mask, (derived from the MNI152 and slightly dilated) is then transformed into the original image space (by inverting the normalizing transform found above) and applied to the brain image. This helps ensure that the original brain extraction does not include unwanted features such as eyeballs. Next, tissue-type segmentation including partial volume estimation is carried out on the masked

brain using FAST (Zhang et al., 2001a) in order to calculate total volume of brain tissue (including separate estimates of volumes of grey matter, white matter, peripheral grey matter and ventricular CSF). For the purpose of between-group comparisons of regional volumetric differences in grey and white matter, all images were then smoothed using an 8mm FWHM Gaussian kernel and normalized to standard MNI space using the previously calculated transformations determined in the SIENAX automated processing pipeline using FMRIB's Linear Registration Tool (FLIRT) (Jenkinson et al., 2002; Smith, 2002).

To summarize, volume measurements for grey and white matter volumes will be calculated using Stereology as the 'gold standard' measurement technique and will be compared to three automated techniques including VBM, FSL FAST and FSL SIENAX (see Figure 4.2). The VBM technique employs a normalization step including linear and non-linear transformations to register each image to standard stereotactic space, and uses *a priori* tissue maps for grey matter, white matter, and CSF during segmentation. Images are modulated to correct for the effect of nonlinear warping where some areas of tissue will grow and other shrink as they are transformed to standard space. In effect, modulation preserves the initial absolute tissue volumes by multiplying each voxel of the segmented image by its Jacobian determinants thus rescaling them back to their original volumes. Finally, all images are smoothed to facilitate statistical group comparisons. By comparison, FSL FAST carries out the image segmentation in native space based on a hidden Markov Random Field Model and Expectation Maximization algorithm (HMRFM-EM) for tissue segmentation. Once the segmentation process is complete, absolute volumes are obtained for each tissue type image. Thus normalization to standard space is not employed and only becomes necessary to facilitate group comparisons. FSL SIENAX incorporates both normalization and segmentation steps to generate measures of grey and white matter volumes. It differs from FAST in that it uses a normalization step based on both brain and skull extraction steps to correct for head size variance and also employs the use of a standard space mask to remove orbits and optic nerves and cut the brain stem. Once the segmentation is completed, the image is then transformed back to its native space by applying the inverse transform and finally yielding a measure of grey and white matter volume.

FIGURE 4.2

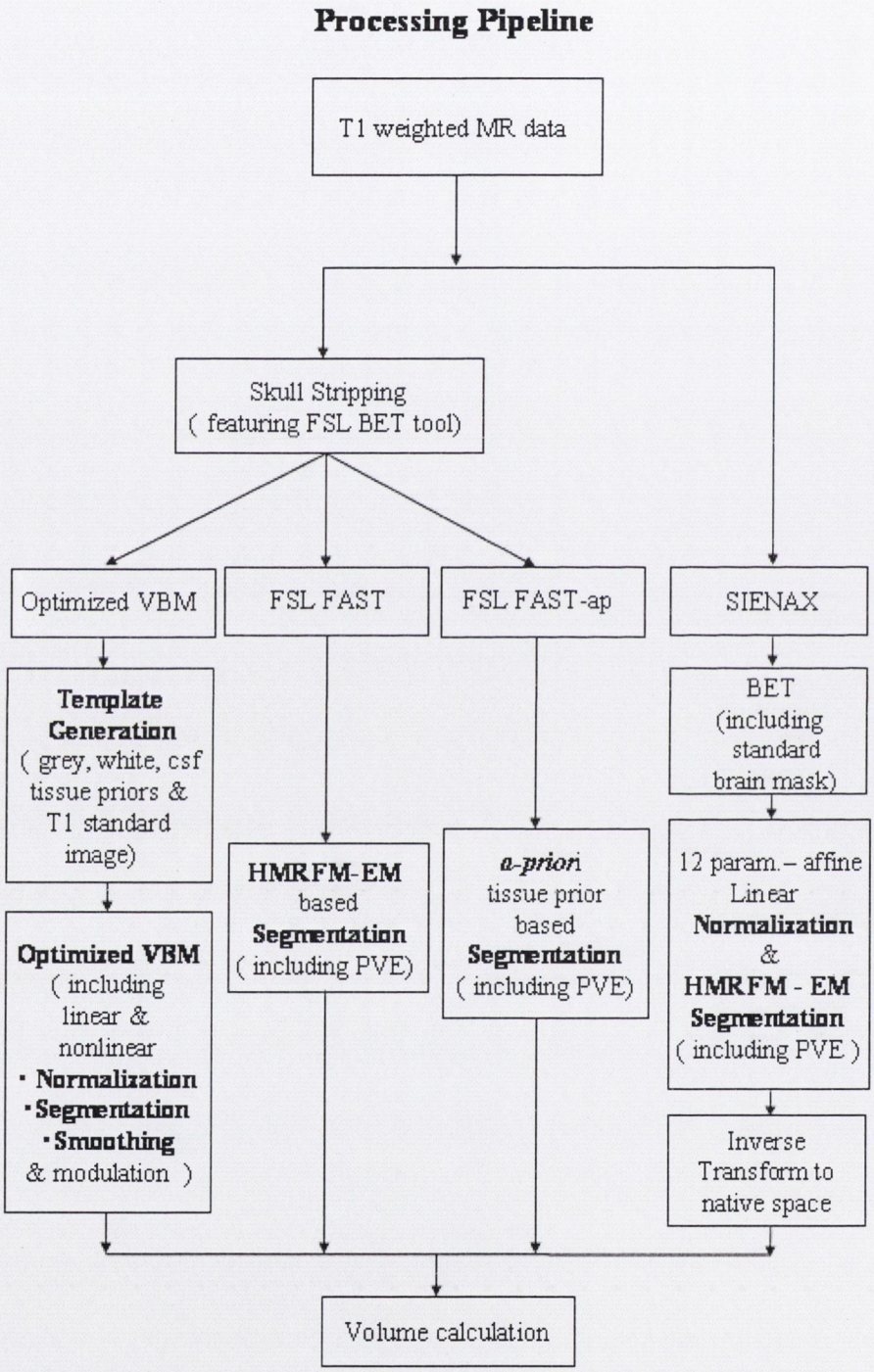


FIGURE 4.2: Flow chart representation detailing each of the automated analysis techniques employed.

A second variation of the FSL FAST method was used to provide an exploratory examination of the effect of an *a priori* based segmentation instead of the default HMRFM-EM based method. This was performed on the data of the controls only to exclude any possible influences attributable to the patient group where normalization, co-registration, and segmentation could be negatively affected by the presence of the clinical condition itself. These results are reported under the FSL-ap category in FIGURES 4.3 and TABLES 4.3

4.2.5 Statistical Comparison of Analysis Strategies

Statistical comparisons were carried out using SPSS (version 12.01 for Windows) and Data Desk (DataDescription, Ithaca, NY). A mixed factorial analysis of variance (ANOVA)(two groups x four measurement techniques) with Bonferroni-corrected *post hoc* pairwise comparisons was conducted for each dependent measure (i.e. grey and white matter volumes, grey/white ratio and TIV). The relationship between stereology measures to those of the automated techniques was initially examined by means of Pearson's r correlation analyses. Although Pearson's r correlation analysis identifies linear relations between two measures, it does not capture baseline shifts between them and may thus be misleading when used to assess agreement between two measures (Bland and Altman, 1986; Bland and Altman, 2003). Consequently, the agreement between stereological measures and each of the automated techniques and hence the interchangeability of the measures determined by two different techniques was not based on correlation values only. Particular attention was paid to the mean difference between the measures, i.e. the bias between the measures where

agreement and interchangeability of the measures is generally accepted to improve as the bias reaches zero (Bland and Altman, 1986; Brazdzionyte and Macas, 2007; Chinn, 1990; Cliff et al., 1999).

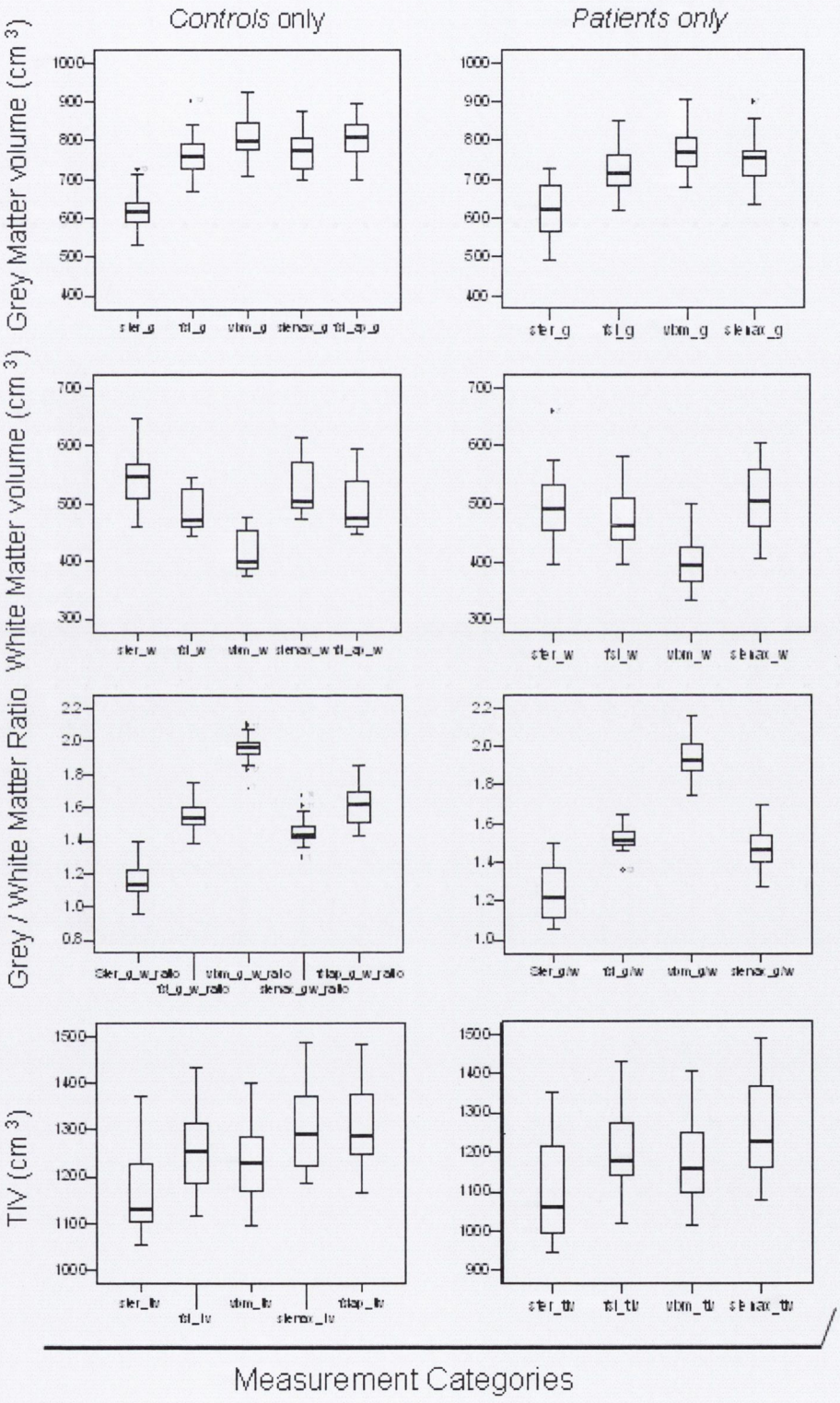
4.2.6 *Statistical Analysis of Voxelwise Volumetric comparisons (fully automated techniques)*

All segmented images were normalized to standard space using the tools of each individual analysis technique (FLIRT for all output images from FSL analysis) or by applying the previously calculated FLIRT transformations to standard space to the segmented images in the case of SIENAX. The modulated segmented images of VBM are in standard space as this step occurs as part of the automated processing pipeline with SPM. All normalized and segmented images were smoothed with an 8 mm FWHM Gaussian filter and were used to conduct a series of voxelwise t-tests comparing the TLE patient group to the control group for each method. Significant voxels passed a voxelwise statistical threshold ($t = 3.02$, $p \leq .005$, $df = 32$) for grey and white matter and were required to be part of a larger cluster of contiguous significant voxels (VBM = 1381 µl and 1343 µl, FSL FAST = 1466 µl and 1466 µl, SIENAX = 1467 µl and 1522 µl, for each methods grey and white matter maps, respectively. The cluster size criterion differed between the various fully automated techniques and tissue-type comparisons as this is based on the number of non-zero voxels in the voxelwise t-tests. The cluster size was determined through Monte Carlo simulations which, when combined with the voxelwise statistical criterion, resulted in a 5% probability (corrected) of a cluster surviving due to chance.

4.3 RESULTS

The mean grey and white matter volumes for all subjects were estimated at 617.3cm^3 (s.d. 63cm^3) and 521.3cm^3 (s.d. 64cm^3) respectively for stereological methods, 791.9cm^3 (s.d. 61cm^3) and 408.7cm^3 (s.d. 39cm^3) respectively for VBM methods, 740cm^3 (s.d. 65cm^3) and 480cm^3 (s.d. 43cm^3) respectively for FSL FAST, and 757cm3 (s.d. 61cm^3) and 518cm^3 (s.d. 55cm^3) respectively for FSL SIENAX (see FIGURE 4.3). In the case of the VBM and FSL FAST techniques used, the effect of *a priori* map segmentation was examined as the FSL toolbox permits the segmentation process to run using the MNI grey and white *a priori* maps option instead of the HMRFM-EM strategy. Based on the restricted sample of controls only data, the FSL FAST analysis was repeated using the *a priori* based segmentation. The results revealed that the measurements for mean grey and white matter volumes increased from 752 to 804 cm^3 and 478 to 495 cm^3, respectively. Thus by using the *a priori* maps for segmentation purposes resulted in an increase in the estimate of mean grey matter volume (52 cm^3 or 6.9% of the original estimate) to the extent where mean grey mater volume from both VBM and FSL-ap were found to match. The white matter volume estimate produced by FSL FAST was found to increase when based on the *a priori* segmentation option, but to a much lesser extent (17 cm^3 or 3.55% of the original estimate).

FIGURE 4.3


Controls only
Patients only
Grey Matter volume (cm 3)
White Matter volume (cm 3)
Grey / White Matter Ratio
TIV (cm 3)
Measurement Categories

4.3.1 Mixed Factorial ANOVA

A mixed factorial ANOVA was performed. The Group x Analysis technique revealed no significant main effect of group for grey matter ($F_{(1, 32)} = 1.72$, $p = 0.20$), white matter ($F_{(1, 32)} = 2.30$, $p = 0.14$), G/W ratio ($F_{(1, 32)} = 0.38$, $p = 0.54$) or TIV ($F_{(1, 32)} = 2.13$, $p = 0.15$). The main effect of measurement technique used was found to be significant for grey matter ($F_{(1.58, 50.68)} = 293.72$, $p \leq 0.0001$), white matter ($F_{(1.59, 50.97)} = 181.028$, $p \leq 0.0001$), G/W ratio ($F_{(1.78, 56.81)} = 393.78$, $p \leq 0.0001$) and TIV ($F_{(1.44, 46.16)} = 122.43$, $p \leq 0.0001$) (see Figure 4.4). *Post-Hoc* pairwise comparisons revealed grey matter volume to be significantly less for stereology relative to each of the fully automated measures ($\alpha = 0.05$ corrected). White matter volume estimates were found to be significantly less for the automated measures relative to stereology with the exception of SIENAX where no significant difference for white matter estimates were found ($\alpha = 0.05$ corrected). The G/W matter ratio differed significantly between stereology and all automated techniques. The TIV differed significantly between stereology and all automated techniques.

FIGURE 4.4

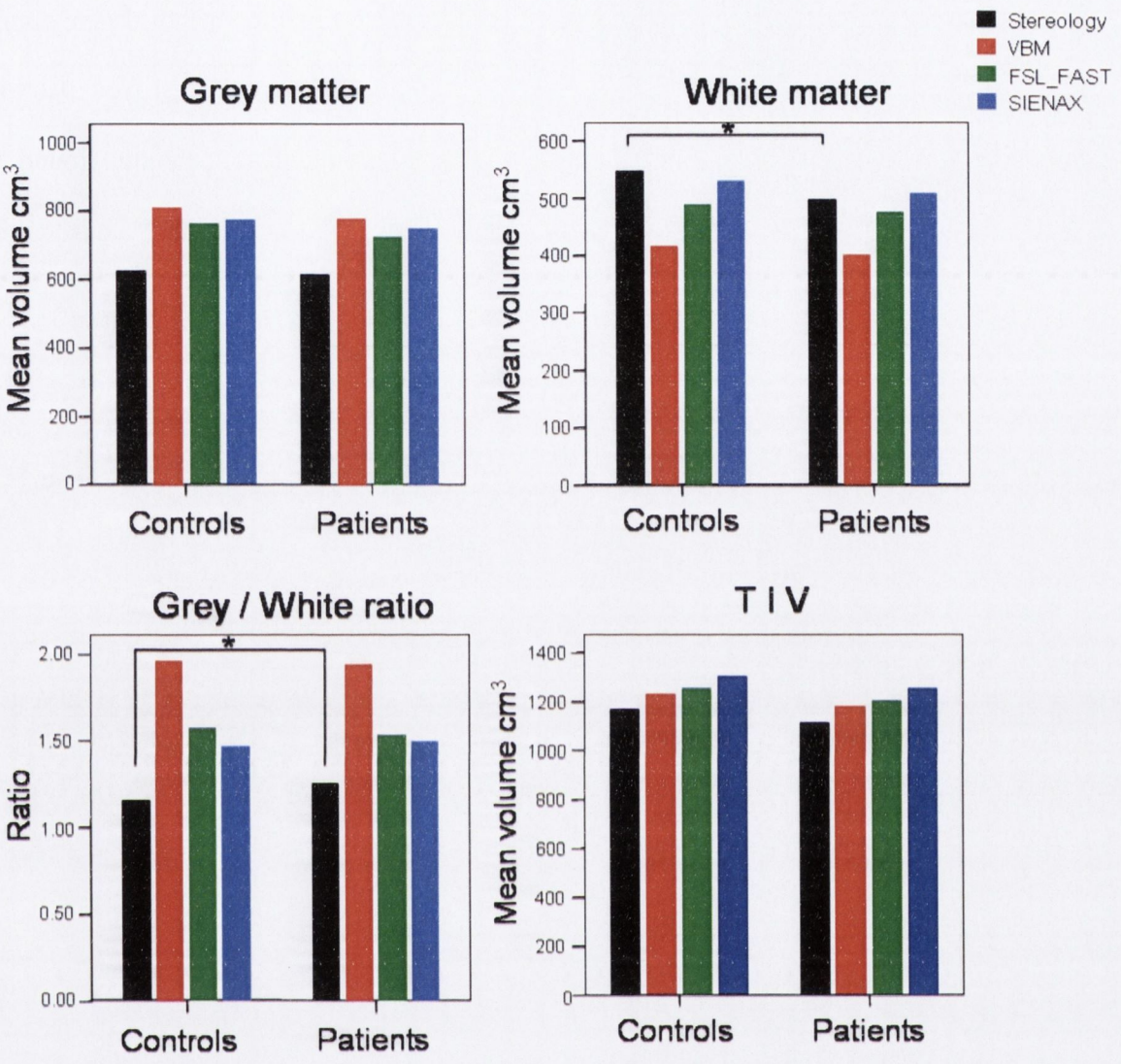


FIGURE 4.4: Bar chart representation of mean grey matter, mean white matter, G/W ratio and TIV for controls and patients. Grey matter measures were significantly different between all methods but no significant differences were identified between grey matter volumes for controls and patients by any of the methods. White matter measures were significantly different between all methods except for those between stereology and SIENAX where no significant difference was found. Stereology identified significant

Finally, group x technique interactions were significant for white matter ($F_{(1.59,\ 50.97)}$ = 4.598, p = 0.02) and G/W ratio ($F_{(1.78,\ 56.81)}$ = 3.744, p = 0.034). *Post-Hoc* pairwise comparisons between Controls and Patients for each measurement technique found no significant group difference for grey matter volume and TIV. Stereological measures for white matter volume and the grey / white ratio were found to differ significantly between the two groups (see TABLE 4.1). By comparison, the fully automated techniques failed to detect any significant between-group differences in any of the dependent measures.

TABLE 4.1

Controls vs. Patients Group mean volume comparison				
Measurement Method	*P-values*			
	Grey matter	White Matter	G/W matter ratio	TIV
Stereology	*0.67*	0.027	0.045	*0.133*
VBM	*0.098*	*0.314*	*0.649*	*0.145*
FSL	*0.088*	*0.434*	*0.16*	*0.161*
Sienax	*0.306*	*0.235*	*0.485*	*0.236*

4.3.2. Correlation Analysis

Correlations between stereology and the automated techniques for the entire dataset demonstrated significant positive correlations for all measures except grey/white ratio. In addition, the measures from all automated techniques demonstrated significant positive correlations with one another ranging from r = 0.93 – 0.99, p < 0.01 for all measures excluding G/W ratio (see TABLE 4.2) and were consistently higher than those between stereology and the automated techniques.

TABLE 4.2

Stereology and Automated Measurement Correlations (Controls and Patients)				
Measurement Comparison	Grey matter Pearson's r / sig	White Matter Pearson's r / sig	G/W ratio Pearson's r / sig	TIV Pearson's r / sig
Stereology vs. VBM	0.71 **	0.74 **	*0.03*	0.87 **
Stereology vs. FSL	0.72 **	0.74 **	*-0.002*	0.88 **
Stereology vs. Sienax	0.71 **	0.75 **	*0.14*	0.87 **
VBM vs. FSL	0.96 **	0.95 **	0.54**	0.99**
VBM vs. SIENAX	0.93 **	0.94 **	0.72**	0.97 **
FSL vs SIENAX	0.94 **	0.95 **	0.64**	0.98 **

Note

** Correlation is significant at 0.01

G/W = grey / white matter Ratio : TIV = total Intracranial volume (grey + white)

Correlations between stereology and the automated techniques the showed only minor improvement when the dataset was restricted to the controls only (see Table 4.3). Measurements based on the restricted dataset also included the additional measurement category of FSL FAST ap (where FAST was forced to use tissue priors for its segmentation).

TABLE 4.3

Stereology and Fully Automated Measurement Correlations (Controls only)				
Measurement Comparison	Grey matter Pearson's r / sig	White Matter Pearson's r / sig	G/W ratio Pearson's r / sig	TIV Pearson's r / sig
Stereology vs. VBM	0.742 **	0.603*	*0.068*	0.820**
Stereology vs. FSL	0.766**	0.571*	*0.129*	0.827**
Stereology vs. Sienax	0.751**	0.684**	*0.398*	0.803**
Stereology vs. FSL-ap	0.732**	0.726**	*0.462*	0.799**
VBM vs. FSL	0.961**	0.943**	0.639**	0.994**
VBM vs. SIENAX	0.935**	0.98**	0.842**	0.984**
FSL vs SIENAX	0.952**	0.948**	0.76**	0.98**
FSL-ap vs VBM	0.933**	0.949**	0.798**	0.989**
FSL-ap vs FSL	0.936**	0.902**	0.564*	0.993**
FSL-ap vs SIENAX	0.956**	0.973**	0.939**	0.976**

Note

** Correlation is significant at 0.01 : * Correlation is significant at .05

Values in italics failed to reach significance

G/W = grey / white matter Ratio : TIV = total Intracranial volume (grey + white)

FSL-ap = FSL FAST using 152 MNI a-prior maps of grey white and CSF for segmentation

The bias as determined by the post-hoc pairwise comparisons from the mixed factorial ANOVA are reported in Table 4.4.

TABLE 4.4

	Patients and Controls								
	Stereology vs VBM			***Stereology vs FSL FAST***			***Stereology vs SIENAX***		
	Standard Deviation (SD)		Bias	Standard Deviation (SD)		Bias	Standard Deviation (SD)		Bias
	(Mean of Measures)	(Diff between Measures)	(mean diff. btn measures)	(Mean of Measures)	(Diff between Measures)	(mean diff. btn measures)	(Mean of Measures)	(Diff between Measures)	(mean diff. btn measures)
GM	58.04	47.86	174.60	60.33	48.45	123.47	58.03	47.70	139.82
WM	48.90	44.02	112.68	50.52	43.60	40.65	56.21	43.77	3.65
G/W ratio	*0.0885*	*0.1726*	*0.7490*	0.0825	*0.1654*	0.3489	*0.0960*	*0.1669*	0.28
TIV	101.12	54.39	61.92	104.67	53.30	82.81	106.75	55.91	136.17

4.3.3. Voxelwise Comparison of fully automated techniques

Complete volumetric analyses at 1mm isotropic voxel resolution were conducted for grey and white matter tissue types using VBM, FSL FAST and SIENAX.

Grey Matter Voxelwise Comparison

VBM yielded eight statistically significant clusters of regional volumetric differences between controls and patients in grey matter. FSL FAST identified 12 regions of localized volumetric change in grey matter (see TABLE 4.5). Nine of these clusters showed a grey matter decrease in patients with respect to controls and three regions (the right uncus, the left middle temporal gyrus and the right uvula) showed a grey matter increase in patients when compared to controls. SIENAX identified nine significant clusters in grey matter. The grey matter cluster maps from each method were combined to form a composite cluster map identifying where the clusters from the three methods overlapped. This resulted in only two overlapping clusters common to all methods, namely in the right declive and the right superior parietal lobule. To determine the extent to which inconsistencies between the different methods were a thresholding artefact, the t-test maps from each method were subjected to various uncorrected threshold levels of $p \leq 0.005$, 0.01, and 0.05. Of the 12 clusters identified by the corrected cluster map from the FSL FAST analysis (chosen as this yielded the largest number of significant clusters), nine showed overlap between all methods (VBM, FSL FAST and SIENAX) at a significance of .05 uncorrected (see Figure 4.5). However, as can be seen in Figure 4.6, at this very low threshold very many other

regions of between-group differences were observed for the different techniques that did not overlap across techniques.

White Matter Voxelwise Comparison

FSL FAST identified nine significant clusters (0.05 corrected) for white matter (see TABLE 4.6 & Figure 4.7). VBM yielded two statistically significant clusters of regional volumetric change in white matter and SIENAX identified none. No white matter cluster overlaps between all three methods were found at 0.05 corrected. Five clusters showed an overlap between all methods at 0.05 uncorrected (see TABLE 4.6), namely in the right uncus, right anterior cingulate, left superior temporal gyrus, left precuneus and right post central gyrus. Overlap in the left parahippocampus based on the 0.05 uncorrected maps from all three automated techniques (VBM, FSL FAST and SIENAX) are shown Figure 4.7 (c) and (d).

TABLE 4.5

Cluster Size (µl)	Location : Lobe /gyrus	X Y Z MNI Coordinates	Brodmann Area	Volume Change direction	Cluster Overlap Between Methods			
					0.05	0.05	0.01	0.005
					corrected	uncorrected		
7528	Right Declive	-10 -88 -30	-	+ve	■	■	■	■
3950	Right Uncus	-20 -6 -48	36	+ve		■		
3773	Left Superior Temporal	58 -16 8	41 / 42	+ve		■		
2784	Right inferior frontal	-60 18 4	45	+ve		■		
2576	Right Uvula	-18 -68 -32	-	-ve		■	■	
2395	Right Superior Parietal	-18 -80 62	7	+ve	■	■	■	■
2124	Right Inferior Temporal	-54 -16 -44	20	+ve		■		
2094	Left Precuneus	44 -82 40	19	+ve		■		
2030	Left Middle Temporal	74 -34 -8	21	-ve				
1908	Left Lingual / Parahippocampal	18 -58 -6	19	+ve				
1831	Left Medial frontal / Anterior cingulate	12 40 28	9	+ve		■	■	
1763	Right Uncus	-32 0 -34		-ve				

Table 4.5 shows significant clusters (0.05 corrected) of grey matter volumetric change determined by FSL FAST. All coordinates given are in MNI standard space based on the MNI 152 brain atlas. The closest Brodmann area for each cluster is given where possible.

The direction of volume change is indicated as +ve where controls show greater grey matter volume than patients and –ve (negative) where controls show reduced grey matter volume compared to patients. The presence of an overlap between all three methods (VBM, FSL FAST and SIENAX) for each cluster determined by FSL FAST is also shown at 0.05 corrected and various uncorrected threshold levels of 0.005, 0.01, and 0.05 as indicated by ■ in each column. The size of each cluster is listed in microlitres.

TABLE 4.6

Cluster Size (μl)	Location : Lobe /gyrus	X Y Z MNI Coordinates	Brodmann Area	Volume Change direction	Overlap 0.05 uncorrected
6005	Right Uncus	-32 -3 -37	36	+ve	■
4659	Right Parahippocampal	-42 -23 -18	20	+ve	
3403	Right Anterior Cingulate	-9 41 5		-ve	■
3200	Right Uvula (cerebellum)	-15 -72 -33		-ve	
2835	Left Medial Frontal	9 41 27	9	+ve	
2747	Left Superior Temporal	64 -22 5		-ve	■
2520	Left precuneus	9 -54 45	7	+ve	■
1724	Right Postcentral	-39 -29 46	40	-ve	■
1477	Left Superior Frontal	13 68 5	10	+ve	

Table 4.6 shows significant clusters (0.05 corrected) of white matter volumetric change determined by FSL FAST. All coordinates given are in MNI standard space based on the MNI 152 brain atlas. The closest Brodmann area for each cluster is given where possible. The direction of volume change is indicated as +ve where controls show greater white matter volume than patients and –ve (negative) where patients show increased white matter volume compared to controls. The presence of an overlap between all three methods (VBM, FSL FAST and SIENAX) for each cluster determined by FSL FAST is also shown at 0.05 uncorrected as indicated by ■ in the table. The size of each cluster is listed in microlitres.

FIGURE 4.5

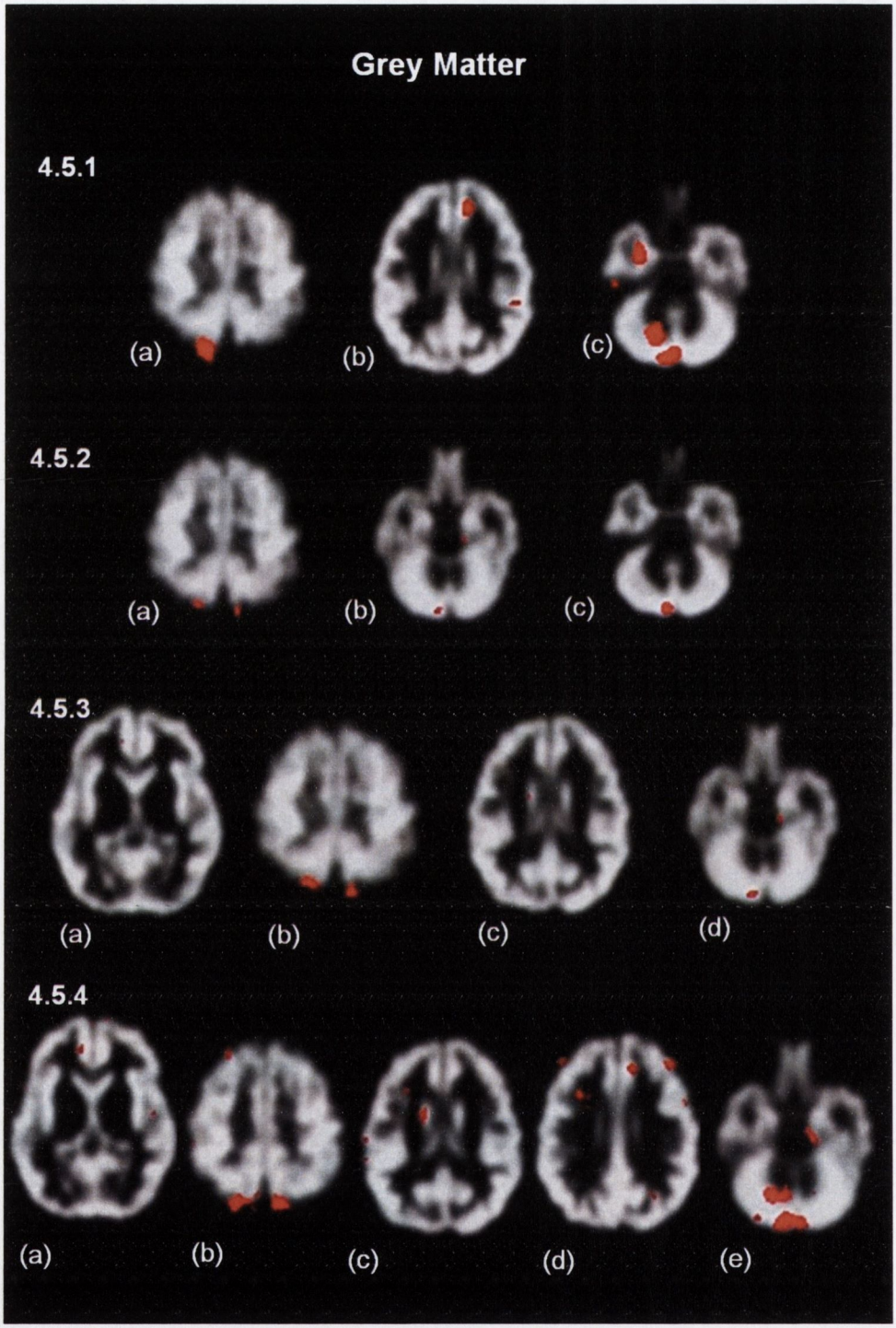


Figure 4.5 shows a voxelwise group t-test comparison of Controls versus TLE patients for grey matter. Figure 4.5.1 identifies regions of volumetric difference determined

by FSL FAST for controls versus TLE Patients (0.05 corrected) where, (a) shows right superior parietal lobule, (b) shows left medial frontal gyrus /anterior cingulate, (c) shows right uvula and declive. Figure 4.5.2 shows identified clusters that form part of an overlap between clusters common to all three methods at an uncorrected threshold of 0.005. The variation in the extent of the overlap between these clusters can be seen at 0.01 uncorrected (Figure 4.5.3) and at 0.05 uncorrected (Figure 4.5.4).

FIGURE 4.6

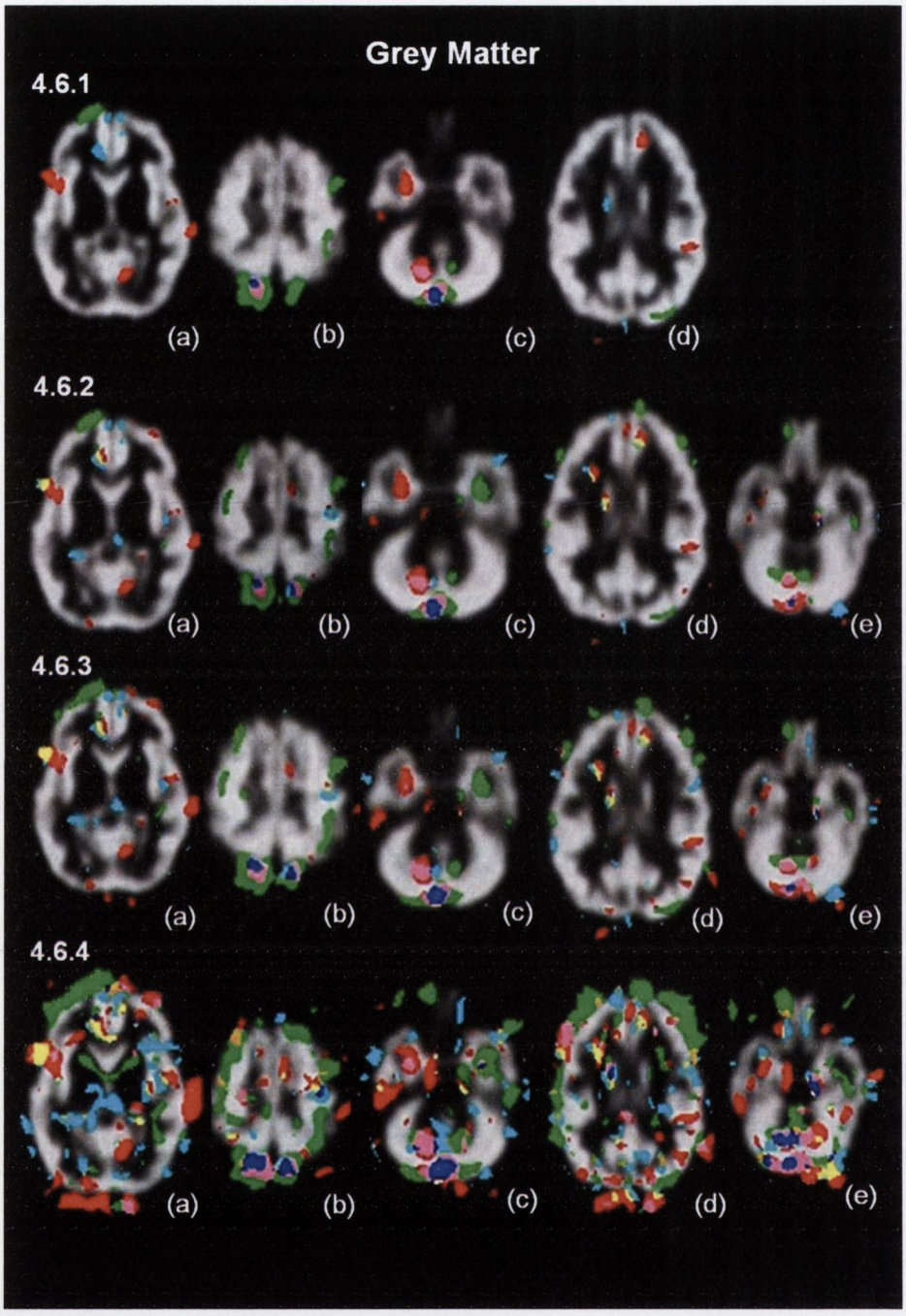


Figure 4.6 shows a composite voxelwise group t-test comparison of Controls versus TLE patients for grey matter featuring clusters identified by VBM (shown in light blue), FSL FAST (shown in red), and SIENAX (shown in green). Regions of overlap between VBM and FAST are shown in yellow, SIENAX and VBM are

shown in orange, FAST and SIENAX shown in pink and finally common overlap featuring all three techniques are shown in dark blue. Figure 4.6.1 identifies regions of volumetric difference for controls versus TLE Patients (0.05 corrected). Figure 4.6.2 shows the composite cluster maps at an uncorrected threshold of 0.005.). Figure 4.6.3 shows the composite cluster maps at an uncorrected threshold of 0.01.). Figure 4.6.4 shows the composite cluster maps at an uncorrected threshold of 0.05.

FIGURE 4.7

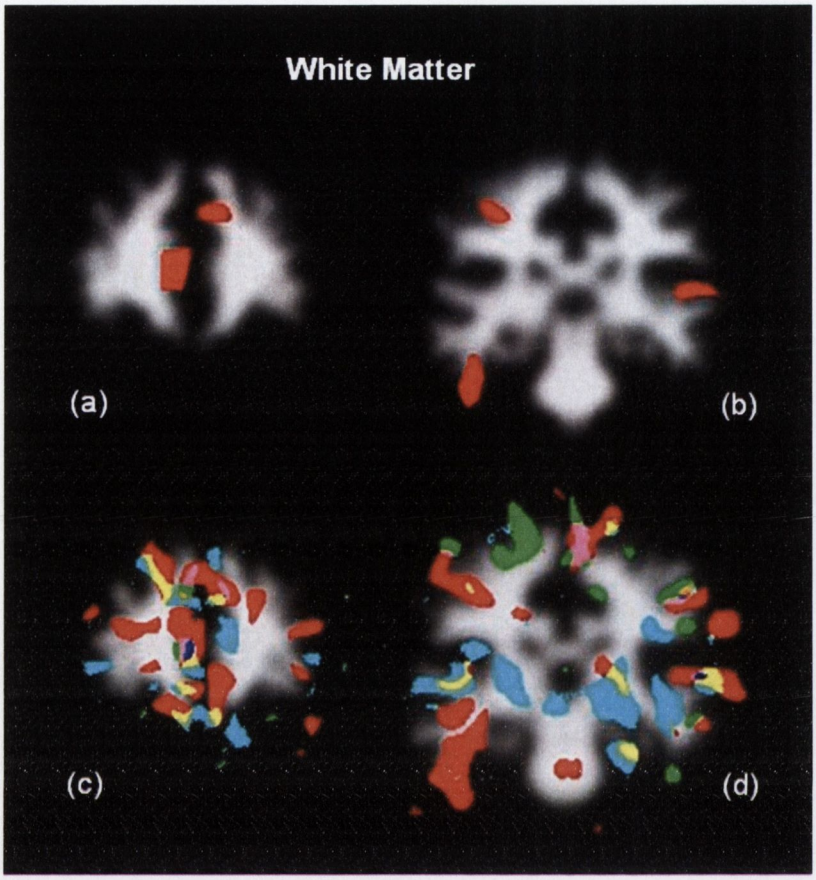


Figure4.7: shows (a) a region of volumetric difference in the right anterior cingulate and (b) the left superior temporal gyrus where patients had significantly less (0.05 corrected) white matter volume than controls as determined by FAST. Composite white matter maps (c) and (d) of all three voxelwise group t-test comparison maps from all automated techniques for Controls versus TLE patients featuring clusters (at an uncorrected threshold of 0.05) identified by VBM (shown in light blue), FSL FAST (shown in red), and SIENAX (shown in green). Regions of overlap between VBM and FAST are shown in yellow, SIENAX and VBM are shown in orange, FAST and SIENAX shown in pink and finally common overlap featuring all three techniques are shown in dark blue.

4.4 DISCUSSION

The choice of stereology as a validation tool for fully automated volumetric measurement techniques is due to the mathematically unbiased nature of the method for geometric property estimation (Gundersen and Jensen, 1987). Several studies have previously demonstrated the accuracy of stereology for volume estimates (Garcia-Finana et al., 2003; Garden and Roberts, 1996; Gong et al., 2004; Gong et al., 2000; Keller et al., 2002a). In this study, whole-brain volume estimates of grey and white matter were found to be significantly different between the stereological measurements and those of the fully automated techniques. The present study's application of the automated techniques would appear to be in line with previous applications. For example, the VBM analysis resulted in a mean absolute grey to white matter ratio of 1.90 which agrees with previous VBM studies where a mean absolute grey to white matter ratio is reported as 1.89 (Good et al., 2001a; Good et al., 2001b; Paillere-Martinot et al., 2001). Our analysis using the FSL software toolbox yielded a mean volume grey to white matter ratio of 1.45 which once again closely agrees with previously published estimates of 1.49 using this method (Fotenos et al., 2005). The preferential atrophy of cerebral white matter over grey matter has previously been reported in the literature (Hermann et al., 2002; Ronan et al., 2007). To exclude the possibility that a loss of grey-white differentiation associated with temporal lobe pathology may affect the reliability of the volume measurements produced by stereology and fully automated techniques, the analyses were repeated with the control only dataset and still revealed significant measurement differences between the techniques (data not shown). In contrast, the correlational analyses observed consistently high correspondences between the

techniques (see Table 4.2). The apparent contradiction between the identification of significant measurement differences between the techniques and the presence of highly correlated measures can be explained by the presence of a baseline shift (tissue bias) between the automated techniques and the stereology measurements wherein the automated techniques consistently overestimate grey matter volume (see Table 4.4). This bias is notable given the preponderance of grey matter differences that are detected with VBM analyses even in diseases where there are known white matter differences such as schizophrenia and TLE. In the present data, the impact of this bias was to obscure group differences in white matter which were detected using the stereology measurements but not the automated measurements with the exception of SIENAX where no significant white matter volume difference was identified when compared to stereological measures as the bias between these two measures was close to zero (see Table 4.4).

To understand the source of this grey matter bias, it should be borne in mind that the automated volume measurements can be influenced by many factors. Geometric properties of the structure being measured where matches between small cortical or deep grey matter structures may not be exact (Good et al., 2001b) or brain regions with large anatomical variability leading to poor image registration and lower sensitivity of VBM to detect changes in these regions (Tisserand et al., 2002), can affect the measurements. The composition of white matter tissue tends to be more fibrous in nature and can often be surrounded by a thick ribbon of cortical grey matter tissue (in the cerebellum for example). Thus, both the size and nature of the white matter could lead to it being mistakenly

classified as grey matter and hence impact the overall accuracy of the white matter volume reported by fully automated techniques. Optimization of the structural image acquisition sequence has been demonstrated to improve the grey and white matter discrimination of small structures which should lead to a more accurate volume measurement if the region of interest incorporates both tissue types (Deichmann et al., 2000).

Registration or 'normalization' involves transforming one image to the coordinate space of another 'template' image. The transformation is then iteratively optimized to minimize the dissimilarity between the two images. Most recent registration methods use image intensity-based cost functions rather than geometrically based functions to perform registration as these have been shown to yield a more accurate result (Insert ref west et al. 1997 here.). Hence, poor registration could lead to localization inaccuracies between the transform image and the template which in turn could affect tissue volume estimates. Both VBM and FSL FLIRT feature intensity based registration. FSL employs 12 stage linear affine registration that features a hybrid global–local optimization method to reduce the likelihood of producing misregistrations due to being trapped by local minima (Jenkinson et al., 2002; Jenkinson and Smith, 2001). VBM utilizes a normalization process incorporating a 12 stage linear affine registration and nonlinear transformations in its processing pipeline to warp all images to a common stereotaxic space. Consequently, optimized VBM does not attempt to match every cortical structure exactly (very high resolution spatial normalization achieved by high dimensional warping) but instead opts for a compromise where global head shape differences are accommodated and modelled. VBM uses a non-label based approach to identify a nonlinear spatial transformation that

minimizes the difference between an object and a template image, where both are treated as unlabeled continuous processes. The nonlinear warping is modelled by a linear combination of smooth basis functions and a fast algorithm for determining the optimum combination of basis functions. Bayesian statistics or 'regularization' is utilized to obtain a more robust fit (Ashburner and Friston, 1999). Hence, both the degree of regularization and the number of basis functions (discrete cosine transforms) can be varied to achieve the extent of the nonlinear warping used. This is not always considered or adjusted when routinely applying the VBM methodology to datasets. Thus, because white matter has more highly curved small structures than grey matter, it is likely that these features may not be modelled as well as the grey matter regions without explicit non-linear parameter consideration and may result in these structures being smoothed out. This may in turn have a negative effect on the amount of white matter measured.

In the case of the FSL FAST technique, the analysis is performed in the image's native space thus avoiding possible sources of error associated with misalignment (Bookstein, 2001; Tisserand et al., 2002). SIENAX uses the brain and skull images derived from the initial step of skull stripping using BET, to carry out constrained registration where the brain and skull images are registered to the standard 152 average MNI brain using the skull as the scaling constraint. Hence, brain tissue volume will be relative to a "normalized" skull size (Smith, 2002; Smith et al., 2004; Zhang et al., 2001a). Poor image registration between the input image and the standard space template image could thus result in certain boundaries and structures being inaccurately localized when transformed to the standard template. When the transformed image undergoes segmentation to identify the different tissue components based on an *a priori* tissue map, this misalignment could result in a

localized region being associated with the wrong tissue parameters as defined by the prior map and ultimately lead to possible tissue misclassification. Thus, the differences between the automated techniques with respect to image registration could act as a source of variability between the methodological measures but further investigation is needed to explore the extent and nature of this possible variability. Regarding the present data, estimates of white matter volumes obtained using SIENAX found no significant differences to those produced by stereology. The brain and skull parameters derived by the initial BET skull stripping and the use a standard brain mask by SIENAX to remove unwanted tissue such as the orbits and neck area, appears to provide an accurate and robust skull stripping mechanism leading to a more accurate tissue segmentation and white subsequent matter volume estimate reported here.

In order to accurately assess a particular volume of interest via a fully automated technique, a clear understanding of the nature of the brain tissue being explored and the correct optimization parameters specific to the method employed is necessary to ensure reliable results. In the case of a region of interest consisting of more than one type of tissue (grey or white for example) the automated technique must be able to accurately assess and quantify each tissue component of the volume. This requires the use of a segmentation process that differentiates between the various tissue types present and then quantifies each identified tissue type (Ashburner and Friston, 1997; Ashburner and Friston, 2005; Held et al., 1997; Salih et al., 2005; Zeng et al., 1999; Zhang et al., 2001a; Zhang et al., 2001b). This is by no means an easy task as confounds such as partial voluming, where a single voxel may consist of multiple tissue types in various proportions, and tissue boundaries where one

tissue type merges with another, frequently complicate the segmentation process (Huppertz et al., 2005).

Possible differences between the segmentation methods of the fully automated techniques employed and the presence and extent of smoothing are other considerations. In general, VBM involves normalization followed by segmentation based on *a priori* tissue type probability maps and finally convolution of the output images with a Gaussian smoothing kernel, as part of its analysis routine (for both standard and optimized versions (Ashburner and Friston, 2000; Good et al., 2001b)). The FSL methodology on the other hand performs the segmentation of the images in their natural space based upon a Hidden Markov Random Field Model and the Expectation-Maximization Algorithm (HMRM-EM) (Zhang et al., 2001a; Zhang et al., 2001b) rather than *a priori* maps for its segmentation routine and smoothing is not a necessary step in the processing pipeline to obtain a volume measure. Both VBM and FSL's FAST tool feature rf image intensity inhomogeneity correction as part of the routine segmentation step to yield a more accurate and reliable tissue segmentation. Certain structures may not have easily identifiable tissue type boundaries or may have complex tissue composition or include small structures which have been shown to suffer bias due to the smoothing kernel used (Salmond et al., 2000; White et al., 2003). For the FSL FAST technique utilizing *a priori* tissue prior segmentation, the results revealed that the measurements for mean grey and white matter volumes increased indicating a possible source of variance that warrants further in depth investigation.

Overall the findings of this voxelwise comparison study appear to agree with those of previous studies that identified both hippocampal and extrahippocampal grey matter volume decreases in TLE patients relative to controls. Localized grey matter volume reductions have been reported in superior parietal regions, cerebellum (Keller et al., 2004; Lawson et al., 2000; Mueller et al., 2006; Woermann et al., 1999) as well as frontal, parietal and occipital lobes (Bonilha et al., 2007; Hermann et al., 2003; Keller et al., 2002a; McMillan et al., 2004; Mueller et al., 2006; Woermann et al., 1999) and parahippocampal and hippocampal regions (Bonilha et al., 2007; Keller et al., 2002a; Keller et al., 2002b; Mueller et al., 2006; Woermann et al., 1999). Increases in grey matter volume in TLE patients compared to controls was not expected but occurred in the right uncus, uvula and left middle temporal gyrus. Localized regions of increased grey matter concentration (unmodulated data in the case of the optimized VBM methodology) have been reported (Keller et al., 2002b; Woermann et al., 1999). This increase in grey matter concentration was hypothesized to be a secondary effect driven by the presence of underlying grey / white matter boundary morphologies where white matter changes in close proximity to grey matter boundaries resulted in increased grey matter concentrations and hence the hypothesized grey matter influences. Two of the regions of grey matter volume increase identified in TABLE 4.5, the right uncus and uvula, both had corresponding adjacent white matter volume changes in close proximity and hence could be the influencing factor in these regions of grey matter volume increase. Unlike grey matter investigations in TLE, comparatively few white matter volumetric comparisons have been conducted. Again our findings appear to agree with previous studies where cerebellar, parahippocampal and temporal white matter changes have been identified.

The extent of variability between the regions identified by each method was surprisingly greater than expected. Obviously, each method utilizes different mechanism within their individual processing pipelines and one would expect this to induce a certain degree of variability in the results but not to the extent uncovered in this study. Apart from the influences of normalization and segmentation methodological differences between the various techniques, the type of statistical thresholding incorporating a minimum cluster size criterion of the type used in this study could offer a possible source of variance between the methods and is constrained by the fact that small highly significant clusters that may show a genuine localized region of effect are ignored if they fail to meet the minimum cluster criteria forced on the data. However, a thresholding artefact is unlikely to be driving the discrepancies between results as the poor overlap between the measures persisted for different statistical thresholds. That said, a General Linear Model (GLM) statistical investigation may prove useful and a more effective mechanism of capturing smaller regions of localized volume change and hence is intended as a future investigation. Another possibility is that this variation is in fact artifactually driven and attributable to some possible source of noise inherent in the data set or the large extent of patient profile variability present. Further investigation is intended with new data from other patient-control comparison studies to determine the robustness of the inaccuracies between the automated techniques. This said, the usefulness of the fully automated techniques as a preliminary investigation tool cannot be overlooked but emphasise the need for caution when interpreting the results of such studies.

In the case of absolute volumetrics such as whole brain volumes our results clearly show that absolute volumes from these automated techniques incur a baseline shift in comparison to 'gold standard estimates' as measured by stereology in this case. Hence absolute volume measurements should be treated with caution and should be used in conjunction with a gold standard quantitative volume estimate such as manual delineation (Giuliani et al., 2005; Tisserand et al., 2002) or the more efficient measurement mechanism now possible with stereology. Further research comparing the measures produced in this body of work to those of a true gold standard would be extremely beneficial and offer the researcher an informative insight into the impact of the measurement technique used to obtain the absolute volume measures and hence the reliability and accuracy of the measurements. Such comparisons would have a vital and significant impact for clinicians where these measures may be under consideration for diagnostic or treatment purposes in the future.

Chapter 5

Correlates of Grey and White matter brain volumetrics using 'optimized' Voxel Based Morphometry with fMRI activation measures and behavioural performance scores.

Abstract

A combined dataset from three event-related fMRI studies of response inhibition and associated anatomical images were used to examine correlates of structural grey matter volumes with activation measures and performance scores related to a GO/NOGO inhibition control task. The present results reveal differences in mean grey matter volume between males and females insofar as males were found to have significantly greater mean grey matter volumes in 11 of the 17 functionally defined regions of interest examined. Only two clusters, the right inferior frontal lobe and right middle frontal gyrus, showed significant differences for both grey matter volume and activation measures in which females, having less grey matter in those regions, had greater activity. These results demonstrate that brain functional measures need not be determined by brain structural differences (at least in the present case of grey matter volumes) underscoring the unique insights offered by functional brain measures. Regional specific sex differences were identified in parietal and frontal regions demonstrating agreement with the literature.

However, the influence that these grey matter volume differences have on the performance of cognitive tasks such as the inhibition related GO / NOGO task featured here remains unclear as no differences in performance between males and females were found. Sex specific *split-group* comparisons indicated an apparent advantage of greater grey matter volumes associated with top performance scores for males. Female top performers revealed no difference in grey matter volumes. These results demonstrate the complexity of the interrelations between grey matter volume, cognitive activation measures and performance during inhibitory control tasks.

5.1 INTRODUCTION

Advances in diagnostic imaging techniques such as Magnetic Resonance Imaging (MRI), offer the research scientist a means to investigate numerous neurophysiological, cognitive and biological mechanisms of the brain. The use of functional magnetic resonance imaging (fMRI) incorporating the principle of blood oxygen level dependent (BOLD) response of the brain, permits an indirect mechanism to capture and quantify brain activations as specific cognitive processes are being performed (Ogawa et al., 1990). Structural high resolution MR imaging offers a detailed *in vivo* anatomical assessment mechanism frequently used for the diagnosis of degenerative disease onset and progression (Bigler et al., 2004; Bonilha et al., 2006; Colchester et al., 2001; Fotenos et al., 2005; Hermann et al., 2003; Hsu et al., 2002; Keller et al., 2002b; Kopelman et al., 2001; Lawson et al., 1998; Perez-Duenas et al., 2006; Selemon et al., 2002; White et al., 2003), oncology diagnosis and treatment assessment (Gong et al., 2004; Schad, 2001; Shi et al., 1998) and age-related studies of both clinical and normal populations (Bartzokis et al., 2000; Bartzokis et al., 2001; Good et al., 2001a; Matsuzawa et al., 2001; Persson et al., 2006).

The relationship between brain volumetrics, brain function, and behavioural and cognitive measures remains elusive. This said, extensive research focusing on various interrelations of these measures has been successful in clarifying to an extent, the complex nature of these mechanisms. For example, cognitive variability due to the presence of degenerative neurological conditions and drug abuse have been extensively reported in the literature

(Bolla et al., 2000; Breiter et al., 1997; Fein et al., 2006b; Fishbein et al., 2005a; Fishbein et al., 2005b; Franklin et al., 2002; Garavan and Stout, 2005; Hester et al., 2006; Hester and Garavan, 2004; Ilan et al., 2004; Kaufman et al., 2003; Kumari et al., 2003; Lawrence et al., 2002; Pope, 2001; Pope, 1996; Rogers and Robbins, 2001; Solowij N, 1997; Solowij et al., 2002a; Solowij et al., 2002b) thus showing the impact on cognitive processes. More recently, studies have reported specific structural deficits associated with drug abuse (Bartzokis et al., 2004; Brody et al., 2004a; Brody et al., 2004b; Cowan et al., 2003; Franklin et al., 2002; Lim et al., 2002; Liu et al., 1998; Matochik et al., 2005; Matochik et al., 2003) helping to clarify the mechanisms of anatomical change in relation to drug abuse. Age-related cognitive decline and associated reductions in grey and white matter volumes have been extensively reported in the literature (Bartzokis et al., 2001; Good et al., 2001b; Good et al., 2001a; Hsu et al., 2002; MacLullich et al., 2002; Matsuzawa et al., 2001; Persson et al., 2006; Scahill et al., 2003; Silbert et al., 2006; Staff et al., 2006; Tisserand et al., 2002; Wolf et al., 2003).

Sources of between-subject variability in normal populations (age, sex, handedness and intelligence and a myriad of other psychological dimensions) and the extent to which these variations affect cognitive activation measures, behavioural performance scores and grey and white matter brain volumetrics have been identified (Garavan et al., 2006; Garavan et al., 2002; Im et al., 2006; MacLullich et al., 2002; Murphy and Garavan, 2004b; Murphy and Garavan, 2004b; Persson et al., 2006; Siegler, 2007; Staff et al., 2006; Witelson et al., 2006; Witelson et al., 1995). The influence of anatomical differences associated with the performance of certain tasks and specific visuomotor abilities typically featuring region of

interest type analysis techniques, has been reported in the literature suggesting that some interactive mechanism relating brain structure and functional activity appears to exist under certain conditions and featuring specific brain regions such as the hippocampus, corpus callosum, motor cortex, and cerebellum (Draganski et al., 2004; Maguire et al., 2000; Maguire et al., 2003; Munte et al., 2002; Schlaug, 2001). However, the specific relationship between grey matter brain volumetrics on cognitive / behavioural measures remains unclear. Is an individual's behavioural test scores related to their associated cognitive activation measures and are these measures, in turn, related to their basic brain anatomy and proportions of grey and white matter tissue? To investigate this question and asses the ability of VBM to capture such grey matter correlates of individual variations in performance, structural image analysis using the technique of 'optimized' Voxel Based Morphometry (VBM) was conducted to examine the relationships between individual neuroanatomical differences with previously reported behavioural performance scores and event-related fMRI activation measures during cognitive inhibitory processes (Garavan et al., 2006). The original fMRI study consisted of a combined dataset of 71 control subjects but the VBM analysis was restricted to a subset of 41 subjects collected on the same scanner and utilizing an identical image acquisition protocol to exclude variability associated with scanner differences in accordance with VBM analysis guidelines.

5.2 METHODS

5.2.1 Participants and Task design

The experimental data set consisted of forty-one right-handed subjects (18 male: mean age 30, range 18-46 and 25 female: mean age 31, range: 18-45) with no history of neurological or psychological impairment. Subjects completed a GO/NOGO task after providing written informed consent. The initial design for the XY GO/NOGO task is described in Garavan et al. (1999) and slight modifications were made in two subsequent studies. In each study, subjects were presented with a serial stream of letters in which frequent Go stimuli (the letters X and Y) were presented in alternating order with subjects instructed to inhibit responding when the alternation was interrupted (e. g., the fifth stimulus in the train X-Y-X-Y-Y-X-Y). In the initial study (Garavan et al., 1999) an average of seven distracter letters (random letters of the alphabet) separated the presentation of X and Y stimuli. There were no distracters in the two subsequent studies included in the present analysis. The version of the task in these two studies contained minor variations of on-screen presentation and inter-stimulus interval timing, varying between 900 msec on-screen presentation / 100 msec ISI (Garavan et al., 2003) and 600/400 (Garavan et al., 2002). In the (Garavan et al., 2002) study, pre-scanning testing identified the timing parameters that produced approximately 50% commission errors, by varying the timing from 600/400 to 900/100.

The GO/NOGO task outlined above and featured in this study has been successfully used in fMRI experiments examining the identification and localization of brain activation patterns in response to inhibitory processes (Garavan et al., 2006; Garavan et al., 2003;

Garavan et al., 1999; Hester et al., 2004a; Hester et al., 2004b; Murphy and Garavan, 2004b). The activation patterns resulting from the task feature right hemisphere networks including prefrontal, parietal sub-cortical and midline regions. More specifically, the GO/NOGO response inhibition task has been successfully used to identify areas specific to error related monitoring such as the anterior cingulate, preSMA, right inferior parietal lobule, bilateral insula and thalamus. Event-related fMRI analyses have shown that the preSMA is not specific to errors but highly sensitive to conflict manipulations arising during the GO/NOGO task. Further localisation specificity identified reaction time to GO with posterior sub-cortical areas and found fronto-parietal regions were prominent in self reported absent mindedness during the task performance.

5.2.2 MRI Scanning Parameters

Scanning for the studies (Garavan et al., 1999, 2002, 2003) was conducted using contiguous 7 mm sagittal slices covering the entire brain from a 1.5T GE Signa scanner using a blipped gradient-echo, echo-planar pulse sequence (TE = 40 msec; TR = 2000 msec; FOV = 24 cm; 64 x 64 matrix; 3.75 mm x 3.75 mm in-plane resolution). High resolution spoiled GRASS anatomic images (TR=24 msec, TE=5msec, flip angle=45^{o}, FOV=24cm, thickness=1.0 mm with no gap, matrix size = 256x256x124) were acquired prior to functional imaging to enable subsequent activation localisation and spatial normalisation. Foam padding was used to limit head movements within the coil. Stimuli were back-projected onto a screen at the subject's feet and were viewed with the aid of prism glasses attached to the inside of the radio-frequency head-coil.

5.2.3 Optimized VBM analysis

The MR images were collected in DICOM format and were converted to the Analyze 7.5 image format via the software package MRIcro; http://people.cas.sc.edu/rorden/mricro.html and a subsequent voxel-based morphometry (VBM) image analysis was performed using the statistical parametric mapping software (SPM2; http://www.fil.ion.ucl.ac.uk/spm/). Voxel-based morphometry is a voxelwise automated analysis technique performed on high resolution structural images to investigate structural differences in local concentrations of grey and white matter and volumetric differences of the brain. The standard VBM methodology incorporated three processing steps, namely (a) normalization to transform all images to a common standard space, (b) segmentation to partition the brain into grey, white and CSF tissue types and finally (c) smoothing by convolving with a Gaussian smoothing kernel to conform to the Gaussian field model and render the data more normally distributed to facilitate statistical analysis. The output from the VBM technique is a probability measure of a voxel being classified as grey or white tissue as determined following normalization and segmentation routines based on an *a-priori* image template used for affine registration and tissue classification maps (see (Ashburner and Friston, 2000) and (Good et al., 2001a)) for detailed descriptions of the standard and optimized VBM methods). The output from the analysis is commonly referred to in the literature as grey/white matter concentration or tissue density and statistical analysis is performed to examine between-group differences in tissue concentrations/densities. More recently, the standard VBM strategy was adapted to overcome some of the criticisms and shortcomings of the technique in what is commonly referred to as the 'optimized VBM' strategy (see the methods section Good et al. 2001a). The optimized VBM strategy employs a 'modulation'

step to correct for partial volume effects resulting from the non-linear normalization process that accommodates the variance in brain size as it is normalized to standard space based on the mathematical principle of curvilinear coordinate transformations which convolve the determinates of the Jacobian transformation matrix with the normalized images to achieve the volume correction as the image is transformed from native space to a standard space to facilitate group comparisons. Volumetric between-group comparisons can thus be investigated using the optimized VBM technique incorporating the volume modulation step. This study incorporated the optimized VBM analysis strategy to specifically examine volumetric change (Keller et al., 2004). A major source of concern with VBM analyses is the error induced by poor image co-registration during transformation into a standard stereotaxic space (Ashburner and Friston, 2001; Bookstein, 2001). The residual error of the mean was reported (Fein et al., 2006a) to be effectively reduced by up to 30% by inputting images with the skull and scalp removed into the initial analysis step. In addition, the use of study-specific templates constructed from the complete dataset of a particular study has been shown to increase the accuracy of the registration and segmentation steps. Thus, all images were skull stripped using FMRIB's Brain Extraction Tool (BET) (Smith, 2002) skull stripping routine; http://www.fmrib.ox.ac.uk/fsl/ and these images were used as the input for the fully automated techniques used in this paper and study specific templates were constructed as outlined below.

5.2.3.1 Template generation

Template images for normalization of grey, white and CSF tissue classification maps were constructed from the complete data set of 41 subjects. All images were spatially normalized

to the same stereotaxic space by a process of linear and non-linear transformations based on the Montreal Neurological Institute (MNI) coordinate system and registered to a template image compiled from the skull stripped 152 brain average of the MNI brain included in the FSL tool box. A mean normalized image was then created from the 41 normalized images and smoothed using an 8mm FWHM Gaussian smoothing kernel. All normalized images were segmented into grey matter, white matter and CSF partitions using *a priori* grey, white and CSF maps provided in the SPM software package which uses a mixture model cluster analysis for the identification of voxel intensities for tissue classification purposes. Study specific templates for grey, white and CSF tissue were constructed from the average segmented image files and smoothed using an 8mm FWHM Gaussian kernel.

The output from the analysis resulted in an optimally normalized, segmented and modulated image file that was smoothed with an 8 mm FWHM kernel. Each smoothed image file was used for statistical analysis to examine regional differences in the volumes of grey matter, white matter and CSF.

5.2.3.2 fMRI Group Analyses and Region of Interest generation

As previously reported (Garavan et al., 2006) the time series data were time-shifted using Fourier interpolation to remove differences in slice acquisition times, and motion-corrected and edge-detected to remove the presence of activations outside the brain. Haemodynamic response functions (HRF's) were calculated using deconvolution techniques for successful response inhibitions (STOPS) during the GO/NOGO task. A multiple regression analysis

estimated the time point parameters of the HRF and these HRF's were modelled voxelwise with a gamma-variate function using non-linear regression. An area-under-the-curve measure of the gamma-variate model was expressed as a percentage of the tonic baseline activity and served as the activation measure for the event-related responses (Murphy and Garavan, 2005). The activation map for STOPS therefore represents activation during successful NOGO events that is significantly greater than during the baseline of ongoing Go trials. Activation maps were resampled to 1 μl and warped into standard Talairach space (Talairach and Tournoux, 1988) and spatially blurred using a 3 mm isotropic rms Gaussian blur. A one-sample t-test against the null hypothesis of zero event-related activation changes (i.e., no change relative to tonic task-related activity) was performed voxel-by-voxel on the percentage area-under-the-curve measure. Significant voxels passed a voxelwise statistical threshold ($t = 4.762$, $p < .00001$) and were required to be part of a larger 71μl cluster of contiguous significant voxels. Thresholding was determined through Monte Carlo simulations and resulted in a 0.1% probability of a cluster surviving due to chance. The functionally-defined group activation map consisting of 17 clusters (see Table 5.1) and based on the restricted sample of 41 subjects was used for the purposes of an ROI analysis of grey matter volume, that is, grey matter volume measures were calculated for each of the regions shown to be functionally active.

Statistical analysis was carried out using the commercially available software package SPSS (version 12.0 for Windows).

5.2.3.3 *Demographic influences on Grey matter volumes.*

Initially, the influence of the demographic profile of the sample was examined. The demographic variables of age and sex were considered to examine the effect they had on mean grey matter volumes in each of the 17 functionally-defined clusters. A series of male verses female independent sample t-test comparisons for each cluster were conducted to investigate the difference between sexes for mean grey matter volumes in each cluster. Next, a series of nonparametric Spearman's Rho correlations were performed for age versus grey matter volume for each defined cluster to identify if grey matter volume was predicted by age.

5.2.3.4 Grey matter volumes and functional activations

Nonparametric Spearman's Rho correlations were calculated for VBM grey matter volume measures versus activation measures (%AUC) for each functionally defined region.

5.2.3.5 Grey matter volume and performance

A series of split-group t-test comparisons between the best (> 90% successful inhibitions: N = 15) and worst performers (< 70% successful inhibitions: N = 14) of the XY GO/NOGO task were conducted for VBM grey matter volume measures. To account for the sex confound between best and worst performance groups, separate split-group comparisons for males and females were carried out (i.e., best-performing females were compared to the poorest performing females while best-performing males were compared to the poorest performing males). In addition, simple correlations were calculated for VBM measures with age, performance score, and activation measures (%AUC) for the whole

dataset and separately for males only and females. This was repeated for %AUC versus age and performance scores. Finally, a series of multiple regression analyses were performed for each cluster with VBM grey matter volume as the dependant variable and age, sex, activation measure and performance as predictors.

5.3 RESULTS

5.3.1 Demographic interactions

Independent sample t-tests between males and females revealed no significant age or performance differences between the groups. The examination of sex differences revealed mean grey matter volume was significantly greater for males in 11 clusters located in the right inferior parietal lobule, superior frontal gyrus, and five clusters in the middle frontal gyrus, bilateral insula and thalamus. Interestingly, in contrast, females had significantly greater activation in 5 clusters ($p < 0.05$) located bilaterally in the inferior parietal lobule, right middle temporal and middle frontal gyrus. No regions had greater activation in males indicating a lack of correspondence between activation measures and grey matter volume.

Nonparametric Spearman's Rho correlation analyses found four clusters that showed a significant negative correlation between age and grey matter volume for males including the right middle frontal gyrus ($s = -0.634$, $p < 0.01$), left insula ($s = -0.578$, $p < 0.05$), left inferior parietal lobule ($s = -0.631$, $p < 0.01$) and right inferior frontal gyrus ($s = -0.0572$, $p < 0.01$). The female-only analysis also revealed four clusters that showed a significant negative correlation between age and grey matter volume including the left insula (s = -

0.422, $p < 0.05$), left inferior parietal lobule ($s = -0.502$, $p < 0.05$ and $s = -0.48$, $p < 0.05$) and the right inferior frontal gyrus ($s = -.533$, $p < 0.01$). Interestingly, both males and females showed a common significant negative correlation between age and grey matter volume in the left insula and left inferior parietal lobule.

5.3.2 Grey matter volume and functional activity

Grey matter volumes were correlated with functional activation measures for male and females separately, given the grey matter volume differences between males and females reported above. Three regions showed a significant positive correlation between grey matter volume and activation for males including the right superior frontal gyrus ($s = 0.626$, $p < 0.01$), the right middle frontal gyrus ($s = 0.662$, $p < 0.01$) and the left thalamus ($s = 0.506$, $p < 0.05$). The equivalent analysis for females found no significant correlations although one region in the left inferior parietal lobule approached significance ($s = 0.392$, $p < 0.053$).

5.3.3 Split-group comparisons of grey matter volume and performance

Grey matter volume was found to be significantly greater for top performers in five regions located bilaterally in the insula, left precuneus and thalamus and right middle frontal gyrus. However, the best and worst performing groups were not matched for sex as the former contained seven males and eight females and the latter three males and eleven females. Consequently, split-group comparisons for best and worst performers and grey matter volume were repeated for males and females separately. Grey matter volume was found to be significantly greater in best male performers than worst male performers in three

regions, the right middle frontal gyrus and bilaterally in the thalamus. Two of these regions, the left thalamus and the right middle frontal gyrus, coincided with those identified in the whole group analysis. In contrast, the female-only split-group comparisons of best/worst performers failed to identify any significant differences in grey matter volumes.

5.3.4 Stepwise Multiple Regression Analyses

Stepwise linear regression analyses with grey matter volume as the dependent variable and age, sex, functional activity and performance were performed for each cluster. Age was found to significantly predict grey matter volume in eight regions, bilaterally in the inferior parietal lobule, bilateral insula, middle frontal gyrus, and the left precuneus. Sex was found to significantly predict grey matter volume in 11 clusters, the right inferior parietal lobule, the right superior frontal gyrus, bilaterally in the insula, five regions in the right middle frontal gyrus and bilaterally in the thalamus. Both functional activity and performance failed to significantly predict grey matter volumes in any regions (see TABLE 5.1).

TABLE 5.1

Lobe	Cluster size (µl)	MNI coordinates X Y Z	Description / Location	Volume Predictors	Brodmann Area
Frontal	4231	2 8 55	R-Superior Frontal gyrus	s	6
	2103	31 -4 48	R-Middle Frontal Gyrus	s	6
	1714	-24 -7 55	L-Middle Frontal gyrus	s,a	6
	1644	41 32 26	R-Middle Frontal gyrus		46
	317	44 1 25	R-Inferior Frontal gyrus		6, 9
	293	45 14 21	R-Inferior Frontal gyrus		9
	216	32 46 22	R-Middle Frontal Gyrus	s	10
	131	46 40 18	R-Middle Frontal Gyrus	s	46 , 10
Parietal	6457	41 -46 45	R-Inferior Parietal lobe	s,a	40
	595	-34 -49 49	L-Inferior Parietal lobe	a	40
	346	-42 -41 44	L-Inferior Prietal Lobe		40
	329	-25 -58 51	L-Precuneus	a	7
Temporal	350	48 -58 6	R-Middle Temporal Gyrus		39
Subcortical	2455	37 13 2	R-Insula	s	13
	1224	-31 14 6	L-Insula	s,a	13
	863	16 -12 6	R-Thalamus,R-Ventral lateral Nucleus	s	NA
	224	-11 -19 10	L-Thalamus	s	NA

Table 5.1: showing significant clusters for successful inhibitions on the XY GO/NOGO task. Coordinates relate to the centre-of-mass of the activated clusters and volumes are in microlitres. Clusters where grey matter volume was significantly predicted by age, denoted by 'a' and sex, denoted by 's' as identified by linear regression analyses with grey matter volume as the dependent variable are identified.

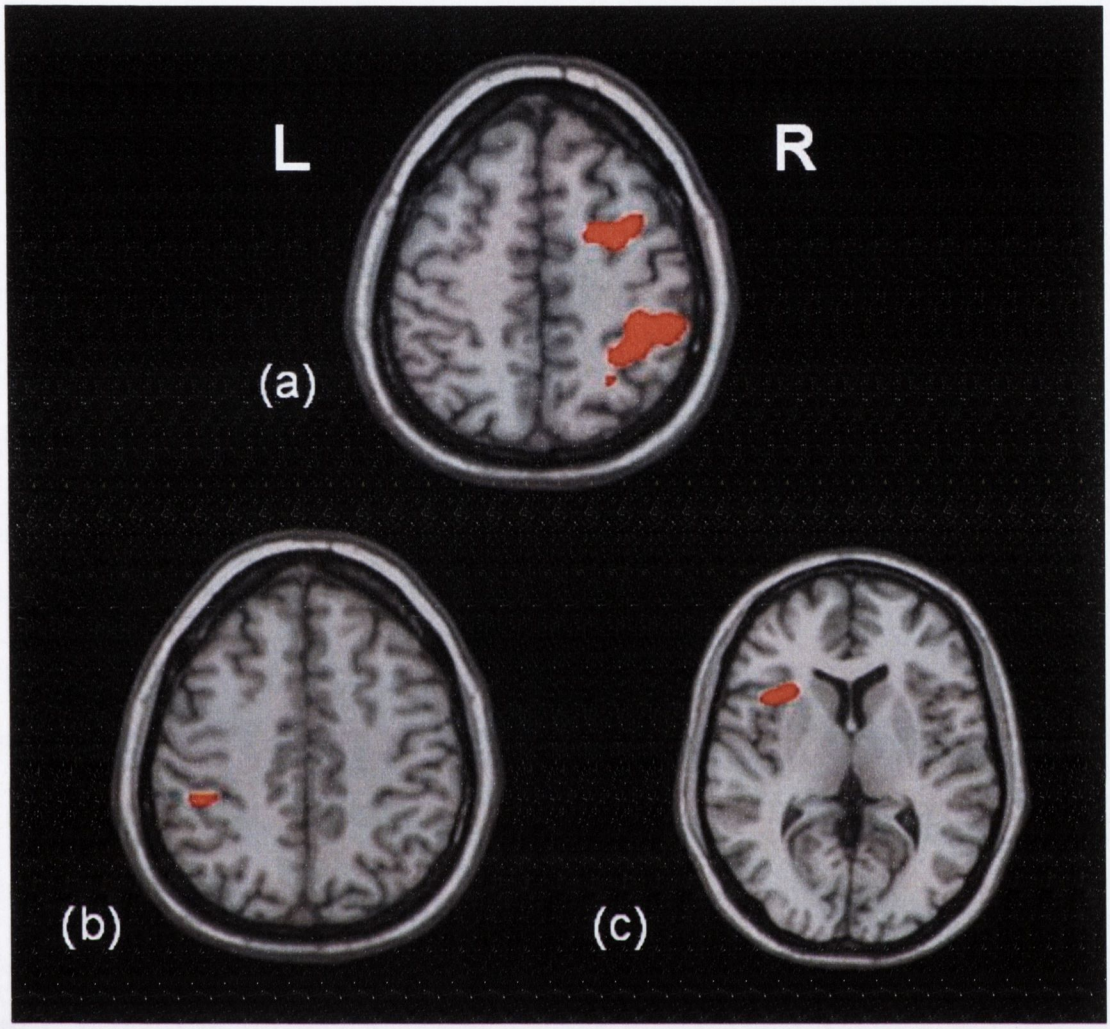


Figure 5.1: (a) showing clusters in the right inferior parietal lobe and right middle frontal gyrus where females had significantly less grey matter volume and a significantly higher activation level than males, (b) showing the left inferior parietal lobule and (c) showing the left insula where grey matter volume showed a negative correlation with age for both sexes.

5.4 DISCUSSION

The present results featuring a more restricted sample size show robust and very similar activation patterns in response to the GO/NOGO response inhibition task to those previously published (Garavan et al., 2006; Garavan et al., 2003; Garavan et al., 1999; Hester et al., 2004a; Hester et al., 2004b; Murphy and Garavan, 2004b), are presented. When correlated with volumetric measures produced for the regions specified by the fMRI activation maps, the present results reveal differences in mean grey matter volume between males and females insofar as males were found to have significantly greater mean grey matter volumes in 11 of the 17 regions of interest examined. Activation measures were significantly greater in females in five of the regions examined, in agreement with even larger sex effects reported in (Garavan et al., 2006) with a larger sample size of N=71. Only two clusters, the right inferior frontal lobe and right middle frontal gyrus (see Figure 5.1(a)) showed significant differences for both grey matter volume and activation measures in which females, having less grey matter in those regions, had greater activity. These results demonstrate that brain functional measures need not be determined by brain structural differences (at least in the present case of grey matter volumes) underscoring the unique insights offered by functional brain measures.

Sex differences in grey matter volume have been previously reported (Chen et al., 2007; Good et al., 2001b; Good et al., 2001a; Im et al., 2006; Luders et al., 2005; Maller et al., 2006; Witelson et al., 2006). Regional specific sex differences have been reported in parietal, frontal and temporal regions (Chen et al., 2007; Good et al., 2001a); seven of the 11 regions of grey matter volume sex difference in the present results were located in

parietal and frontal lobes. However, the influence that these grey matter volume differences have on the performance of cognitive tasks such as the inhibition related GO / NOGO task featured here remains unclear as no differences in performance between males and females were found. The lack of performance-structure relationships and the inverse relationship between structure and function points towards a complex set of interactions.

Age-related grey matter volumetric degeneration has been extensively identified (Bartzokis et al., 2001; Fotenos et al., 2005; Good et al., 2001a; Raz et al., 1998; Resnick et al., 2000; Scahill et al., 2003; Tisserand et al., 2002; van der Flier et al., 2005) When grouped by sex, negative correlations were identified between grey matter volume and age in four clusters for females and five for males with common regions of age-related decline for both sexes in the left inferior parietal lobule (see Figure 5.1.(b)) and the left insula (see Figure 5.1.(c)), agreeing with previous finding that show greater age-related volumetric differences associated with parietal regions (Resnick et al., 2000). The sensitivity of VBM to detect age related volumetric change is clearly demonstrated here given the limited age range (18-45 years) of the present sample.

Split-group comparisons based on best and worst performers for the complete dataset identified five regions in which the better performers had significantly more grey matter volume. Sex-specific versions of the split-group comparisons were performed given the differences in volumes between the sexes and the disproportionate number of males in the best performer group. This identified two regions of significantly increased grey matter volume in best performers in males in left thalamus and right middle frontal gyrus but no

differences in females. Interpretation of these results must consider the reduced range in performance when conducting the sex-specific contrasts. The relationship between cognitive performance declines and age-related decline in total brain volumetrics has been reported (Bigler et al., 2004). Intelligence quota (IQ) and verbal IQ have successfully been correlated with whole brain volumes and right hippocampal volumes (Toulopoulou et al., 2004). Hippocampal atrophy has been shown to correlate with executive dysfunction (Frodl et al., 2006) and affect cognitive performance associated with memory tasks. Increased functional activations in the prefrontal cortex during episodic encoding have been demonstrated with negatively correlated DTI-measured fractional anisotropy in the corpus callosum (Persson et al., 2006). Hence the complex mechanism that relates structure, function and cognitive performance measures where the focus of the three measures can often traverse multiple brain regions encompassing various tissue types, highlights the complexity of the underlying mechanisms that may or may not be localized to a common region of effect. Unfortunately the presence of a gender bias in our sample appears to have impacted our results as the known gender volume differences may have made it difficult to assess a generic relationship between grey matter volumes and functional activation and associated performance marks for a cognitive inhibition task as used here. The importance of careful demographic profiling to remove the effects of sex bias due to disproportionate numbers of males versus females in the subject sample is very apparent with the notable differences in the findings based on the sex specific (be it somewhat limited sample size) analyses. The underlying mechanisms of the possible relationship between structure, function and performance measures may be accentuated or diminished depending of the sex of the group and although some generic characteristics may relate these measures,

separate sex specific mechanism may also be at play, as revealed in the apparent advantage of greater grey matter volumes associated with best performance scores in males. This said the comparison of best/worst performers revealed greater grey matter volumes for best performers in the right middle frontal gyrus, bilaterally in the insula, left precuneus and left thalamus. The sex specific split group comparisons indicated that this relationship was more pronounced in males (N=16, seven best performers ranging from 100-92%, mean = 93.5% and nine worst performers ranging from 88-33.75%, mean = 68.9%) revealing two regions of greater grey matter volume associated with higher performance. Females, N=25, 13 best performers ranging from 96-84.62%, mean = 91% and 12 worst performers ranging from 79-41%, mean 60.35%, revealed no difference in grey matter volumes. Further investigations featuring a larger, sex matched sample permitting a greater performance score differential between best and worst performers may offer a clearer understanding of the mechanisms that could influence grey matter volume, performance scores and functional activation and facilitate the identification of possible correlations that encompass all three markers of performance, grey matter volume and functional activation.

5.5 *Summary*

The influence of sex on relationship between grey matter volume, performance scores and cognitive activation levels remains unclear, largely influenced by the heterogeneous nature of the dataset with regard to gender. Careful consideration to ensure an equal distribution of sexes or gender-specific investigations is very apparent from the results. Sex-specific comparisons appear to suggest that grey matter volume is unrelated to functional activation and performance measures although obtaining best performance scores appears to be

positively influenced by the presence of greater grey matter volumes and this effect appears more pronounced in males. Further investigation is needed on a large sample of subjects to facilitate a clearer understanding of the complex interrelations between grey matter volume, cognitive activation measures and performance during inhibitory control tasks.

Chapter 6

6.1 *Discussion*

This thesis presented a body of research consisting of four studies to investigate methodological variability in both functional and structural MR image analysis and assess the interactions between brain structure and functional activation and performance measures. The findings offer the researcher a valuable insight into the practical considerations and confounds typically encountered with structural and functional MR image analyses. The flexibility and sensitivity of both analysis techniques is clearly demonstrated over a wide range of clinical and drug using groups as well as control populations. However, these results also stress the importance of carefully selecting the optimum methodological approach and subsequent image analysis parameters for a particular research question to facilitate meaningful investigations. Armed with a clearer understanding of the methodological considerations at hand, specific questions concerning the flexibility of fMRI to cope with haemodynamic variations were addressed. The ability and sensitivity of voxelwise volumetric automated analysis techniques were demonstrated by comparing three independent drug using groups with known neuroanatomical regional specificity. The accuracy and reliability of results from such automated volumetric techniques were assessed by direct quantification and comparison of grey and white matter volumes with a 'Gold Standard' technique. Finally, the specific inter-relations between the

various structural, functional and performance measures were explored to assess the underlying mechanisms of brain structure and anatomy to functional activations and performance scores.

6.2 *Summary of results*

The first study in Chapter 2 specifically focused on a novel modelling analysis technique for event-related fMRI. Haemodynamic responses have been shown to contain inherent sources of both inter- and intra-subject variability (vasculature, and anatomical localization and specific structural differences to name but a few). The integrity of the BOLD response in light of these considerations must be insured to provide meaningful results based on fMRI. Frequently, analyses test for goodness of fit between the observed haemodynamic responses of the data and a predetermined HRF. When these observed haemodynamic properties vary from the predetermined response, with for example, variations in onset time by as little as one second between the standard HRF and the observed data has been shown to impact false negative rates (Handwerker et al., 2004). Voxels that are responsive to the particular stimulus having a HRF different to the predetermined response could be missed. The nonlinear modelling technique was applied to a dataset of 58 control subjects where quantitative descriptors of each voxel's haemodynamic response were obtained from the gamma-variate modelling function. These results show that although there are variations in the time to onset, rise time, decay time and time-to-peak for every voxel across the whole brain, the modelling technique can successfully accommodate these variations and correctly identify and hence capture and model the BOLD response. These results are potentially very useful for the event-related fMRI analyst as the modelling technique is

easily adaptable to capture a wide range of haemodynamic properties while reducing the influences of false positives.

The arguments concerning the validity of VBM and other similar voxelwise structural image analysis techniques continue to rage and remain the focus of extensive research (Bookstein, 2001; Crum et al., 2003; Thacker et al., 2004). Although these doubts remain at the forefront of structural image analysis, few can deny that these analysis tools display an extraordinary ability to capture localized structural changes. Chapter 3 investigated the sensitivity of VBM to capture and localize drug-related volumetric changes in both the grey and white tissue partitions of the brain. Three distinct drug using samples with known regional effects associated with the individual pharmacological, cognitive and psychological effects of each drug [cannabis:(Block et al., 2002; Bolla et al., 2002; Campbell, 2001; Crippa et al., 2005; Downer et al., 2003; Ernst et al., 2001; Evans, 1992; Iversen, 2003; Lane et al., 2005; Matochik et al., 2005; O'Leary et al., 2002; Pope, 2001; Pope, 1996; Solowij N, 1997; Solowij et al., 2002b); cocaine: (Bolla et al., 1998; Bolla et al., 2000; Bolla et al., 1999; Cadet and Bolla, 1996; Garavan et al., 2000a; Garavan et al., 2000b; Hester and Garavan, 2004; Matochik et al., 2003); nicotine: (Bolla et al., 1998; Bolla et al., 2000; Bolla et al., 1999; Brody et al., 2004a; Brody et al., 2004b; Brody et al., 2004c; Cadet and Bolla, 1996; Court et al., 2000; Domino et al., 2000; Domino et al., 2004; Garavan et al., 2000a; Garavan et al., 2000b; Graham et al., 2002; Guan et al., 2003; Hester and Garavan, 2004; Kumari et al., 2003; Lawrence et al., 2002; Matochik et al., 2003; Opanashuk et al., 2001)] were compared to controls using the 'optimized' VBM protocol to probe for evidence of specific structural changes. The ability of VBM to identify drug-

specific and common volumetric regional effects was demonstrated providing further supportive evidence of anatomical change associated with substance abuse consistent with literature (Bloom et al., 1999; Brody et al., 2004a; Csernansky, 2001; Garavan and Stout, 2005; Goldstein and Volkow, 2002; Matochik et al., 2005; Matochik et al., 2003; Stein, 2001; Stein, 1999).

The results found that the most extensive grey matter changes were observed in cocaine users with reductions observed in bilateral thalamus / red nucleus, left inferior semi lunar lobule, right cerebellar tonsil and left inferior parietal lobe. Parietal, occipital and temporal volume reductions were also identified in the nicotine using group. Grey matter volume reductions were identified in the left parahippocampus and left thalamus for cocaine and cannabis users while cerebellar deficits were observed for both nicotine and cocaine users. White matter morphologies (both increases and decreases) were noted for all drug-using groups, with cocaine users again demonstrating the most pronounced effects.

Having successfully demonstrated the selectivity and sensitivity of VBM for the identification and localisation of structural volumetric changes, Chapter 4 introduced a study featuring an epilepsy and control sample that specifically focused on a direct comparison of the differences in whole brain volume measures and identified localized regions of volumetric change output by three fully automated analysis techniques, VBM, FSL FAST and FSL SIENAX. An in depth quantitative volumetric comparison of the grey and white matter volumes assessed by each technique was performed by comparing the results to the 'gold standard' quantitative volumetric measures obtained using Stereology.

This quantitative volumetric comparison has important implications for researchers and clinicians alike as it specifically examined the reliability and accuracy and hence interchangeability of the absolute volume measures for whole-brain grey and white matter output by these automated techniques. Derived variables of grey / white matter ratio and total intracranial volume, TIV, (grey matter + white matter) were also generated. The results demonstrated that the fully automated techniques (VBM and FSL FAST and FSL SIENAX) identified significantly greater grey matter volume and VBM and FSL FAST identified significantly smaller white matter volume measurements compared to those measured using Stereology. No significant differences were found between Stereology and SIENAX for white matter volume. Hence, all fully automated techniques utilized here appear to display a systematic bias towards grey matter tissue at the expense of white matter which has implications for the reliability of whole brain grey and white matter absolute volumes reported using these techniques. In a comparison between the epilepsy patients and controls, statistical analysis revealed agreement (Bland and Altman, 1986) between VBM, FSL, FSL SIENAX and Stereology measures for the identification of cerebral grey matter, white matter and total intracranial volume (TIV) differences. The measurements produced by the automated technique were consistent with published estimates for the grey / white matter ratio. Stereological results indicated significant group differences between patients and controls in white matter volumes, and the grey / white matter ratio. The fully automated techniques failed to detect these effects. Further research is needed to examine absolute volume measurement from the automated techniques that will focus on region specific measures and not on whole brain volumetrics as detailed in Chapter 4. The possibility that grey and white matter measures may be confounded by the

inclusion of the cerebellum, for example, which has very complex tissue architecture. White matter tissue typically has very small fibrous characteristics that may impact the segmentation performance of the automated techniques and skew the overall grey/ white tissue measures. Thus a similar investigation restricted to the cerebrum may offer a clearer insight in the whole brain grey tissue bias reported in this body of work. Further region specific investigations of particular brain structures may also prove useful as the tissue bias may or may not be as pronounced depending on the nature of the region of interest being explored. Such detail would permit the researcher to identify particular brain regions where reliable absolute volumetrics as measured by the automated techniques occur or particular structures where these automated measures become unreliable.

The findings of the voxelwise comparison study appear to agree with those of previous studies that identified both hippocampal and extrahippocampal (frontal, parietal and cerebellar) grey matter volume decreases in TLE patients relative to controls. Results of the voxelwise volumetric white matter regions appear to agree with previous studies where cerebellar, parahippocampal and temporal white matter changes were identified. The extent of variability between the regions identified by each method was surprisingly greater than expected. Each method utilized different analysis mechanisms within their individual processing pipelines that could induce a certain degree of variability in the results but not to the extent uncovered in this study and hence further investigation is intended with new data from other patient-control comparison studies to determine the robustness of the inaccuracies between the automated techniques.

The complex relationship between brain anatomy, brain function and cognitive performance is by no means fully understood. Structural variations and or changes have been implicated in cognitive performance differences in particular groups such as musicians and taxi drivers where structural brain plasticity is evident and associated with an enhanced ability to perform certain tasks. Evidence of the effects of structural change on cognitive ability is apparent in patients with traumatic brain injuries yet a general mechanism that relates brain structure to brain function remains unclear. Chapter 5 draws on the findings from the three previous studies of this thesis by utilizing the novel nonlinear modelling approach for fMRI event-related analysis featured in Chapter 2 to quantify and define functional activation maps associated with the performance of a GO/NOGO cognitive task and correlate these measures with structural volumetrics for the functionally defined regions as assessed by optimized VBM to explore their interactions. In contrast to the results in Chapter 3 investigating drug related volumetric changes, possible volumetric variations were examined in specific functionally defined regions. Thus the analysis strategy employed in Chapter 5 differs from Chapter 3. Here the focus of investigation changed from the exploration of drug induced whole brain structural changes to a more subtle volumetric examination confined to brain regions based on the pattern of functional activations in response to the GO/NOGO cognitive task. Hence the influence of possible structural differences and their relationship to functional and cognitive measures in specific brain regions became the focus. The results while not conclusive, suggest that in general, brain structure appears not to directly influence functional activity and cognitive performance. This said, the results offer tentative evidence that a more restricted and

localized mechanism of structure / function interactions may be at play in which larger grey matter volumes in certain brain regions may result in increased performance during an inhibition type task. These findings stress the need for further extensive research to unravel the true nature of neuroanatomy and how it relates to cognitive ability in general.

6.3 *Proposed optimum VBM analysis strategy*

Chapter 3, while investigating the sensitivity of VBM to accurately identify regional effects of particular drugs, also enabled the identification of many of the parameters that should be considered when performing such voxelwise volumetric investigations. Hence one could suggest a possible analysis routine to yield more robust and reliable results. Firstly, I feel all the input images to the automated analysis software should be skull stripped using one of the numerous software tools present in many of the freely available analysis packages. This has been shown to reduce registration errors and increase the sensitivity of the analysis (Fein et al., 2006a). Next, the researcher should use custom made study specific templates to sensitize the analysis to the particular dataset under investigation rather than the more general template files available in the software suites (Keller et al., 2004). Having explored the impact of the different segmentation routines available in both FSL and SPM2, the intensity based segmentation routine within FSL rather than a routine that utilizes tissue priors appears to offer a slightly more sensitive segmentation performance and more accurate partial volume estimate. The registration step used to transpose an image from one coordinate system to a standard coordinate space such as MNI space can feature linear transformations as in the case of FSL SIENAX or linear and non linear transformations as in the case SPM2 VBM. The latest version of FSL featuring FSL-VBM, now offers an

expanded registration mechanism incorporating both linear and nonlinear transforms similar to the SPM2 approach (not available during the investigations contained in this thesis). This appears to be the suggested preferred registration method rather than linear registrations only and thus the optimum VBM approach should feature both linear and nonlinear registration transformations which may in turn reduce the differences between the voxelwise maps of SPM2 VBM and FSL's SIENAX and FAST reported in the voxelwise comparisons reported in Chapter 4.

Particular attention should be applied to the selection of the smoothing kernel used as this can also have a large impact on the findings as mentioned in Chapters 3 and 4. A good 'rule of thumb' should be to let the data and research question drive the extent of the blur, where the smaller FWHM kernels may be more useful when investigating subtle or possible small scale structural effects. The larger smoothing size may be appropriate when examining possible volumetric changes that may be very robust or extensive. This in reality may require multiple iterations of the analysis with various smoothing kernels to selectively sensitize the data to the particular effect or research question at hand. The important message here is that there is no overall golden rule for the selection of the smoothing kernel used.

Chapter 4 demonstrated that whole brain absolute measures determined by fully automated techniques incur a baseline shift and bias the measures in favour of grey matter. Thus although a highly correlated pattern of volume change appears to be consistent between both the automated techniques and those of stereology and can offer an insight into the over

overall trends in the data, whole brain measures must be used in conjunction with 'Gold Standard' measures to accurately assess absolute volumetrics. This effect may become less pronounced when structures such as the cerebellum are excluded or smaller regions with clearly defined tissue boundaries are being investigated but this question requires further investigation.

Finally, it necessary to briefly mention some particular considerations involved in the statistical analyses. In order to perform the voxelwise volumetric analysis the assumption that the data is normally distributed must be adhered to ensure the validity of the statistical tests when performing parametric tests. The statistical design must also be well balanced to ensure this normality remains and avoid undesirable sources of bias being introduced into the data. The use of smoothing is typically employed to render the data more normally distributed and the extent of the smoothing kernel used can be increased in size to above 12mm FWHM where the deign is typically unbalanced (i.e. where a single subject is being compared to a control sample in case studies). Another option is to use nonparametric statistical tests where no assumptions about the data are required. These nonparametric statistical tests feature in the new FSL-VBM analysis toolbox as well as optional statistical toolboxes within SPM and remove the restrictions of the data being normally distributed but can be less sensitive and require a larger sample size to obtain similar patterns of effect. Again this is data dependent and should be considered when the specifics of the data are understood. Hence, the factors outlined above present the researcher with a useful insight into some of the key analytical issues when conducting volumetric structural analysis and

stress the importance of these considerations while attempting to optimise the analysis strategy to perform volumetric analysis.

6.4 *Interpretations: The big picture.*

This body of work has explored the mechanisms of structural image analysis and has demonstrated the necessity for a clear understanding of the methodological consideration when performing such analyses. Due to the high degree of automation in these software packages used for volumetric analyses, it is very easy to overlook the complexities of the parameter selection and how these setting can directly influence the findings. Thus it is apparent that the process of parameter selection must be considered with particular attention to the overall research question being addressed. These automated techniques have become very powerful and indeed flexible research tools at the disposal of the research scientist. The use of these automated techniques for whole brain absolute volumetrics appears to suffer a tissue bias in favour of grey matter and resulting in more grey matter being estimated compared to stereological measures. This should act as cautionary note to the research as further research is needed to explore the nature of this tissue bias and investigate if this bias remains when the region of interest becomes more distinct in location and doesn't encompass the whole brain. Finally, the need for a very flexible and sensitive fMRI analysis technique is outlined with the description and application of a nonlinear modelling technique for event-related fMRI analysis. This technique is utilized within this body of work to facilitate the exploration of the complex interactions between structural, functional activation and cognitive performance measures. The results in Chapter 5 identify an analysis strategy to perform inter-modal interactions

that capture the brain function and structure on various levels. It also highlights the degree of attention needed for demographic profiling of participants to ensure that as many confounds are removed as possible before the onset of analysis. Overall, these techniques can be used successfully to further our understanding of the complex workings of the brain.

6.5 *Future directions*

The theme of this body of work has highlighted some of the key methodological consideration facing the researcher when employing MRI analysis techniques to investigate human neuroanatomy and cognition. Technological advancement in this area continues and facilitates the diversification of imaging modalities and analysis techniques available to the researcher. Numerous studies have begun to utilize complex analysis techniques featuring different imaging modalities that when combined, offer the researcher a clearer view of the research question being addressed. I believe that this type of multi-modal imaging approach can offer the research scientist the opportunity to explore the mechanisms of brain function and anatomy at a resolution unseen before. When taken independently, imaging techniques such as fMRI, volumetric analysis and more recently diffusion tensor imaging (DTI) are powerful and sophisticated techniques of exploration but to truly exploit their potential, I feel a multi-faceted imaging approach combining numerous techniques will enhance our perspective of numerous research questions and offer a level of insight exceeding that of each individual imaging modality.

It is my intention to expand upon the methodological considerations investigated in this thesis and incorporate an analytical battery of techniques routinely featuring and combining fMRI, VBM, and DTI as well as cognitive behavioral testing. To date, I have piloted this

approach where my current focus of research investigates the effects of marijuana on the brain (a portion of my research conducted for this thesis but incomplete at the time of submission), and schizophrenia. I feel the future offers exciting challenges and untapped potential into the vast area of brain research in general. Further optimization of the analysis techniques will ensue, in particular focusing on the recently released software analysis package from the FMRIB Software Library featuring FSL-VBM. This software includes a non parametric statistical toolbox suggested to offer a robust permutation based inference tool for nonparametric statistical thresholding that avoids the constraint of normally distributed data and stationarity limitations that must be adhered to with SPM2 at the present (Ashburner and Friston, 2000). FSL also offers an extensive analysis toolbox for diffusion weighted image (DWI) analysis and offers the researcher the mechanisms to conduct DTI analysis, fibre tractography, and fractional anisotropy (FA) analysis, routinely considered as a robust indicator of white matter tissue integrity, and all of which I am are currently investigating as part of the proposed routine multi-modal analysis strategy.

6.6 *Conclusions*

Structural image analysis is an exciting and ongoing area of research that is methodologically complex and extremely diverse in possible avenues of exploration. This thesis attempts to stress the necessity of a clear understanding of the methodological considerations and pitfalls facing the researcher and hence inform the reader of some of the possible confounds and variability associated with structural image analysis. The results demonstrated the sensitivity of these automated structural image analysis techniques to identify and quantify regional volumetric changes in a wide variety of clinical and normal

samples, the variability between the techniques and the importance of careful systematic interpretation of findings. These techniques can be very useful tools when treated with appropriate caution and could prove vital in providing a better understanding of intricate and frequently complex workings of the human brain.

REFERENCES

Aguirre, G. K., Detre, J. A., Zarahn, E., and Alsop, D. C. (2002). Experimental design and the relative sensitivity of BOLD and perfusion fMRI. Neuroimage *15*, 488-500.

Aguirre, G. K., Zarahn, E., and D'Esposito, M. (1998). The variability of human, BOLD hemodynamic responses. Neuroimage *8*, 360-369.

Ashburner, J., and Friston, K. (1997). Multimodal image coregistration and partitioning--a unified framework. Neuroimage *6*, 209-217.

Ashburner, J., and Friston, K. (1999). Nonlinear Spatial Normalization Using Basis Functions. Hum Brain Mapp *7*, 254-266.

Ashburner, J., and Friston, K. J. (2000). Voxel-based morphometry--the methods. Neuroimage *11*, 805-821.

Ashburner, J., and Friston, K. J. (2001). Why voxel-based morphometry should be used. Neuroimage *14*, 1238-1243.

Ashburner, J., and Friston, K. J. (2005). Unified segmentation. Neuroimage *26*, 839-851.

Bandettini, P. A., Wong, E. C., Hinks, R. S., Tikofsky, R. S., and Hyde, J. S. (1992). Time course EPI of human brain function during task activation. Magn Reson Med *25*, 390-397.

Barta, P. E., Petty, R. G., McGilchrist, I., Lewis, R. W., Jerram, M., Casanova, M. F., Powers, R. E., Brill, L. B., 2nd, and Pearlson, G. D. (1995). Asymmetry of the planum temporale: methodological considerations and clinical associations. Psychiatry Res *61*, 137-150.

Bartzokis, G., Beckson, M., Lu, P. H., Edwards, N., Bridge, P., and Mintz, J. (2002). Brain maturation may be arrested in chronic cocaine addicts. Biol Psychiatry *51*, 605-611.

Bartzokis, G., Beckson, M., Lu, P. H., Edwards, N., Rapoport, R., Bridge, P., and Mintz, J. (2004). Cortical gray matter volumes are associated with subjective responses to cocaine infusion. Am J Addict *13*, 64-73.

Bartzokis, G., Beckson, M., Lu, P. H., Edwards, N., Rapoport, R., Wiseman, E., and Bridge, P. (2000). Age-related brain volume reductions in amphetamine and cocaine addicts and normal controls: implications for addiction research. Psychiatry Res *98*, 93-102.

Bartzokis, G., Beckson, M., Lu, P. H., Nuechterlein, K. H., Edwards, N., and Mintz, J. (2001). Age-related changes in frontal and temporal lobe volumes in men: a magnetic resonance imaging study. Arch Gen Psychiatry *58*, 461-465.

Bell, E. C., Willson, M. C., Wilman, A. H., Dave, S., and Silverstone, P. H. (2006). Males and females differ in brain activation during cognitive tasks. Neuroimage *30*, 529-538.

Bigler, E. D., Neeley, E. S., Miller, M. J., Tate, D. F., Rice, S. A., Cleavinger, H., Wolfson, L., Tschanz, J., and Welsh-Bohmer, K. (2004). Cerebral volume loss, cognitive deficit and neuropsychological performance: comparative measures of brain atrophy: I. Dementia. J Int Neuropsychol Soc *10*, 442-452.

Bland, J. M., and Altman, D. G. (1986). Statistical methods for assessing agreement between two methods of clinical measurement. Lancet *1*, 307-310.

Bland, J. M., and Altman, D. G. (2003). Applying the right statistics: analyses of measurement studies. Ultrasound Obstet Gynecol *22*, 85-93.

Block, R. I., O'Leary, D. S., Hichwa, R. D., Augustinack, J. C., Boles Ponto, L. L., Ghoneim, M. M., Arndt, S., Hurtig, R. R., Watkins, G. L., Hall, J. A., *et al.* (2002). Effects of frequent marijuana use on memory-related regional cerebral blood flow. Pharmacol Biochem Behav *72*, 237-250.

Bloom, A. S., Hoffmann, R. G., Fuller, S. A., Pankiewicz, J., Harsch, H. H., and Stein, E. A. (1999). Determination of drug-induced changes in functional MRI signal using a pharmacokinetic model. Hum Brain Mapp *8*, 235-244.

Bolla, K., Ernst, M., Kiehl, K., Mouratidis, M., Eldreth, D., Contoreggi, C., Matochik, J., Kurian, V., Cadet, J., Kimes, A., *et al.* (2004). Prefrontal cortical dysfunction in abstinent cocaine abusers. J Neuropsychiatry Clin Neurosci *16*, 456-464.

Bolla, K. I., Brown, K., Eldreth, D., Tate, K., and Cadet, J. L. (2002). Dose-related neurocognitive effects of marijuana use. Neurology *59*, 1337-1343.

Bolla, K. I., Cadet, J. L., and London, E. D. (1998). The neuropsychiatry of chronic cocaine abuse. J Neuropsychiatry Clin Neurosci *10*, 280-289.

Bolla, K. I., Eldreth, D. A., London, E. D., Kiehl, K. A., Mouratidis, M., Contoreggi, C., Matochik, J. A., Kurian, V., Cadet, J. L., Kimes, A. S., *et al.* (2003). Orbitofrontal cortex dysfunction in abstinent cocaine abusers performing a decision-making task. Neuroimage *19*, 1085-1094.

Bolla, K. I., Eldreth, D. A., Matochik, J. A., and Cadet, J. L. (2005). Neural substrates of faulty decision-making in abstinent marijuana users. Neuroimage *26*, 480-492.

Bolla, K. I., Funderburk, F. R., and Cadet, J. L. (2000). Differential effects of cocaine and cocaine alcohol on neurocognitive performance. Neurology *54*, 2285-2292.

Bolla, K. I., Rothman, R., and Cadet, J. L. (1999). Dose-related neurobehavioral effects of chronic cocaine use. J Neuropsychiatry Clin Neurosci *11*, 361-369.

Bonilha, L., Rorden, C., Halford, J. J., Eckert, M., Appenzeller, S., Cendes, F., and Li, L. M. (2006). Asymmetrical extra-hippocampal gray matter loss related to hippocampal atrophy in patients with medial temporal lobe epilepsy. J Neurol Neurosurg Psychiatry.

Bonilha, L., Rorden, C., Halford, J. J., Eckert, M., Appenzeller, S., Cendes, F., and Li, L. M. (2007). Asymmetrical extra-hippocampal grey matter loss related to hippocampal atrophy in patients with medial temporal lobe epilepsy. J Neurol Neurosurg Psychiatry *78*, 286-294.

Bookstein, F. L. (2001). "Voxel-based morphometry" should not be used with imperfectly registered images. Neuroimage *14*, 1454-1462.

Braver, T. S., and Barch, D. M. (2002). A theory of cognitive control, aging cognition, and neuromodulation. Neurosci Biobehav Rev *26*, 809-817.

Brazdzionyte, J., and Macas, A. (2007). Bland-Altman analysis as an alternative approach for statistical evaluation of agreement between two methods for measuring hemodynamics during acute myocardial infarction. Medicina (Kaunas) *43*, 208-214.

Breiter, H. C., Gollub, R. L., Weisskoff, R. M., Kennedy, D. N., Makris, N., Berke, J. D., Goodman, J. M., Kantor, H. L., Gastfriend, D. R., Riorden, J. P., *et al.* (1997). Acute effects of cocaine on human brain activity and emotion. Neuron *19*, 591-611.

Bremner, J. D., and Narayan, M. (1998). The effects of stress on memory and the hippocampus throughout the life cycle: Implications for childhood development and aging. Dev Psychopathol *10*, 871-885.

Brody, A. L., Mandelkern, M. A., Jarvik, M. E., Lee, G. S., Smith, E. C., Huang, J. C., Bota, R. G., Bartzokis, G., and London, E. D. (2004a). Differences between smokers and nonsmokers in regional gray matter volumes and densities. Biol Psychiatry *55*, 77-84.

Brody, A. L., Mandelkern, M. A., Lee, G., Smith, E., Sadeghi, M., Saxena, S., Jarvik, M. E., and London, E. D. (2004b). Attenuation of cue-induced cigarette craving and anterior cingulate cortex activation in bupropion-treated smokers: a preliminary study. Psychiatry Res *130*, 269-281.

Brody, A. L., Olmstead, R. E., London, E. D., Farahi, J., Meyer, J. H., Grossman, P., Lee, G. S., Huang, J., Hahn, E. L., and Mandelkern, M. A. (2004c). Smoking-induced ventral striatum dopamine release. Am J Psychiatry *161*, 1211-1218.

Buckner, R. L., Bandettini, P. A., O'Craven, K. M., Savoy, R. L., Petersen, S. E., Raichle, M. E., and Rosen, B. R. (1996). Detection of cortical activation during averaged single trials of a cognitive task using functional magnetic resonance imaging. Proc Natl Acad Sci U S A *93*, 14878-14883.

Bush, G., Frazier, J. A., Rauch, S. L., Seidman, L. J., Whalen, P. J., Jenike, M. A., Rosen, B. R., and Biederman, J. (1999). Anterior cingulate cortex dysfunction in attention-deficit/hyperactivity disorder revealed by fMRI and the Counting Stroop. Biol Psychiatry *45*, 1542-1552.

Bush, G., Valera, E. M., and Seidman, L. J. (2005). Functional neuroimaging of attention-deficit/hyperactivity disorder: a review and suggested future directions. Biol Psychiatry *57*, 1273-1284.

Cadet, J. L., and Bolla, K. I. (1996). Chronic cocaine use as a neuropsychiatric syndrome: a model for debate. Synapse *22*, 28-34.

Calhoun, V. D., Adali, T., Pearlson, G. D., and Pekar, J. J. (2001). Spatial and temporal independent component analysis of functional MRI data containing a pair of task-related waveforms. Hum Brain Mapp *13*, 43-53.

Calhoun, V. D., Stevens, M. C., Pearlson, G. D., and Kiehl, K. A. (2004). fMRI analysis with the general linear model: removal of latency-induced amplitude bias by incorporation of hemodynamic derivative terms. Neuroimage *22*, 252-257.

Campbell, V. A. (2001). Tetrahydrocannabinol-induced apoptosis of cultured cortical neurones is associated with cytochrome c release and caspase-3 activation. Neuropharmacology *40*, 702-709.

Carmona, S., Vilarroya, O., Bielsa, A., Tremols, V., Soliva, J. C., Rovira, M., Tomas, J., Raheb, C., Gispert, J. D., Batlle, S., and Bulbena, A. (2005). Global and regional gray matter reductions in ADHD: a voxel-based morphometric study. Neurosci Lett *389*, 88-93.

Carpentier, A., Galanaud, D., Puybasset, L., Muller, J. C., Lescot, T., Boch, A. L., Riedl, V., Cornu, P., Coriat, P., Dormont, D., and van Effenterre, R. (2006). Early morphologic and spectroscopic magnetic resonance in severe traumatic brain injuries can detect "invisible brain stem damage" and predict "vegetative states". J Neurotrauma *23*, 674-685.

Castellanos, F. X., Giedd, J. N., Berquin, P. C., Walter, J. M., Sharp, W., Tran, T., Vaituzis, A. C., Blumenthal, J. D., Nelson, J., Bastain, T. M., *et al.* (2001). Quantitative brain magnetic resonance imaging in girls with attention-deficit/hyperactivity disorder. Arch Gen Psychiatry *58*, 289-295.

Castellanos, F. X., Giedd, J. N., Marsh, W. L., Hamburger, S. D., Vaituzis, A. C., Dickstein, D. P., Sarfatti, S. E., Vauss, Y. C., Snell, J. W., Lange, N., *et al.* (1996). Quantitative brain magnetic resonance imaging in attention-deficit hyperactivity disorder. Arch Gen Psychiatry *53*, 607-616.

Cavanna, A. E., and Trimble, M. R. (2006). The precuneus: a review of its functional anatomy and behavioural correlates. Brain *129*, 564-583.

Chen, X., Wen, W., Malhi, G. S., Ivanovski, B., and Sachdev, P. S. (2007). Regional gray matter changes in bipolar disorder: a voxel-based morphometric study. Aust N Z J Psychiatry *41*, 327-336.

Chinn, S. (1990). The assessment of methods of measurement. Stat Med *9*, 351-362.

Cliff, I. J., Evans, A. H., Pantin, C. F., and Baldwin, D. R. (1999). Comparison of two new methods for the measurement of lung volumes with two standard methods. Thorax *54*, 329-333.

Cohen, M. S. (1997). Parametric analysis of fMRI data using linear systems methods. Neuroimage *6*, 93-103.

Cohen, R. A., Grieve, S., Hoth, K. F., Paul, R. H., Sweet, L., Tate, D., Gunstad, J., Stroud, L., McCaffery, J., Hitsman, B., *et al.* (2006). Early Life Stress and Morphometry of the Adult
Anterior Cingulate Cortex and Caudate Nuclei. BIOL PSYCHIATRY *59*, 975-982.

Colchester, A., Kingsley, D., Lasserson, D., Kendall, B., Bello, F., Rush, C., Stevens, T. G., Goodman, G., Heilpern, G., Stanhope, N., and Kopelman, M. D. (2001). Structural MRI volumetric analysis in patients with organic amnesia, 1: methods and comparative findings across diagnostic groups. J Neurol Neurosurg Psychiatry *71*, 13-22.

Court, J. A., Martin-Ruiz, C., Graham, A., and Perry, E. (2000). Nicotinic receptors in human brain: topography and pathology. J Chem Neuroanat *20*, 281-298.

Cowan, R. L., Frederick, B. B., Rainey, M., Levin, J. M., Maas, L. C., Bang, J., Hennen, J., Lukas, S. E., and Renshaw, P. F. (2000). Sex differences in response to red and blue light in human primary visual cortex: a bold fMRI study. Psychiatry Res *100*, 129-138.

Cowan, R. L., Lyoo, I. K., Sung, S. M., Ahn, K. H., Kim, M. J., Hwang, J., Haga, E., Vimal, R. L., Lukas, S. E., and Renshaw, P. F. (2003). Reduced cortical gray matter density in human MDMA (Ecstasy) users: a voxel-based morphometry study. Drug Alcohol Depend *72*, 225-235.

Cox, R. W. (1996). AFNI: software for analysis and visualization of functional magnetic resonance neuroimages. Comput Biomed Res *29*, 162-173.

Crippa, J. A., Lacerda, A. L., Amaro, E., Busatto Filho, G., Zuardi, A. W., and Bressan, R. A. (2005). [Brain effects of cannabis--neuroimaging findings]. Rev Bras Psiquiatr *27*, 70-78.

Crum, W. R., Griffin, L. D., Hill, D. L., and Hawkes, D. J. (2003). Zen and the art of medical image registration: correspondence, homology, and quality. Neuroimage *20*, 1425-1437.

Csernansky, J. G. (2001). Structural MRI as a tool for the study of neurotoxicity and neurodegenerative disorders. J Anal Toxicol *25*, 414-418.

Dale, A. M. (1999). Optimal experimental design for event-related fMRI. Hum Brain Mapp *8*, 109-114.

Daumann, J., Jr., Fischermann, T., Heekeren, K., Thron, A., and Gouzoulis-Mayfrank, E. (2004). Neural mechanisms of working memory in ecstasy (MDMA) users who continue or discontinue ecstasy and amphetamine use: evidence from an 18-month longitudinal functional magnetic resonance imaging study. Biol Psychiatry *56*, 349-355.

De Carli, D., Garreffa, G., Colonnese, C., Giulietti, G., Labruna, L., Briselli, E., Ken, S., Macri, M. A., and Maraviglia, B. (2007). Identification of activated regions during a language task. Magn Reson Imaging.

Deblieck, C., Pesenti, G., Scifo, P., Fazio, F., Bricolo, E., Lo Russo, G., Scialfa, G., Cossu, M., Bottini, G., and Paulesu, E. (2003). Preserved functional competence of perilesional areas in drug-resistant epilepsy with lesion in supplementary motor cortex: fMRI and neuropsychological observations. Neuroimage *20*, 2225-2234.

Deichmann, R., Good, C. D., Josephs, O., Ashburner, J., and Turner, R. (2000). Optimization of 3-D MP-RAGE sequences for structural brain imaging. Neuroimage *12*, 112-127.

Desmond, J. E., Chen, S. H., DeRosa, E., Pryor, M. R., Pfefferbaum, A., and Sullivan, E. V. (2003). Increased frontocerebellar activation in alcoholics during verbal working memory: an fMRI study. Neuroimage *19*, 1510-1520.

D'Esposito, M., Zarahn, E., and Aguirre, G. K. (1999). Event-related functional MRI: implications for cognitive psychology. Psychol Bull *125*, 155-164.

Domino, E. F., Minoshima, S., Guthrie, S. K., Ohl, L., Ni, L., Koeppe, R. A., Cross, D. J., and Zubieta, J. (2000). Effects of nicotine on regional cerebral glucose metabolism in awake resting tobacco smokers. Neuroscience *101*, 277-282.

Domino, E. F., Ni, L., Xu, Y., Koeppe, R. A., Guthrie, S., and Zubieta, J. K. (2004). Regional cerebral blood flow and plasma nicotine after smoking tobacco cigarettes. Prog Neuropsychopharmacol Biol Psychiatry *28*, 319-327.

Downer, E. J., Fogarty, M. P., and Campbell, V. A. (2003). Tetrahydrocannabinol-induced neurotoxicity depends on CB1 receptor-mediated c-Jun N-terminal kinase activation in cultured cortical neurons. Br J Pharmacol *140*, 547-557.

Draganski, B., Gaser, C., Busch, V., Schuierer, G., Bogdahn, U., and May, A. (2004). Neuroplasticity: changes in grey matter induced by training. Nature *427*, 311-312.

Eldreth, D. A., Matochik, J. A., Cadet, J. L., and Bolla, K. I. (2004). Abnormal brain activity in prefrontal brain regions in abstinent marijuana users. Neuroimage *23*, 914-920.

Elfgren, C., van Westen, D., Passant, U., Larsson, E. M., Mannfolk, P., and Fransson, P. (2006). fMRI activity in the medial temporal lobe during famous face processing. Neuroimage *30*, 609-616.

Ernst, M., Matochik, J. A., Heishman, S. J., Van Horn, J. D., Jons, P. H., Henningfield, J. E., and London, E. D. (2001). Effect of nicotine on brain activation during performance of a working memory task. Proc Natl Acad Sci U S A *98*, 4728-4733.

Evans, W. E., Schentag, J.J, and Jusko, W.J. (1992). Applied Pharmacokinetics: Principles of
Therapeutic Drug Monitoring. (Vancouver, WA: Applied Therapeutics, Inc.,).

Ewing-Cobbs, L., Kramer, L., Prasad, M., Canales, D. N., Louis, P. T., Fletcher, J. M., Vollero, H., Landry, S. H., and Cheung, K. (1998). Neuroimaging, physical, and developmental findings after inflicted and noninflicted traumatic brain injury in young children. Pediatrics *102*, 300-307.

Fein, G., Landman, B., Tran, H., Barakos, J., Moon, K., Di Sclafani, V., and Shumway, R. (2006a). Statistical parametric mapping of brain morphology: sensitivity is dramatically increased by using brain-extracted images as inputs. Neuroimage *30*, 1187-1195.

Fein, G., Landman, B., Tran, H., McGillivray, S., Finn, P., Barakos, J., and Moon, K. (2006b). Brain atrophy in long-term abstinent alcoholics who demonstrate impairment on a simulated gambling task. Neuroimage.

Fernandes, M. A., Moscovitch, M., Ziegler, M., and Grady, C. (2005). Brain regions associated with successful and unsuccessful retrieval of verbal episodic memory as revealed by divided attention. Neuropsychologia *43*, 1115-1127.

Fillmore, M. T., and Rush, C. R. (2002). Impaired inhibitory control of behavior in chronic cocaine users. Drug Alcohol Depend *66*, 265-273.

Fishbein, D., Hyde, C., Eldreth, D., London, E. D., Matochik, J., Ernst, M., Isenberg, N., Steckley, S., Schech, B., and Kimes, A. (2005a). Cognitive performance and autonomic reactivity in abstinent drug abusers and nonusers. Exp Clin Psychopharmacol *13*, 25-40.

Fishbein, D. H., Eldreth, D. L., Hyde, C., Matochik, J. A., London, E. D., Contoreggi, C., Kurian, V., Kimes, A. S., Breeden, A., and Grant, S. (2005b). Risky decision making and the anterior cingulate cortex in abstinent drug abusers and nonusers. Brain Res Cogn Brain Res *23*, 119-136.

Fotenos, A. F., Snyder, A. Z., Girton, L. E., Morris, J. C., and Buckner, R. L. (2005). Normative estimates of cross-sectional and longitudinal brain volume decline in aging and AD. Neurology *64*, 1032-1039.

Franklin, T. R., Acton, P. D., Maldjian, J. A., Gray, J. D., Croft, J. R., Dackis, C. A., O'Brien, C. P., and Childress, A. R. (2002). Decreased gray matter concentration in the insular, orbitofrontal, cingulate, and temporal cortices of cocaine patients. Biol Psychiatry *51*, 134-142.

Frings, L., Wagner, K., Quiske, A., Schwarzwald, R., Spreer, J., Halsband, U., and Schulze-Bonhage, A. (2006). Precuneus is involved in allocentric spatial location encoding and recognition. Exp Brain Res.

Frodl, T., Schaub, A., Banac, S., Charypar, M., Jager, M., Kummler, P., Bottlender, R., Zetzsche, T., Born, C., Leinsinger, G., *et al.* (2006). Reduced hippocampal volume correlates with executive dysfunctioning in major depression. J Psychiatry Neurosci *31*, 316-323.

Garavan, H., Hester, R., Murphy, K., Fassbender, C., and Kelly, C. (2006). Individual differences in the functional neuroanatomy of inhibitory control. Brain Res *1105*, 130-142.

Garavan, H., Morgan, R. E., Mactutus, C. F., Levitsky, D. A., Booze, R. M., and Strupp, B. J. (2000a). Prenatal cocaine exposure impairs selective attention: evidence from serial reversal and extradimensional shift tasks. Behav Neurosci *114*, 725-738.

Garavan, H., Pankiewicz, J., Bloom, A., Cho, J. K., Sperry, L., Ross, T. J., Salmeron, B. J., Risinger, R., Kelley, D., and Stein, E. A. (2000b). Cue-induced cocaine craving: neuroanatomical specificity for drug users and drug stimuli. Am J Psychiatry *157*, 1789-1798.

Garavan, H., Ross, T. J., Kaufman, J., and Stein, E. A. (2003). A midline dissociation between error-processing and response-conflict monitoring. Neuroimage *20*, 1132-1139.

Garavan, H., Ross, T. J., Murphy, K., Roche, R. A., and Stein, E. A. (2002). Dissociable executive functions in the dynamic control of behavior: inhibition, error detection, and correction. Neuroimage *17*, 1820-1829.

Garavan, H., Ross, T. J., and Stein, E. A. (1999). Right hemispheric dominance of inhibitory control: an event-related functional MRI study. Proc Natl Acad Sci U S A *96*, 8301-8306.

Garavan, H., and Stout, J. C. (2005). Neurocognitive insights into substance abuse. Trends Cogn Sci *9*, 195-201.

Garcia-Finana, M., Cruz-Orive, L. M., Mackay, C. E., Pakkenberg, B., and Roberts, N. (2003). Comparison of MR imaging against physical sectioning to estimate the volume of human cerebral compartments. Neuroimage *18*, 505-516.

Garden, A. S., and Roberts, N. (1996). Fetal and fetal organ volume estimations with magnetic resonance imaging. Am J Obstet Gynecol *175*, 442-448.

Gazzaley, A., and D'Esposito, M. (2007). Top-down modulation and normal aging. Ann N Y Acad Sci *1097*, 67-83.

Geuze, E., Vermetten, E., and Bremner, J. D. (2005). MR-based in vivo hippocampal volumetrics: 2. Findings in neuropsychiatric disorders. Mol Psychiatry *10*, 160-184.

Giuliani, N. R., Calhoun, V. D., Pearlson, G. D., Francis, A., and Buchanan, R. W. (2005). Voxel-based morphometry versus region of interest: a comparison of two methods for analyzing gray matter differences in schizophrenia. Schizophr Res *74*, 135-147.

Goldstein, R. Z., and Volkow, N. D. (2002). Drug addiction and its underlying neurobiological basis: neuroimaging evidence for the involvement of the frontal cortex. Am J Psychiatry *159*, 1642-1652.

Gong, Q. Y., Eldridge, P. R., Brodbelt, A. R., Garcia-Finana, M., Zaman, A., Jones, B., and Roberts, N. (2004). Quantification of tumour response to radiotherapy. Br J Radiol *77*, 405-413.

Gong, Q. Y., Phoenix, J., Kemp, G. J., Garcia-Finana, M., Frostick, S. P., Brodie, D. A., Edwards, R. H., Whitehouse, G. H., and Roberts, N. (2000). Estimation of body composition in muscular dystrophy by MRI and stereology. J Magn Reson Imaging *12*, 467-475.

Good, C. D., Johnsrude, I., Ashburner, J., Henson, R. N., Friston, K. J., and Frackowiak, R. S. (2001a). Cerebral asymmetry and the effects of sex and handedness on brain structure: a voxel-based morphometric analysis of 465 normal adult human brains. Neuroimage *14*, 685-700.

Good, C. D., Johnsrude, I., Ashburner, J., Henson, R. N., Friston, K. J., and Frackowiak, R. S. (2001b). Cerebral asymmetry and the effects of sex and handedness on brain structure: a voxel-based morphometric analysis of 465 normal adult human brains. Neuroimage *14*, 685-700.

Good, C. D., Johnsrude, I. S., Ashburner, J., Henson, R. N., Friston, K. J., and Frackowiak, R. S. (2001b). A voxel-based morphometric study of ageing in 465 normal adult human brains. Neuroimage *14*, 21-36.

Good, C. D., Johnsrude, I. S., Ashburner, J., Henson, R. N., Friston, K. J., and Frackowiak, R. S. (2001a). A voxel-based morphometric study of ageing in 465 normal adult human brains. Neuroimage *14*, 21-36.

Gorbet, D. J., and Sergio, L. E. (2007). Preliminary sex differences in human cortical BOLD fMRI activity during the preparation of increasingly complex visually guided movements. Eur J Neurosci *25*, 1228-1239.

Graham, A. J., Martin-Ruiz, C. M., Teaktong, T., Ray, M. A., and Court, J. A. (2002). Human brain nicotinic receptors, their distribution and participation in neuropsychiatric disorders. Curr Drug Targets CNS Neurol Disord *1*, 387-397.

Grossman, M., Cooke, A., DeVita, C., Alsop, D., Detre, J., Chen, W., and Gee, J. (2002). Age-related changes in working memory during sentence comprehension: an fMRI study. Neuroimage *15*, 302-317.

Guan, Z. Z., Yu, W. F., and Nordberg, A. (2003). Dual effects of nicotine on oxidative stress and neuroprotection in PC12 cells. Neurochem Int *43*, 243-249.

Gundersen, H. J., and Jensen, E. B. (1987). The efficiency of systematic sampling in stereology and its prediction. J Microsc *147*, 229-263.

Gurvits, T. V., Shenton, M. E., Hokama, H., Ohta, H., Lasko, N. B., and Gilbertson, M. W. (1996). Magnetic resonance imaging study of hippocampal volume in chronic, combat-related posttraumatic stress disorder. Biol Psychiatry *40*, 1091-1099.

Gusnard, D. A., Akbudak, E., Shulmann, G. L., and Raichle, M. E. (2001). Medial prefrontal cortex and self-referential mental activity :relation to a default mode of brain function. Proc Natl Acad Sci U S A *98*, 4259-4264.

Gusnard, D. A., and Raichle, M. E. (2001). Searching for a baseline: functional imaging and resting human brain. Nat Rev Neurosci *2*, 685-694.

Handwerker, D. A., Ollinger, J. M., and D'Esposito, M. (2004). Variation of BOLD hemodynamic responses across subjects and brain regions and their effects on statistical analyses. Neuroimage *21*, 1639-1651.

Held, K., Rota Kops, E., Krause, B. J., Wells, W. M., 3rd, Kikinis, R., and Muller-Gartner, H. W. (1997). Markov random field segmentation of brain MR images. IEEE Trans Med Imaging *16*, 878-886.

Hermann, B., Jones, J., Sheth, R., Dow, C., Koehn, M., and Seidenberg, M. (2006). Children with new-onset epilepsy: neuropsychological status and brain structure. Brain *129*, 2609-2619.

Hermann, B., Seidenberg, M., Bell, B., Rutecki, P., Sheth, R., Ruggles, K., Wendt, G., D., O. L., and Magnotta, V. (2002). The neurodevelopmental impact of childhood-onset temporal lobe epilepsy on brain structure and function. Epilepsia *43*, 1062-1071.

Hermann, B., Seidenberg, M., Bell, B., Rutecki, P., Sheth, R. D., Wendt, G., O'Leary, D., and Magnotta, V. (2003). Extratemporal quantitative MR volumetrics and neuropsychological status in temporal lobe epilepsy. J Int Neuropsychol Soc *9*, 353-362.

Hesselmann, V., Zaro Weber, O., Wedekind, C., Krings, T., Schulte, O., Kugel, H., Krug, B., Klug, N., and Lackner, K. J. (2001). Age related signal decrease in functional magnetic resonance imaging during motor stimulation in humans. Neurosci Lett *308*, 141-144.

Hester, R., Dixon, V., and Garavan, H. (2006). A consistent attentional bias for drug-related material in active cocaine users across word and picture versions of the emotional Stroop task. Drug Alcohol Depend *81*, 251-257.

Hester, R., Fassbender, C., and Garavan, H. (2004a). Individual differences in error processing: a review and reanalysis of three event-related fMRI studies using the GO/NOGO task. Cereb Cortex *14*, 986-994.

Hester, R., and Garavan, H. (2004). Executive dysfunction in cocaine addiction: evidence for discordant frontal, cingulate, and cerebellar activity. J Neurosci *24*, 11017-11022.

Hester, R. L., Murphy, K., Foxe, J. J., Foxe, D. M., Javitt, D. C., and Garavan, H. (2004b). Predicting success: patterns of cortical activation and deactivation prior to response inhibition. J Cogn Neurosci *16*, 776-785.

Himanen, L., Portin, R., Isoniemi, H., Helenius, H., Kurki, T., and Tenovuo, O. (2005). Cognitive functions in relation to MRI findings 30 years after traumatic brain injury. Brain Inj *19*, 93-100.

Hoshida, T., Sakaki, T., Morimoto, T., Hashimoto, H., Kurokawa, S., Nakase, H., Hirabayashi, H., Kawaguchi, S., Tsunoda, S., Uematsu, S., and et al. (1995). Manual and digitizer measurements of amygdalohippocampal volume: reliability in comparison to computer-based measurement. Psychiatry Clin Neurosci *49*, S223-225.

Howard, M. A., Roberts, N., Garcia-Finana, M., and Cowell, P. E. (2003). Volume estimation of prefrontal cortical subfields using MRI and stereology. Brain Res Brain Res Protoc *10*, 125-138.

Hsu, Y. Y., Schuff, N., Du, A. T., Mark, K., Zhu, X., Hardin, D., and Weiner, M. W. (2002). Comparison of automated and manual MRI volumetry of hippocampus in normal aging and dementia. J Magn Reson Imaging *16*, 305-310.

Huppertz, H. J., Grimm, C., Fauser, S., Kassubek, J., Mader, I., Hochmuth, A., Spreer, J., and Schulze-Bonhage, A. (2005). Enhanced visualization of blurred gray-white matter

junctions in focal cortical dysplasia by voxel-based 3D MRI analysis. Epilepsy Res *67*, 35-50.

Ilan, A. B., Smith, M. E., and Gevins, A. (2004). Effects of marijuana on neurophysiological signals of working and episodic memory. Psychopharmacology (Berl) *176*, 214-222.

Im, K., Lee, J. M., Lee, J., Shin, Y. W., Kim, I. Y., Kwon, J. S., and Kim, S. I. (2006). Gender difference analysis of cortical thickness in healthy young adults with surface-based methods. Neuroimage *31*, 31-38.

Iversen, L. (2003). Cannabis and the brain. Brain *126*, 1252-1270.

Jenkinson, M., Bannister, P., Brady, M., and Smith, S. (2002). Improved optimization for the robust and accurate linear registration and motion correction of brain images. Neuroimage *17*, 825-841.

Jenkinson, M., and Smith, S. (2001). A global optimisation method for robust affine registration of brain images. Med Image Anal *5*, 143-156.

Jimenez-Rivera, C. A., Segarra, O., Jimenez, Z., and Waterhouse, B. D. (2000). Effects of intravenous cocaine administration on cerebellar Purkinje cell activity. Eur J Pharmacol *407*, 91-100.

Joe, B. N., Fukui, M. B., Meltzer, C. C., Huang, Q. S., Day, R. S., Greer, P. J., and Bozik, M. E. (1999). Brain tumor volume measurement: comparison of manual and semiautomated methods. Radiology *212*, 811-816.

Jones, D. K., Symms, M. R., Cercignani, M., and Howard, R. J. (2005). The effect of filter size on VBM analyses of DT-MRI data. Neuroimage *26*, 546-554.

Kamada, K., Sawamura, Y., Takeuchi, F., Kuriki, S., Kawai, K., Morita, A., and Todo, T. (2007). Expressive and receptive language areas determined by a non-invasive reliable method using functional magnetic resonance imaging and magnetoencephalography. Neurosurgery *60*, 296-305; discussion 305-296.

Kastrup, A., Li, T. Q., Glover, G. H., Kruger, G., and Moseley, M. E. (1999). Gender differences in cerebral blood flow and oxygenation response during focal physiologic neural activity. J Cereb Blood Flow Metab *19*, 1066-1071.

Kaufman, J. N., Ross, T. J., Stein, E. A., and Garavan, H. (2003). Cingulate hypoactivity in cocaine users during a GO-NOGO task as revealed by event-related functional magnetic resonance imaging. J Neurosci *23*, 7839-7843.

Keller, S. S., Mackay, C. E., Barrick, T. R., Wieshmann, U. C., Howard, M. A., and Roberts, N. (2002a). Voxel-based morphometric comparison of hippocampal and

extrahippocampal abnormalities in patients with left and right hippocampal atrophy. Neuroimage *16*, 23-31.

Keller, S. S., Wieshmann, U. C., Mackay, C. E., Denby, C. E., Webb, J., and Roberts, N. (2002b). Voxel based morphometry of grey matter abnormalities in patients with medically intractable temporal lobe epilepsy: effects of side of seizure onset and epilepsy duration. J Neurol Neurosurg Psychiatry *73*, 648-655.

Keller, S. S., Wilke, M., Wieshmann, U. C., Sluming, V. A., and Roberts, N. (2004). Comparison of standard and optimized voxel-based morphometry for analysis of brain changes associated with temporal lobe epilepsy. Neuroimage *23*, 860-868.

Kitayama, N., Quinn, S., and Bremner, J. D. (2006). Smaller volume of anterior cingulate cortex in abuse-related
posttraumatic stress disorder. Journal of Affective Disorders *90*, 171-174.

Kopelman, M. D., Lasserson, D., Kingsley, D., Bello, F., Rush, C., Stanhope, N., Stevens, T., Goodman, G., Heilpern, G., Kendall, B., and Colchester, A. (2001). Structural MRI volumetric analysis in patients with organic amnesia, 2: correlations with anterograde memory and executive tests in 40 patients. J Neurol Neurosurg Psychiatry *71*, 23-28.

Krause, B. J., Schmidt, D., Mottaghy, F. M., Taylor, J., Halsband, U., Herzog, H., Tellmann, L., and Muller-Gartner, H. W. (1999). Episodic retrieval activates the precuneus irrespective of the imagery content of word pair associates. A PET study. Brain *122 (Pt 2)*, 255-263.

Krimer, L. S., Muly, E. C., 3rd, Williams, G. V., and Goldman-Rakic, P. S. (1998). Dopaminergic regulation of cerebral cortical microcirculation. Nat Neurosci *1*, 286-289.

Kubler, A., Murphy, K., and Garavan, H. (2005). Cocaine dependence and attention switching within and between verbal and visuospatial working memory. Eur J Neurosci *21*, 1984-1992.

Kumari, V., Gray, J. A., ffytche, D. H., Mitterschiffthaler, M. T., Das, M., Zachariah, E., Vythelingum, G. N., Williams, S. C., Simmons, A., and Sharma, T. (2003). Cognitive effects of nicotine in humans: an fMRI study. Neuroimage *19*, 1002-1013.

Kurca, E., Sivak, S., and Kucera, P. (2006). Impaired cognitive functions in mild traumatic brain injury patients with normal and pathologic magnetic resonance imaging. Neuroradiology *48*, 661-669.

Kwong, K. K., Belliveau, J. W., Chesler, D. A., Goldberg, I. E., Weisskoff, R. M., Poncelet, B. P., Kennedy, D. N., Hoppel, B. E., Cohen, M. S., Turner, R., and et al. (1992). Dynamic magnetic resonance imaging of human brain activity during primary sensory stimulation. Proc Natl Acad Sci U S A *89*, 5675-5679.

Lane, S. D., Cherek, D. R., Lieving, L. M., and Tcheremissine, O. V. (2005). Marijuana effects on human forgetting functions. J Exp Anal Behav *83*, 67-83.

Lawrence, N. S., Ross, T. J., and Stein, E. A. (2002). Cognitive mechanisms of nicotine on visual attention. Neuron *36*, 539-548.

Lawson, J. A., Cook, M. J., Bleasel, A. F., Nayanar, V., Morris, K. F., and Bye, A. M. (1997). Quantitative MRI in outpatient childhood epilepsy. Epilepsia *38*, 1289-1293.

Lawson, J. A., Cook, M. J., Vogrin, S., Litewka, L., Strong, D., Bleasel, A. F., and Bye, A. M. (2002). Clinical, EEG, and quantitative MRI differences in pediatric frontal and temporal lobe epilepsy. Neurology *58*, 723-729.

Lawson, J. A., Nguyen, W., Bleasel, A. F., Pereira, J. K., Vogrin, S., Cook, M. J., and Bye, A. M. (1998). ILAE-defined epilepsy syndromes in children: correlation with quantitative MRI. Epilepsia *39*, 1345-1349.

Lawson, J. A., Vogrin, S., Bleasel, A. F., Cook, M. J., and Bye, A. M. (2000). Cerebral and cerebellar volume reduction in children with intractable epilepsy. Epilepsia *41*, 1456-1462.

Lee, A. T., Glover, G. H., and Meyer, C. H. (1995). Discrimination of large venous vessels in time-course spiral blood-oxygen-level-dependent magnetic-resonance functional neuroimaging. Magn Reson Med *33*, 745-754.

Li, S. J., Wang, Y., Pankiewicz, J., and Stein, E. A. (1999). Neurochemical adaptation to cocaine abuse: reduction of N-acetyl aspartate in thalamus of human cocaine abusers. Biol Psychiatry *45*, 1481-1487.

Lim, K. O., Choi, S. J., Pomara, N., Wolkin, A., and Rotrosen, J. P. (2002). Reduced frontal white matter integrity in cocaine dependence: a controlled diffusion tensor imaging study. Biol Psychiatry *51*, 890-895.

Liu, X., Matochik, J. A., Cadet, J. L., and London, E. D. (1998). Smaller volume of prefrontal lobe in polysubstance abusers: a magnetic resonance imaging study. Neuropsychopharmacology *18*, 243-252.

Logothetis, N. K. (2002). The neural basis of the blood-oxygen-level-dependent functional magnetic resonance imaging signal. Philos Trans R Soc Lond B Biol Sci *357*, 1003-1037.

Lu, Y., Bagshaw, A. P., Grova, C., Kobayashi, E., Dubeau, F., and Gotman, J. (2006). Using voxel-specific hemodynamic response function in EEG-fMRI data analysis. Neuroimage *32*, 238-247.

Luders, E., Narr, K. L., Thompson, P. M., Woods, R. P., Rex, D. E., Jancke, L., Steinmetz, H., and Toga, A. W. (2005). Mapping cortical gray matter in the young adult brain: effects of gender. Neuroimage *26*, 493-501.

Mackay, C. E., Webb, J. A., Eldridge, P. R., Chadwick, D. W., Whitehouse, G. H., and Roberts, N. (2000). Quantitative magnetic resonance imaging in consecutive patients evaluated for surgical treatment of temporal lobe epilepsy. Magn Reson Imaging *18*, 1187-1199.

MacLullich, A. M., Ferguson, K. J., Deary, I. J., Seckl, J. R., Starr, J. M., and Wardlaw, J. M. (2002). Intracranial capacity and brain volumes are associated with cognition in healthy elderly men. Neurology *59*, 169-174.

Maguire, E. A., Gadian, D. G., Johnsrude, I. S., Good, C. D., Ashburner, J., Frackowiak, R. S., and Frith, C. D. (2000). Navigation-related structural change in the hippocampi of taxi drivers. Proc Natl Acad Sci U S A *97*, 4398-4403.

Maguire, E. A., Spiers, H. J., Good, C. D., Hartley, T., Frackowiak, R. S., and Burgess, N. (2003). Navigation expertise and the human hippocampus: a structural brain imaging analysis. Hippocampus *13*, 250-259.

Maller, J. J., Reglade-Meslin, C., Anstey, K. J., and Sachdev, P. (2006). Sex and symmetry differences in hippocampal volumetrics: before and beyond the opening of the crus of the fornix. Hippocampus *16*, 80-90.

Massana, G., Salgado-Pineda, P., Junque, C., Perez, M., Baeza, I., Pons, A., Massana, J., Navarro, V., Blanch, J., Morer, A., *et al.* (2005). Volume changes in gray matter in first-episode neuroleptic-naive schizophrenic patients treated with risperidone. J Clin Psychopharmacol *25*, 111-117.

Matochik, J. A., Eldreth, D. A., Cadet, J. L., and Bolla, K. I. (2005). Altered brain tissue composition in heavy marijuana users. Drug Alcohol Depend *77*, 23-30.

Matochik, J. A., London, E. D., Eldreth, D. A., Cadet, J. L., and Bolla, K. I. (2003). Frontal cortical tissue composition in abstinent cocaine abusers: a magnetic resonance imaging study. Neuroimage *19*, 1095-1102.

Matsuzawa, J., Matsui, M., Konishi, T., Noguchi, K., Gur, R. C., Bilker, W., and Miyawaki, T. (2001). Age-related volumetric changes of brain gray and white matter in healthy infants and children. Cereb Cortex *11*, 335-342.

McCloskey, D. P., Hintz, T. M., Pierce, J. P., and Scharfman, H. E. (2006). Stereological methods reveal the robust size and stability of ectopic hilar granule cells after pilocarpine-induced status epilepticus in the adult rat. Eur J Neurosci *24*, 2203-2210.

McGowan, J. C., Yang, J. H., Plotkin, R. C., Grossman, R. I., Umile, E. M., Cecil, K. M., and Bagley, L. J. (2000). Magnetization transfer imaging in the detection of injury associated with mild head trauma. AJNR Am J Neuroradiol *21*, 875-880.

McKeown, M. J., Makeig, S., Brown, G. G., Jung, T. P., Kindermann, S. S., Bell, A. J., and Sejnowski, T. J. (1998). Analysis of fMRI data by blind separation into independent spatial components. Hum Brain Mapp *6*, 160-188.

McMillan, A. B., Hermann, B. P., Johnson, S. C., Hansen, R. R., Seidenberg, M., and Meyerand, M. E. (2004). Voxel-based morphometry of unilateral temporal lobe epilepsy reveals abnormalities in cerebral white matter. Neuroimage *23*, 167-174.

Mechelli, A., Henson, R. N., Price, C. J., and Friston, K. J. (2003). Comparing event-related and epoch analysis in blocked design fMRI. Neuroimage *18*, 806-810.

Miezin, F. M., Maccotta, L., Ollinger, J. M., Petersen, S. E., and Buckner, R. L. (2000). Characterizing the hemodynamic response: effects of presentation rate, sampling procedure, and the possibility of ordering brain activity based on relative timing. Neuroimage *11*, 735-759.

Miller, M. B., and Van Horn, J. D. (2007). Individual variability in brain activations associated with episodic retrieval: a role for large-scale databases. Int J Psychophysiol *63*, 205-213.

Molina, V., Reig, S., Sanz, J., Palomo, T., Benito, C., Sanchez, J., Sarramea, F., Pascau, J., and Desco, M. (2005). Increase in gray matter and decrease in white matter volumes in the cortex during treatment with atypical neuroleptics in schizophrenia. Schizophr Res *80*, 61-71.

Molina-Holgado, E., Vela, J. M., Arevalo-Martin, A., Almazan, G., Molina-Holgado, F., Borrell, J., and Guaza, C. (2002). Cannabinoids promote oligodendrocyte progenitor survival: involvement of cannabinoid receptors and phosphatidylinositol-3 kinase/Akt signaling. J Neurosci *22*, 9742-9753.

Moulton, E. A., Keaser, M. L., Gullapalli, R. P., Maitra, R., and Greenspan, J. D. (2006). Sex differences in the cerebral BOLD signal response to painful heat stimuli. Am J Physiol Regul Integr Comp Physiol *291*, R257-267.

Mueller, S. G., Laxer, K. D., Cashdollar, N., Buckley, S., Paul, C., and Weiner, M. W. (2006). Voxel-based optimized morphometry (VBM) of gray and white matter in temporal lobe epilepsy (TLE) with and without mesial temporal sclerosis. Epilepsia *47*, 900-907.

Munte, T. F., Altenmuller, E., and Jancke, L. (2002). The musician's brain as a model of neuroplasticity. Nat Rev Neurosci *3*, 473-478.

Murphy, K., Dixon, V., Lagrave, K., Kaufman, J., Risinger, R., Bloom, A., and Garavan, H. (2006). A validation of event-related FMRI comparisons between users of cocaine, nicotine, or cannabis and control subjects. Am J Psychiatry *163*, 1245-1251.

Murphy, K., and Garavan, H. (2004a). An empirical investigation into the number of subjects required for an event-related fMRI study. Neuroimage *22*, 879-885.

Murphy, K., and Garavan, H. (2004b). Artifactual fMRI group and condition differences driven by performance confounds. Neuroimage *21*, 219-228.

Murphy, K., and Garavan, H. (2004b). Artifactual fMRI group and condition differences driven by performance confounds. Neuroimage *21*, 219-228.

Murphy, K., and Garavan, H. (2005). Deriving the optimal number of events for an event-related fMRI study based on the spatial extent of activation. Neuroimage *27*, 771-777.

Naqvi, N. H., Rudrauf, D., Damasio, H., and Bechara, A. (2007). Damage to the insula disrupts addiction to cigarette smoking. Science *315*, 531-534.

Nelder, J. A., and Mead, R. (1965). A simplex method for function minimization. Computer Journal *7*, 308-313.

Nester, L., Roberts, G., Graravan, H., and Hester, R. (2008). Deficits in learning and memory: parahippocampla hyperactivity and frontocortical hypoactivity in cannabis users. Neuroimage *40*, 1328-1339.

Neumann, J., Lohmann, G., Zysset, S., and von Cramon, D. Y. (2003). Within-subject variability of BOLD response dynamics. Neuroimage *19*, 784-796.

Nielson, K. A., Langenecker, S. A., and Garavan, H. (2002). Differences in the functional neuroanatomy of inhibitory control across the adult life span. Psychol Aging *17*, 56-71.

Nielson, K. A., Langenecker, S. A., Ross, T. J., Garavan, H., Rao, S. M., and Stein, E. A. (2004). Comparability of functional MRI response in young and old during inhibition. Neuroreport *15*, 129-133.

Oddo, S., Solis, P., Consalvo, D., Giagante, B., Silva, W., D'Alessio, L., Centurion, E., Saidon, P., and Kochen, S. (2003). Mesial temporal lobe epilepsy and hippocampal sclerosis: cognitive function assessment in Hispanic patients. Epilepsy Behav *4*, 717-722.

Ogawa, S., Lee, T. M., Kay, A. R., and Tank, D. W. (1990). Brain magnetic resonance imaging with contrast dependent on blood oxygenation. Proc Natl Acad Sci U S A *87*, 9868-9872.

O'Leary, D. S., Block, R. I., Koeppel, J. A., Flaum, M., Schultz, S. K., Andreasen, N. C., Ponto, L. B., Watkins, G. L., Hurtig, R. R., and Hichwa, R. D. (2002). Effects of smoking marijuana on brain perfusion and cognition. Neuropsychopharmacology *26*, 802-816.

Opanashuk, L. A., Pauly, J. R., and Hauser, K. F. (2001). Effect of nicotine on cerebellar granule neuron development. Eur J Neurosci *13*, 48-56.

Pae, E. K., Chien, P., and Harper, R. M. (2005). Intermittent hypoxia damages cerebellar cortex and deep nuclei. Neurosci Lett *375*, 123-128.

Paillere-Martinot, M. L., Caclin, A., Artiges, E., Poline, J. B., Joliot, M., Mallet, L., Recasens, C., Attar-Levy, D., and Martinot, J. L. (2001). Cerebral grey and white matter reductions and clinical correlates in patients with early onset schizophrenia. Schizophrenia Research *50*, 19 - 26.

Parkinson, R. B., Hopkins, R. O., Cleavinger, H. B., Weaver, L. K., Victoroff, J., Foley, J. F., and Bigler, E. D. (2002). White matter hyperintensities and neuropsychological outcome following carbon monoxide poisoning. Neurology *58*, 1525-1532.

Perez-Duenas, B., Pujol, J., Soriano-Mas, C., Ortiz, H., Artuch, R., Vilaseca, M. A., and Campistol, J. (2006). Global and regional volume changes in the brains of patients with phenylketonuria. Neurology *66*, 1074-1078.

Persson, J., Nyberg, L., Lind, J., Larsson, A., Nilsson, L. G., Ingvar, M., and Buckner, R. L. (2006). Structure-function correlates of cognitive decline in aging. Cereb Cortex *16*, 907-915.

Pihlajamaki, M., Tanila, H., Kononen, M., Hanninen, T., Hamalainen, A., Soininen, H., and Aronen, H. J. (2004). Visual presentation of novel objects and new spatial arrangements of objects differentially activates the medial temporal lobe subareas in humans. Eur J Neurosci *19*, 1939-1949.

Pins, D., Meyer, M. E., Foucher, J., Humphreys, G., and Boucart, M. (2004). Neural correlates of implicit object identification. Neuropsychologia *42*, 1247-1259.

Pogarell, O., Mulert, C., and Hegerl, U. (2006). Event related potentials and fMRI in neuropsychopharmacology. Clin EEG Neurosci *37*, 99-107.

Pope, H., Gruber, A., Hudson, J., Huestis, M., Yurgelun-Todd, D. (2001). Neuropsychological performance in long-term cannabis users. Arch Gen Psychiatry *58*, 909-915.

Pope, H., Yurgelun-Todd, D. (1996). The residual cognitive effects of heavy marijuana use in college students. Journal of the American Medical Association *275*, 521-527.

Pouratian, N., Bookheimer, S. Y., Rex, D. E., Martin, N. A., and Toga, A. W. (2002). Utility of preoperative functional magnetic resonance imaging for identifying language cortices in patients with vascular malformations. J Neurosurg *97*, 21-32.

Pradat-Diehl, P., Masure, M. C., Lauriot-Prevost, M. C., Vallat, C., and Bergego, C. (1999). [Impairment of visual recognition after a traumatic brain injury]. Rev Neurol (Paris) *155*, 375-382.

Raichle, M. E., MacLeod, A. M., Snyder, A. Z., Powers, W. J., Gusnard, D. A., and Shulmann, G. L. (2001). A default mode of brain function. Proc Natl Acad Sci U S A *98*, 676-682.

Raz, N., Gunning-Dixon, F. M., Head, D., Dupuis, J. H., and Acker, J. D. (1998). Neuroanatomical correlates of cognitive aging: evidence from structural magnetic resonance imaging. Neuropsychology *12*, 95-114.

Resnick, S. M., Goldszal, A. F., Davatzikos, C., Golski, S., Kraut, M. A., Metter, E. J., Bryan, R. N., and Zonderman, A. B. (2000). One-year age changes in MRI brain volumes in older adults. Cereb Cortex *10*, 464-472.

Rezvani, A. H., and Levin, E. D. (2001). Cognitive effects of nicotine. Biol Psychiatry *49*, 258-267.

Risinger, R. C., Salmeron, B. J., Ross, T. J., Amen, S. L., Sanfilipo, M., Hoffmann, R. G., Bloom, A. S., Garavan, H., and Stein, E. A. (2005). Neural correlates of high and craving during cocaine self-administration using BOLD fMRI. Neuroimage *26*, 1097-1108.

Roberts, N., Garden, A. S., Cruz-Orive, L. M., Whitehouse, G. H., and Edwards, R. H. (1994). Estimation of fetal volume by magnetic resonance imaging and stereology. Br J Radiol *67*, 1067-1077.

Roberts, N., Hogg, D., Whitehouse, G. H., and Dangerfield, P. (1998). Quantitative analysis of diurnal variation in volume and water content of lumbar intervertebral discs. Clin Anat *11*, 1-8.

Roberts, N., Puddephat, M. J., and McNulty, V. (2000). The benefit of stereology for quantitative radiology. Br J Radiol *73*, 679-697.

Rogers, R. D., and Robbins, T. W. (2001). Investigating the neurocognitive deficits associated with chronic drug misuse. Curr Opin Neurobiol *11*, 250-257.

Ronan, L., Doherty, C. P., Delanty, N., Thornton, J., and Fitzsimons, M. (2006). Quantitative MRI: a reliable protocol for measurement of cerebral gyrification using stereology. Magn Reson Imaging *24*, 265-272.

Ronan, L., Murphy, K., Delanty, N., Doherty, C., Maguire, S., Scanlon, C., and Fitzsimons, M. (2007). Cerebral cortical gyrification: a preliminary investigation in temporal lobe epilepsy. Epilepsia *48*, 211-219.

Rosen, G. D., and Harry, J. D. (1990). Brain volume estimation from serial section measurements: a comparison of methodologies. J Neurosci Methods *35*, 115-124.

Roth, R. M., and Saykin, A. J. (2004). Executive dysfunction in attention-deficit/hyperactivity disorder: cognitive and neuroimaging findings. Psychiatr Clin North Am *27*, 83-96, ix.

Rubia, K., Smith, A. B., Brammer, M. J., Toone, B., and Taylor, E. (2005). Abnormal brain activation during inhibition and error detection in medication-naive adolescents with ADHD. Am J Psychiatry *162*, 1067-1075.

Rypma, B., Eldreth, D. A., and Rebbechi, D. (2007). Age-related differences in activation-performance relations in delayed-response tasks: a multiple component analysis. Cortex *43*, 65-76.

Sakai, K. L., Miura, K., Narafu, N., and Muraishi, Y. (2004). Correlated functional changes of the prefrontal cortex in twins induced by classroom education of second language. Cereb Cortex *14*, 1233-1239.

Salih, Q. A., Ramli, A. R., Mahmud, R., and Wirza, R. (2005). Brain white and gray matter anatomy of MRI segmentation based on tissue evaluation. MedGenMed *7*, 1.

Salman, Y. M., Assal, M. A., Badaw, A. M., Alian, S. M., and El-Bayome, M. E. (2005a). Validation Techniques for Quantitative Brain Tumors Measurements. Paper presented at: Engineering in Medicine and Biology 27th Annual Conference (Shanghai, China).
Salman, Y. M., Assal, M. A., Badaw, A. M., Alian, S. M., and El-Bayome, M. E. (2005b). Validation Techniques for Quantitative Brain Tumors Measurements. In Engineering in Medicine and Biology 27th Annual Conference (Shanghai, China), pp. 4.

Salmond, C. H., Ashburner, J., Vargha-Khadem, F., Gadian, D. G., and Friston, K. J. (2000). Detecting bilateral abnormalities with voxel-based morphometry. Hum Brain Mapp *11*, 223-232.

Scahill, R. I., Frost, C., Jenkins, R., Whitwell, J. L., Rossor, M. N., and Fox, N. C. (2003). A longitudinal study of brain volume changes in normal aging using serial registered magnetic resonance imaging. Arch Neurol *60*, 989-994.

Schad, L. R. (2001). Improved target volume characterization in stereotactic treatment planning of brain lesions by using high-resolution BOLD MR-venography. NMR Biomed *14*, 478-483.

Schlaug, G. (2001). The brain of musicians. A model for functional and structural adaptation. Ann N Y Acad Sci *930*, 281-299.

Schmithorst, V. J., and Holland, S. K. (2004). Comparison of three methods for generating group statistical inferences from independent component analysis of functional magnetic resonance imaging data. J Magn Reson Imaging *19*, 365-368.

Seidman, L. J., Valera, E. M., and Bush, G. (2004). Brain function and structure in adults with attention-deficit/hyperactivity disorder. Psychiatr Clin North Am *27*, 323-347.

Sekiyama, K., Kanno, I., Miura, S., and Sugita, Y. (2003). Auditory-visual speech perception examined by fMRI and PET. Neurosci Res *47*, 277-287.

Selemon, L. D., Kleinman, J. E., Herman, M. M., and Goldman-Rakic, P. S. (2002). Smaller frontal gray matter volume in postmortem schizophrenic brains. Am J Psychiatry *159*, 1983-1991.

Semrud-Clikeman, M., Pliszka, S. R., Lancaster, J., and Liotti, M. (2006). Volumetric MRI differences in treatment-naive vs chronically treated children with ADHD. Neurology *67*, 1023-1027.

Shi, W. M., Wildrick, D. M., and Sawaya, R. (1998). Volumetric measurement of brain tumors from MR imaging. J Neurooncol *37*, 87-93.

Siegler, R. S. (2007). Cognitive variability. Dev Sci *10*, 104-109.

Sigman, M., Pan, H., Yang, Y., Stern, E., Silbersweig, D., and Gilbert, C. D. (2005). Top-down reorganization of activity in the visual pathway after learning a shape identification task. Neuron *46*, 823-835.

Silbert, L. C., Nelson, C., Holman, S., Eaton, R., Oken, B. S., Lou, J. S., and Kaye, J. A. (2006). Cortical excitability and age-related volumetric MRI changes. Clin Neurophysiol *117*, 1029-1036.

Sim, M. E., Lyoo, I. K., Streeter, C. C., Covell, J., Sarid-Segal, O., Ciraulo, D. A., Kim, M. J., Kaufman, M. J., Yurgelun-Todd, D. A., and Renshaw, P. F. (2007). Cerebellar gray matter volume correlates with duration of cocaine use in cocaine-dependent subjects. Neuropsychopharmacology *32*, 2229-2237.

Smith, C. D., Chebrolu, H., Wekstein, D. R., Schmitt, F. A., Jicha, G. A., Cooper, G., and Markesbery, W. R. (2007). Brain structural alterations before mild cognitive impairment. Neurology *68*, 1268-1273.

Smith, S. M. (2002). Fast robust automated brain extraction. Hum Brain Mapp *17*, 143-155.

Smith, S. M., Jenkinson, M., Woolrich, M. W., Beckmann, C. F., Behrens, T. E. J., Johansen-Berg, H., Bannister, P. R., De Luca, M., Drobnjak, I., Flitney, D. E., *et al.* (2004). Advances in functional and structural MR image analysis and implementation as FSL. Neuroimage *23*, 208-219.

Soeda, A., Nakashima, T., Okumura, A., Kuwata, K., Shinoda, J., and Iwama, T. (2005). Cognitive impairment after traumatic brain injury: a functional magnetic resonance imaging study using the Stroop task. Neuroradiology *47*, 501-506.

Sokhi, D. S., Hunter, M. D., Wilkinson, I. D., and Woodruff, P. W. (2005). Male and female voices activate distinct regions in the male brain. Neuroimage *27*, 572-578.

Solowij N, G. B., Peters R, Chesher G (1997). Long term cannabis use impairs memory processes and frontal lobe function. In. Paper presented at: Symposium on the cannabinoids (Burlington, VT).

Solowij, N., Stephens, R., Roffman, R. A., and Babor, T. (2002a). Does marijuana use cause long-term cognitive deficits? Jama *287*, 2653-2654; author reply 2654.

Solowij, N., Stephens, R. S., Roffman, R. A., Babor, T., Kadden, R., Miller, M., Christiansen, K., McRee, B., and Vendetti, J. (2002b). Cognitive functioning of long-term heavy cannabis users seeking treatment. Jama *287*, 1123-1131.

Staff, R. T., Murray, A. D., Deary, I. J., and Whalley, L. J. (2006). Generality and specificity in cognitive aging: a volumetric brain analysis. Neuroimage *30*, 1433-1440.

Stein, E. A. (2001). fMRI: a new tool for the in vivo localization of drug actions in the brain. J Anal Toxicol *25*, 419-424.

Stein, E. A., Risinger, R. and Bloom, A.S. (1999). FMRI in Pharmacology. In Medical Radiology. Diadnostic Imaging, C. Moonen, Bandettini, P.A., ed. (Verlag, Springer), pp. 525-538.

Sunshine, J. L., Lewin, J. S., Wu, D. H., Miller, D. A., Findling, R. L., Manos, M. J., and Schwartz, M. A. (1997). Functional MR to localize sustained visual attention activation in patients with attention deficit hyperactivity disorder: a pilot study. AJNR Am J Neuroradiol *18*, 633-637.

Talairach, J., and Tournoux, P. (1988). Co-Palnar stereotaxic atlas of the human brain (New York).

Tang, Y. (1997). Age-induced white matter changes in the human brain: a stereological investigation. Neurobiology of Aging *18*, 609-615.

Taniwaki, T., Okayama, A., Yoshiura, T., Togao, O., Nakamura, Y., Yamasaki, T., Ogata, K., Shigeto, H., Ohyagi, Y., Kira, J. I., and Tobimatsu, S. (2007). Age-related alterations of the functional interactions within the basal ganglia and cerebellar motor loops in vivo. Neuroimage.

Tatsuno, Y., and Sakai, K. L. (2005). Language-related activations in the left prefrontal regions are differentially modulated by age, proficiency, and task demands. J Neurosci *25*, 1637-1644.

Teoh, S. K., Mendelson, J. H., Woods, B. T., Mello, N. K., Hallgring, E., Anfinsen, P., Douglas, A., and Mercer, G. (1993). Pituitary volume in men with concurrent heroin and cocaine dependence. J Clin Endocrinol Metab *76*, 1529-1532.

Thacker, N. A., Williamson, D. C., and Pokric, M. (2004). Voxel based analysis of tissue volume from MRI data. Br J Radiol *77 Spec No 2*, S114-125.

Thompson, P. M., Hayashi, K. M., de Zubicaray, G., Janke, A. L., Rose, S. E., Semple, J., Herman, D., Hong, M. S., Dittmer, S. S., Doddrell, D. M., and Toga, A. W. (2003). Dynamics of gray matter loss in Alzheimer's disease. J Neurosci *23*, 994-1005.

Thompson, P. M., Hayashi, K. M., Simon, S. L., Geaga, J. A., Hong, M. S., Sui, Y., Lee, J. Y., Toga, A. W., Ling, W., and London, E. D. (2004). Structural abnormalities in the brains of human subjects who use methamphetamine. J Neurosci *24*, 6028-6036.

Tisserand, D. J., Pruessner, J. C., Sanz Arigita, E. J., van Boxtel, M. P., Evans, A. C., Jolles, J., and Uylings, H. B. (2002). Regional frontal cortical volumes decrease differentially in aging: an MRI study to compare volumetric approaches and voxel-based morphometry. Neuroimage *17*, 657-669.

Toulopoulou, T., Grech, A., Morris, R. G., Schulze, K., McDonald, C., Chapple, B., Rabe-Hesketh, S., and Murray, R. M. (2004). The relationship between volumetric brain changes and cognitive function: a family study on schizophrenia. Biol Psychiatry *56*, 447-453.

van der Flier, W. M., Middelkoop, H. A., Weverling-Rijnsburger, A. W., Admiraal-Behloul, F., Bollen, E. L., Westendorp, R. G., and van Buchem, M. A. (2005). Neuropsychological correlates of MRI measures in the continuum of cognitive decline at old age. Dement Geriatr Cogn Disord *20*, 82-88.

Verdejo-Garcia, A. J., Lopez-Torrecillas, F., Aguilar de Arcos, F., and Perez-Garcia, M. (2005). Differential effects of MDMA, cocaine, and cannabis use severity on distinctive components of the executive functions in polysubstance users: a multiple regression analysis. Addict Behav *30*, 89-101.

Villarreal, G., Hamilton, D. A., Petropoulos, H., Driscoll, I., Rowland, L. M., and Griego, J. A. (2002). Reduced hippocampal volume and total white matter volume in posttraumatic stress disorder. Biol Psychiatry *52*, 119-125.

Volkow, N. D., Fowler, J. S., Wang, G. J., and Goldstein, R. Z. (2002). Role of dopamine, the frontal cortex and memory circuits in drug addiction: insight from imaging studies. Neurobiol Learn Mem *78*, 610-624.

Volkow, N. D., Wang, G. J., Ma, Y., Fowler, J. S., Zhu, W., Maynard, L., Telang, F., Vaska, P., Ding, Y. S., Wong, C., and Swanson, J. M. (2003). Expectation enhances the regional brain metabolic and the reinforcing effects of stimulants in cocaine abusers. J Neurosci *23*, 11461-11468.

Ward, B., Garavan, H., Ross, T. J., Bloom, A., Cox, R., and Stein, E. A. (1998). Nonlinear regression for fMRI time series analysis. Neuroimage *7*.

Wenger, K. K., Visscher, K. M., Miezin, F. M., Petersen, S. E., and Schlaggar, B. L. (2004). Comparison of sustained and transient activity in children and adults using a mixed blocked/event-related fMRI design. Neuroimage *22*, 975-985.

Wexler, B. E., Gottschalk, C. H., Fulbright, R. K., Prohovnik, I., Lacadie, C. M., Rounsaville, B. J., and Gore, J. C. (2001). Functional magnetic resonance imaging of cocaine craving. Am J Psychiatry *158*, 86-95.

White, N. S., Alkire, M. T., and Haier, R. J. (2003). A voxel-based morphometric study of nondemented adults with Down Syndrome. Neuroimage *20*, 393-403.

Witelson, S. F., Beresh, H., and Kigar, D. L. (2006). Intelligence and brain size in 100 postmortem brains: sex, lateralization and age factors. Brain *129*, 386-398.

Witelson, S. F., Glezer, II, and Kigar, D. L. (1995). Women have greater density of neurons in posterior temporal cortex. J Neurosci *15*, 3418-3428.

Woermann, F. G., Free, S. L., Koepp, M. J., Ashburner, J., and Duncan, J. S. (1999). Voxel-by-voxel comparison of automatically segmented cerebral gray matter--A rater-independent comparison of structural MRI in patients with epilepsy. Neuroimage *10*, 373-384.

Wolf, H., Kruggel, F., Hensel, A., Wahlund, L. O., Arendt, T., and Gertz, H. J. (2003). The relationship between head size and intracranial volume in elderly subjects. Brain Res *973*, 74-80.

Wolf, I., Tost, H., Ruf, M., Schmidt, M. H., and Ende, G. (2005). [Functional imaging of neurocognitive dysfunction in attention deficit hyperactivity disorder]. Radiologe *45*, 169-177.

Yamasue, H., Kasai, K., Iwanami, A., Ohtani, T., Yamada, H., Abe, O., Kuroki, N., Fukuda, R., Tochigi, M., Furukawa, S., *et al.* (2003). Voxel-based analysis of MRI reveals anterior
cingulate gray-matter volume reduction in
posttraumatic stress disorder due to terrorism. PNAS *100*, 9039-9043.

Zang, Y. F., Jin, Z., Weng, X. C., Zhang, L., Zeng, Y. W., Yang, L., Wang, Y. F., Seidman, L. J., and Faraone, S. V. (2005). Functional MRI in attention-deficit hyperactivity disorder: evidence for hypofrontality. Brain Dev *27*, 544-550.

Zeng, X., Staib, L. H., Schultz, R. T., and Duncan, J. S. (1999). Segmentation and measurement of the cortex from 3-D MR images using coupled-surfaces propagation. IEEE Trans Med Imaging *18*, 927-937.

Zhang, Y., Brady, M., and Smith, S. (2001a). Segmentation of brain MR images through a hidden Markov random field model and the expectation-maximization algorithm. IEEE Trans Med Imaging *20*, 45-57.

Zhang, Y., Goldszal, A., Butman, J., and Choyke, P. (2001b). Improving image contrast using principal component analysis for subsequent image segmentation. J Comput Assist Tomogr *25*, 817-822.

Zubieta, J. K., Heitzeg, M. M., Xu, Y., Koeppe, R. A., Ni, L., Guthrie, S., and Domino, E. F. (2005). Regional cerebral blood flow responses to smoking in tobacco smokers after overnight abstinence. Am J Psychiatry *162*, 567-577.